



PB99-155046

Fabric For Reinforcement and Separation In Unpaved Roads



REPRODUCED BY
U.S. DEPARTMENT OF COMMERCE
NATIONAL TECHNICAL
INFORMATION SERVICE
SPRINGFIELD, VA 22161

Minnesota Local Road
Research Board

Funding Acknowledgment

This project was conducted with funding provided by the Minnesota Local Road Research Board (LRRB). The LRRB's purpose is to develop and manage a program of research for county and municipal state aid road improvements. Funding for LRRB research projects comes from designated fund equivalent to half of one percent of the annual state aid for county and city roads.

1. Report No. MN/RC - 1999-04		2.		3. Re  PB99-155046	
4. Title and Subtitle FABRIC FOR REINFORCEMENT AND SEPARATION IN UNPAVED ROADS				5. Report Date December 1998	
7. Author(s) Julie B. Bearden Joseph F. Labuz				8. Performing Organization Report No.	
9. Performing Organization Name and Address University of Minnesota Department of Civil Engineering 500 Pillsbury Drive, S.E. Minneapolis, MN 55455				10. Project/Task/Work Unit No.	
				11. Contract (C) or Grant (G) No. (C) 74708 TOC # 12	
12. Sponsoring Organization Name and Address Minnesota Department of Transportation 395 John Ireland Boulevard Mail Stop 330 St. Paul, Minnesota 55155				13. Type of Report and Period Covered Final Report - 1996 - 1998	
				14. Sponsoring Agency Code	
15. Supplementary Notes					
16. Abstract (Limit: 200 words) <p>Researchers performed laboratory experiments on soil-fabric-aggregate systems to evaluate the effect of a geotextile on unpaved road performance. Direct shear tests performed on gravel indicated a 42 degree friction angle. Similar tests performed on soil-fabric-aggregate systems resulted in an interface friction value for the nonwoven geotextile system similar to that of the gravel alone. The slit film and heavy weight woven systems generated friction angles about 20 percent lower.</p> <p>Observations of model tests showed that in terms of rut depths, the nonwoven performed better than the slit film woven geotextile for all gravel thicknesses, most likely because of the nonwoven's higher frictional characteristics. The rut diameters for the slit film and nonwoven reinforced systems tended to be larger than those observed for the unreinforced systems indicating an increased load-spread angle through the gravel. Based on rutting alone, the unreinforced model with 200 mm (8 in.) gravel was equivalent to that of the slit film in reinforced model with 150 mm (6 in.) gravel and the nonwoven model with 100 mm (4 in.) gravel. A so-called bearing capacity factor for the unreinforced models was approximately 50 percent less than the nonwoven reinforced models, in reasonable agreement with theory.</p>					
17. Document Analysis/Descriptors geotextiles geosynthetics rutting				18. Availability Statement No restrictions. Document available from: National Technical Information Services, Springfield, Virginia 22161	
19. Security Class (this report)		20. Security Class (this page)		21. No. of Pages	
Unclassified		Unclassified		132	
				22. Price	



FABRIC FOR REINFORCEMENT AND SEPARATION IN UNPAVED ROADS

Final Report

Prepared by

Julie B. Bearden
Joseph F. Labuz

Department of Civil Engineering
University of Minnesota
500 Pillsbury Drive S.E.
Minneapolis, Minnesota 55455-0220

December 1998

Published by

Minnesota Department of Transportation
Office of Research Services, First Floor
395 John Ireland Boulevard, MS 330
St. Paul, Minnesota 55155

The contents of this report reflect the views of the authors who are responsible for the facts and accuracy of the data presented herein. The contents do not necessarily reflect the views or policies of the Minnesota Department of Transportation at the time of publication. This report does not constitute a standard, specification, or regulation.

PROTECTED UNDER INTERNATIONAL COPYRIGHT
ALL RIGHTS RESERVED.
NATIONAL TECHNICAL INFORMATION SERVICE
U.S. DEPARTMENT OF COMMERCE



ACKNOWLEDGEMENTS

The Local Road Research Board (LRRB) through the Minnesota Department of Transportation (Mn/DOT) funded the research presented in this report. Without the participation of Mn/DOT personnel this work would not have been possible. The support of LRRB is also gratefully acknowledged.



Table of Contents

Executive Summary	i
Chapter 1 Introduction	1
Chapter 2 Literature Review	5
2.1 Description of Geotextiles and Their Functions	5
2.2 Reinforcement in Unpaved Roads	8
2.2.1 Membrane Reinforcement	9
2.2.2 Shear Reinforcement	21
2.2.3 Factors Affecting Reinforced Unpaved Roads	33
2.3 Separation in Unpaved Roads	36
2.4 Case Studies	39
2.5 Summary	42
Chapter 3 Direct Shear Tests	49
3.1 Apparatus and Setup	50
3.1.1 Apparatus Description	50
3.1.2 Apparatus Setup	51
3.2 Test Materials and Test Setup	52
3.2.1 Test Materials	52
3.2.2 Test Setup	54
3.3 Test Matrix	55
3.3.1 Clay Placement	55
3.3.2 Geotextile and Gravel Placement	55
3.4 Results	59
3.5 Summary	64

Chapter 4	Model Tests	65
4.1	Apparatus and Setup	65
4.1.1	Determination of SFA System	65
4.1.2	Cylinder Design	68
4.1.3	Testing System and Configuration	70
4.2	Materials	72
4.3	Practice Tests	76
4.3.1	Anchored Slit Film Reinforcement	77
4.3.2	Unanchored Nonwoven Reinforcement	77
4.4	Test Matrix	78
4.5	Results	81
4.5.1	Test Parameters and Final Rut Depths	81
4.5.2	Shape of Rut	83
4.5.3	Equivalency Charts	87
4.5.4	Bearing Capacity	91
4.6	Summary	93
Chapter 5	Conclusions	95
	References	97
Appendix A	Vendor Recommended Design Procedures	A-1
A.1	FHWA Geosynthetic Design and Construction Guidelines [22]	A-3
A.2	U.S. Forest Service [7]	A-11
A.3	Barenberg [3]	A-13

List of Figures

Figure 1.1: Section of reinforced unpaved road	2
Figure 2.1: Testing apparatus	9
Figure 2.2: Dual wheel axle configuration	16
Figure 2.3: Pyramidal load distribution	17
Figure 2.4: Plastic zone	17
Figure 2.5: Geotextile deformed shape	18
Figure 2.6: Section of stretched geotextile	22
Figure 2.7: Geometry of deformed geotextile	29
Figure 2.8: Load distribution through aggregate	31
Figure 3.1: Section of reinforced unpaved road	49
Figure 3.2: Direct shear box	50
Figure 3.3: Bladder calibration curve	51
Figure 3.4: Silty-clay compaction curve	52
Figure 3.5: Gravel gradation curve	53
Figure 3.6: Results of gravel direct shear tests	53
Figure 3.7: Geotextile clamping and sliding schematic	56
Figure 3.8: Geotextile clamping system on the direct shear machine (Fig. 3.2)	56
Figure 3.9: Results from slit film sliding on gravel (test number 11)	59
Figure 3.10: Results from direct shear tests on the SFA systems	60
Figure 3.11: Change in aggregate volume for three geotextiles: gravel and clay sliding	63
Figure 4.1: Tire print configuration	66
Figure 4.2: Interface pressure	67
Figure 4.3: Pressure isobar	68
Figure 4.4: Loading of a cylindrical pressure vessel	69
Figure 4.5: Schematic of cylinder design	70
Figure 4.6: Operation of closed-loop, servo-controlled testing machine	71
Figure 4.7: Loading history	71

Figure 4.8: Geotextile location for model tests	73
Figure 4.9: Bottom fill compaction curve	74
Figure 4.10: Top fill compaction curve	74
Figure 4.11: Compaction curve for silty-clay after completion of model tests	76
Figure 4.12: Anchorage scenarios	76
Figure 4.13: Rut mapping measurements	80
Figure 4.14: Rut depth histogram with table of test parameters (* extrapolated rut depth values)	82
Figure 4.15: Extrapolated rut depths for X41 and X61	82
Figure 4.16: Rut geometry interpretation	83
Figure 4.17: Coordinate system used to develop Eq. 4.4	84
Figure 4.18: Rut geometry as a function of reinforcement	85
Figure 4.19: Rut geometry as a function of gravel thickness	86
Figure 4.20: Equivalency charts after 10, 100, 1,000, and 10,000 cycles for subgrade with average (final) shear strength of 75 kPa	90
Figure 4.21: Bearing capacity factors for the unreinforced, slit film reinforced, and nonwoven reinforced tests	91
Figure A.1: Thickness design curve for single wheel loads [7]	A-8
Figure A.2: Thickness design curve for dual wheel loads [7]	A-9
Figure A.3: Thickness design curve for tandem wheel loads [7]	A-10
Figure A.4: Haul-road stabilization design curves for a 22 kN (5,000 lb) wheel load [3]	A-16
Figure A.5: Haul-road stabilization design curves for a 44.5 kN (10,000 lb) wheel load [3]	A-17
Figure A.6: Haul-road stabilization design curves for a 67 kN (15,000 lb) wheel load [3]	A-18
Figure A.7: Haul-road stabilization design curves for a 90 kN (20,000 lb) wheel load [3]	A-19

List of Tables

Table 2.1: Summary of literature review findings	42
Table 3.1: Physical and mechanical properties of the geotextiles	54
Table 3.2: Direct shear test order	58
Table 3.3: Summary of shear tests	61
Table 3.4: Interface friction angles	61
Table 4.1: Eleven model tests and their moisture contents	79
Table 4.2: Comparison of measured and calculated values for S	84
Table 4.3: Correction for stroke	87
Table 4.4: Rut depths at different cycle intervals	88
Table 4.5: Results from Steward et al. [7]	93
Table A.1: Construction survivability ratings [Task Force 25, 46]	A-4
Table A.2: Physical property requirements ¹	A-5
Table A.3: Bearing capacity factors	A-6
Table A.4: Drainage and filtration requirements	A-7



Executive Summary

When a vertical load from a vehicle is applied to an unpaved road involving a gravel aggregate-clay subgrade system, horizontal and vertical stresses are generated. The horizontal stresses in the aggregate result in outward shear stresses on the surface of the subgrade. These shear stresses reduce the bearing capacity of the clay to as little as one half the value for purely vertical loading. If fabric is present, these shear stresses can possibly be carried by the reinforcement (depending on interface friction), allowing the full bearing capacity of the clay to be mobilized.

Laboratory experiments were performed on soil-fabric-aggregate systems to evaluate the effect a geotextile has on the performance of an unpaved road. A series of 18 direct shear tests on soil-fabric-aggregate systems and 13 model tests on various unpaved road designs were conducted. The direct shear tests indicated that the nonwoven geotextile system developed an interface friction value similar to the gravel alone (42° - 45°), while the slit film and heavyweight woven systems generated friction angles about 20% lower (about 34°).

By performing model tests on similar pavement systems it was observed that, in terms of rut depths, the nonwoven performed better than the slit film woven geotextile for all gravel thicknesses, most likely due to the nonwoven's higher frictional characteristics. For all tests, geotextile anchorage was observed to be unimportant, as the geotextile appeared to be stretched only within the distributed load area at that location. The rut diameters for the slit film and nonwoven reinforced systems tended to be larger than those observed for the unreinforced systems indicating that gravel-geotextile interlocking produced some confinement within the gravel resulting in an increased load-spread angle through the gravel.

Based on rutting alone, the unreinforced model with 200 mm (8 in.) of gravel was equivalent to that of the slit film model with 150 mm (6 in.) of gravel and the nonwoven model with 100 mm (4 in.) of gravel, although the rutting was significant (60 mm or 40% of the load plate diameter). The bearing capacity factor (the ratio of maximum applied stress and shear strength) for the nonwoven reinforced models was approximately 1.5-2 times greater than the unreinforced models, in reasonable agreement with theory.



Chapter 1

Introduction

Fabric in an unpaved road can reduce the amount of aggregate needed by *reinforcing* the road and can eliminate the need for additional aggregate to account for mixing at the soil-gravel interface by *separating* the two materials. Cost savings have been recognized through the reinforcing and separating mechanisms provided by a fabric. Many agencies have successfully used geotextiles in unpaved road design. Some agencies have also experienced failures. Through both the successes and failures, it is clear that many questions remain as to how reinforced unpaved roads are designed. For example: what are the mechanisms that control road design? Is there some system property that can be efficiently evaluated and used as a deciding parameter in design?

Many factors in a soil-fabric-aggregate system affect performance:

- gravel and subgrade material properties;
- interface friction and stiffness of the geotextile;
- separation properties of the geotextile such as apparent opening size, permeability and transmissivity.

A number of researchers have looked at the mechanisms or system properties that affect the performance of geotextile reinforced unpaved roads. Barenberg et al. [1] developed a design procedure assuming that significant rutting occurs; it was also assumed that the deflected shape of the geotextile was a circular arc and no slip of the geotextile occurred at the interface. It was determined that for reinforced unpaved roads the permissible value for allowable subgrade stress is $6c_u$ and for unreinforced roads is $3.2c_u$, where c_u is the subgrade's undrained shear strength.

Kinney [2] found that geotextile properties, such as the modulus, have a significant effect on the behavior of soil-fabric-aggregate (SFA) systems. The fabric tension model was developed so as to take these effects into account. Included in the model were methods for determining geotextile shear and normal stresses as well as geotextile strain energy. The fabric tension model

is the basis for the design procedure developed for use with Mirafi[®] 140 and 500 X geotextiles [3].

Giroud and Noiray [4] developed an equation for determining the required aggregate layer thickness for a geotextile reinforced unpaved road as a function of loading, subgrade shear strength, and geotextile properties. In developing the design procedure, the reinforcement at the gravel-subgrade interface was assumed to distort a certain way under a wheel load and it was assumed that the geotextile does not slip relative to the soil and gravel. It was also assumed that the geotextile was firmly anchored at some point outside the loaded area, allowing the strain in the reinforcement to be calculated. Assuming an amount of permissible rutting and knowing the stiffness of the reinforcement, geotextile tension can be determined and, because of the assumed rut geometry, a difference between the applied pressure above and below the reinforcement (the tensioned membrane effect) could be calculated. The membrane effect was taken into account through the use of an enhanced bearing capacity factor in the road design.

Several analyses of the reinforced unpaved road problem have been published along with design charts, but all are based on essentially the same concepts as those adopted by Giroud and Noiray [4] and Barenberg [3]. Recently, Milligan et al. [5] developed a method for the design of reinforced unpaved roads where only *small* rutting is permitted. Their work was based on the concept that the principal function of geotextile reinforcement is to carry shear stresses that would otherwise be applied to the soft subgrade (Fig. 1.1).

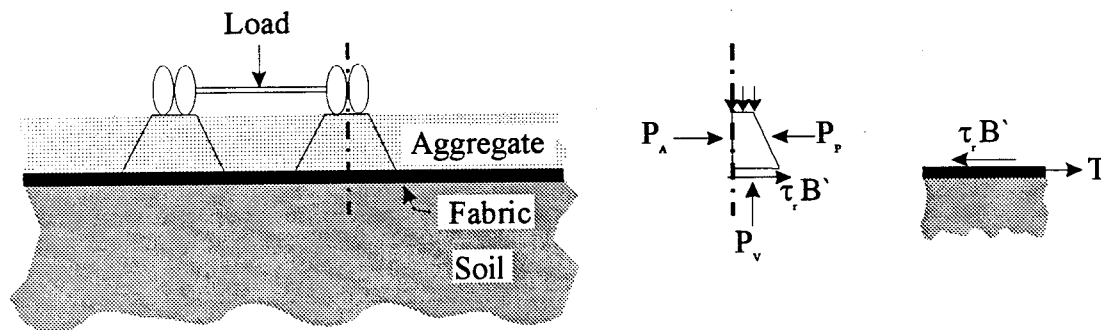


Figure 1.1: Section of reinforced unpaved road

A series of 18 direct shear tests and 13 unpaved road model tests were performed to evaluate how system properties such as interface friction affect the road's performance. Three types of geotextiles were used: a lightweight slit film, heavyweight woven, and a nonwoven. The subgrade soil was silty-clay and the aggregate was crushed gravel. Gravel thickness was varied for the model tests and the moisture content of the silty-clay was monitored so as to remain 3-7% above optimum ($w = 23-27\%$).

The model test apparatus consisted of a 560 mm (22 in.) diameter thin-walled steel cylinder that was filled with clay during testing. The inside cylinder wall was covered with plastic foam to reduce the effects of the boundaries by allowing sufficient displacement at the cylinder wall. The geotextile was placed unanchored on the clay surface and covered with either 100, 150, or 200 mm (4, 6, or 8 in.) of gravel. Approximately 10,000 cycles were applied to each modeled system at a frequency of 0.2 Hz.

Chapter 2

Literature Review

2.1 Description of Geotextiles and Their Functions

According to ASTM [6], a *geosynthetic* is defined as a planar product manufactured from a polymeric material used with soil, rock, earth, or other geotechnical-related materials as an integral part of a civil engineering project, structure, or system. A *geotextile* is a permeable geosynthetic made of textile materials. There are other types of geosynthetics such as *geogrids* and *geomembranes*. Geogrids are primarily used for reinforcement and are formed by a regular network of tensile elements with apertures of sufficient size to interlock with surrounding fill material. Geomembranes are low-permeability geosynthetics used as fluid barriers.

Elements such as fibers or yarns are combined into planar textile structures to manufacture geotextiles. The fibers can be continuous filaments, which are very long thin strands of a polymer, or staple fibers, which are short filaments, typically 20-150 mm (0.75-6 in.) long. The fibers may also be produced by slitting an extruded plastic sheet of film to form thin flat tapes. In both filaments and slit films, the extrusion or drawing process elongates the polymers in the direction of the draw and increase the filament strength.

Geotextile type is determined by the method used to combine the filaments or tapes into the planar structure. The vast majority of geotextiles are either *woven* or *nonwoven*. Woven geotextiles are made of monofilament, multifilament, or fibrillated yarns, or of slit films and tapes. The weaving process is like that of textile cloth-making. Nonwoven textile manufacturing is a modern process in which synthetic polymer fibers or filaments are continuously extruded and spun, blown or otherwise laid on to a moving belt. Then the mass of filaments or fibers are either needlepunched, in which the filaments are mechanically entangled by a series of small needles, or heat bonded, in which the fibers are welded together by heat and/or pressure at their points of contact in the nonwoven mass.

Geosynthetics have six primary functions: filtration, drainage, separation, reinforcement, fluid barrier, and protection. Geotextiles can be used as filters to prevent soil migration, as drains to allow transmission of water through low permeability materials, as separators to prevent mixing of subgrade and gravel in unpaved roads, and as reinforcement to add shear strength to a soil matrix.

There are three different reinforcing mechanisms a geotextile is commonly believed to provide to a geotextile reinforced unpaved road, commonly referred to as a soil-fabric-aggregate (SFA) system. The first mechanism is that of membrane support or membrane reinforcement. Giroud and Noiray [4] introduced the concept of membrane support for an unpaved road reinforced with a geotextile and described it as follows:

In the case of wheel loadings on a geotextile reinforced unpaved road, the normal stress applied through the aggregate and onto the geotextile is greater than the normal stress applied through the geotextile and onto the subgrade. The stress against its aggregate face is higher than the stress against its subgrade face. This stress difference is attributed to membrane support.

Membrane support is produced only if the geotextile is stretched. For stretching to occur, significant rutting of the unpaved road must take place. The tensioned geotextile takes on a wavy form due to the rutting, producing a vertical component of tensile force that relieves the subgrade of some vertical stress.

Shear reinforcement is commonly believed to be a second reinforcing mechanism a geotextile provides. Shear stresses exist at the base of a gravel layer under loading. If geotextile reinforcement is absent, these damaging stresses are transferred directly to the subgrade material. Of course, this is not a serious problem if the subgrade is a competent material. However, if the subgrade material is weak it may not be able to support these stresses. A geotextile placed at the interface between the gravel and subgrade materials provides shear reinforcement by carrying these shear stresses and not transferring them to the subgrade.

A third type of reinforcing mechanism is that of lateral confinement which is connected to the shear reinforcing mechanism. For shear stresses to be transferred to the geotextile there needs to be some gravel-geotextile interlock. When this interlock occurs the load-spread angle through the gravel may be increased resulting in lower pressures at the geotextile interface.

This chapter summarizes a review of literature pertaining to the use of geotextiles for reinforcement and separation in unpaved roads, and is organized by the following topics:

- Reinforcement in Unpaved Roads
- Separation in Unpaved Roads
- Case Studies

Research surrounding the design of geotextile reinforced unpaved roads seemingly started with work performed at the University of Illinois by Barenberg et al. [1] and Kinney [2]. This work ultimately led to the development of reinforced unpaved low-volume road design charts by Giroud and Noiray [4]. The research and interest in the topic of reinforcing unpaved roads with geotextiles quickly escalated after the publication of the work by Giroud and Noiray [4]. Based on observations of field performance, Steward et al. [7] recommended a design procedure to the U.S. Forest Service for using geotextile reinforcement in unpaved roads. However, all of these design procedures assumed that large rutting occurs and develops geotextile membrane support. Recently, Milligan et al. [5] studied reinforced unpaved roads where large rutting is not permitted. For low-deformation systems membrane support is not developed. The reinforcement mechanism may be a result of increased shear resistance at the gravel-geotextile interface.

While the use of geotextiles for reinforcing unpaved roads continued to be investigated, others started to look at the use of geotextiles purely for separation in unpaved roads. Douglas et al. [8] found that the reinforcement function of geotextiles in unpaved roads was insignificant and that the primary reason for improved performance was separation. It is well known that many engineering properties of granular materials, such as shear strength, permeability, resilient modulus and frost action potential, are adversely affected by an increase in fines content. For example, about 20% by weight of subgrade soil mixed into the aggregate base can reduce the bearing capacity of the aggregate base to that of the subgrade soil [9]. Thus, the mixing of aggregate and subgrade could compromise the structural integrity of the road.

Brorsson and Eriksson [10] reported on the long-term properties of geotextiles and their function as a separator. Geotextiles were placed on soft and saturated frost susceptible clayey-silt and silty-clay subgrades to act as a separator between the aggregate base and subgrade. After five and ten years, geotextile samples were excavated and the subgrade and base materials were

examined. All of the geotextiles sampled were found to have performed the separation function satisfactorily. It was observed that the subgrade material was firm, dry, and well consolidated. These findings point to the idea that separation is a useful function while the subgrade is consolidating. Haliburton and Barron [11] stated that, although the use of fabric for separation does not in itself strengthen the road system, it does allow for the dissipation of excess pore pressures and subgrade consolidation, which will lead to long-term subgrade strength improvement. This allows the road to improve, rather than degrade, with time and number of load repetitions.

2.2 Reinforcement in Unpaved Roads

This section deals specifically with the research on geotextile reinforced unpaved roads that was conducted by the following four groups:

- Barenberg [1, 3] and Kinney [2] – University of Illinois, Urbana-Champaign
- Giroud and Noiray [4] – Woodward-Clyde Consultants
- Milligan et al. [5], Burd and Brocklehurst [12], Houlsby and Jewel [13] – Oxford University
- Espinoza [14] and Espinoza and Bray [15] – University of California, Berkeley

A vast amount of research on geotextiles for reinforcement in unpaved roads has occurred over the last 20 years. A major advancement in this area was the development of an analytical treatment of unpaved road design with geotextile reinforcement performed by Giroud and Noiray [4], based on the concept of membrane-type reinforcement. The membrane effect refers to the reinforcement provided by a geosynthetic when large rutting is permitted, stretching and allowing the geotextile to provide some vertical (membrane) support.

Giroud and Noiray's [4] design procedure for geotextile reinforced unpaved roads came shortly after Kinney [2] completed a study on large deformation soil-fabric-aggregate systems (commonly referred to as SFA systems), where a so-called fabric tension model was introduced. This model used the notion that when a fabric is stretched over a curved surface, there is a higher normal stress on the aggregate side of the geotextile than on the subgrade side. Kinney [2] defined this difference in normal stresses as the fabric induced normal stress. Giroud and Noiray

[4] defined it as membrane support. Prior to Kinney's work with SFA systems where large rutting was permitted, Barenberg [1] developed a design procedure for the use of Mirafi® 140 in SFA systems. Membrane type reinforcement is now commonly recognized and applied to the design of unpaved haul or access roads where large rutting is permitted. Since it is necessary to have rutting to generate membrane support, researchers have recently started investigating other possible reinforcing mechanisms that may be present without rutting. Milligan et al. [5] and Espinoza [14, 15] looked at a possible shear reinforcing mechanism that may be present for small rut depths and unaffected by anchorage.

2.2.1 Membrane Reinforcement

Barenberg et al. [1] and Bender and Barenberg [16] developed design criteria for the use of Mirafi® 140 and 280 in SFA systems, from which design charts were generated. The design criterion was based on the results of small-scale laboratory tests on SFA systems (Fig. 2.1).

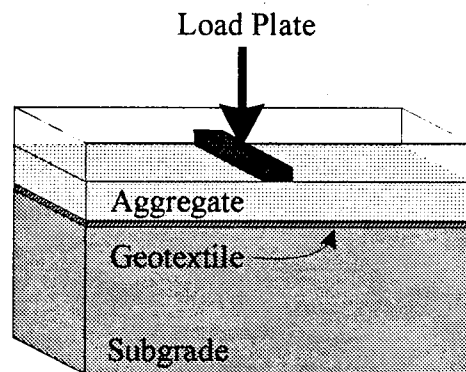


Figure 2.1: Testing apparatus

For the tests performed using the apparatus shown in Fig. 2.1, no significant difference in the performance of the systems with Mirafi® 140 and 280 was observed. The systems with fabric tended to reach some level of permanent deformation after which the system stabilized and further load applications of the same magnitude caused little or no additional permanent deformation. The critical stress level to cause excessive permanent deformation was found to be about $3.2c_u$ for systems without fabric and $6c_u$ for systems with fabric, where c_u is the undrained shear strength.

It was recommended that if the number of load cycles is greater than 10,000, the required aggregate depth should be increased by 10% above that calculated using the critical stress levels given above. This correction factor should be applied for each increment of 10,000 loads above the initial level of excessive loading (that is, the first 10,000 loads). This correction is purely empirical and based on work performed by the Army Corps of Engineers [17]. Barenberg [1] also found that fabrics were effective in preventing the intrusion of subgrade soil into the aggregate layer and stabilizing the aggregate. For certain conditions, the use of fabric was found to result in significant aggregate savings, with approximately a *one-third* reduction in aggregate thickness.

Kinney [2] developed a so-called fabric tension model, which is a mechanistic description of the behavior of the geotextile in an SFA system. It included methods for determining the geotextile induced shear and normal stresses and the strain energy stored in the geotextile. This model was based on the concept that the outward movement of aggregate and clay under loading causes outward shear stresses on the fabric, creating tension in the fabric. Also, when the fabric is stretched over a curved surface higher normal stresses are generated on the aggregate side of the fabric than on the subgrade side. The fabric resists stretching, causing inward-directed shear stresses on the gravel and the clay. Hence, the fabric indirectly causes changes in the behavior of the system.

Expressions were developed for calculating the induced shear and normal stresses knowing the tension in the geotextile and the deformed shape of the geotextile. The sum of the shear stresses on the two sides of the fabric was set equal to the rate of change in the tension-per-unit-width of the fabric along its length. The geotextile-induced shear stresses could only be determined if the fabric is assumed to be slipping with respect to one or both of the surrounding materials. If slip is assumed, the shear stress on the slipping side can be set equal to the maximum available, which is governed by the friction and adhesion between the fabric and the adjoining material and by the normal stress on that interface. The geotextile induced normal stress was set equal to the tension in the geotextile per unit width divided by the radius of curvature.

Kinney's [2] fabric tension model represented in Eq. 2.1 and 2.2 takes into account the modulus of the geotextile. Kinney found that the fabric's modulus significantly affected the performance of an SFA system. Higher modulus fabrics tended to perform better than lower

modulus fabrics. The normal stress on the geotextile, shear stress developed by the geotextile on the aggregate and subgrade, and strain energy stored in the geotextile can be determined using this model.

$$E_f = \int_s \left[\int T d\varepsilon \right] dS \quad (2.1)$$

$$E_f = \frac{W}{2E_s} \int_L (T_p^2 - T_i^2) dL \quad (2.2)$$

where

- E_f = strain energy stored in geotextile
- T = tensile force per unit width
- ε = strain
- S = geotextile surface area
- W = geotextile width being stressed
- T_p = tensile force per unit width under peak load
- T_i = residual tensile force per unit width between loading
- E_s = modulus
- L = geotextile length

Barenberg's [1] earlier design procedure for SFA systems was based on the concept of limiting, to acceptable values, the ratio of vertical stress (σ_z) transmitted to the subgrade to subgrade strength (c_u). A limitation of Barenberg's procedure was that it was based on tests performed on only two fabric types, Mirafi® 140 and 280. At the time of Barenberg's [1] work, the effect of fabric properties on the behavior and performance of an SFA system was unknown. Kinney [2] found that the fabric's modulus significantly affected the performance of an SFA system with higher modulus fabrics performing better than lower modulus fabrics. This relationship was incorporated into Kinney's [2] fabric tension model.

Barenberg's [3] revised design procedure included the fabric tension model developed by Kinney [2] with the previously developed design criteria and procedures for using Mirafi® 140 and 280 in unpaved roads. The revised procedure was developed to also be used with the

Mirafi® 500X geotextile. Barenberg [3] showed that when a load is applied to an SFA system, the normal stress transmitted to the subgrade may exceed the allowable stress. As the rut deepens, the fabric deforms and takes on a permanent tension, and a portion of the load is then carried by the fabric. Rutting continues to deepen with an increase in the fabric's tension until the normal stress transmitted to the subgrade is equal to the permissible subgrade stress. At this point, the system becomes stable and no further rutting occurs. Barenberg [3] recommended that a permissible stress on the subgrade, σ , be adjusted to compensate for the effect of the fabric modulus on the failure criterion. This was done by setting $\sigma = A * \pi * c_u$ where A is a coefficient related to the confining effects of the fabric on the soil (A equals 1 when no fabric is used and varies up to 2 when fabric is used), and c_u is the undrained shear strength of the soil. In developing the revised design procedure the geometry of the deflected shape of the fabric was assumed as a circular arc and the estimated rut depth was calculated based on this assumption. Design curves have been developed for different wheel loads using this model and assuming an average contact pressure per wheel of 550 kPa (80 psi).

Barenberg [3] Design Procedure

1. Determine the wheel load and contact pressure anticipated on the surface of the SFA system.

For dual tires as a single load, a contact pressure of 0.7-0.8 times the air pressure can be assumed. All loaded areas are assumed to have uniform pressure over a circular area.

2. Determine the maximum allowable stress, σ_{all} , for the subgrade:

$$\sigma_{all} = 3.2 A c_u \tag{2.3}$$

where c_u = subgrade undrained shear strength

A = coefficient related to the confining effects of fabric

Recommended Values for Coefficient A	
Fabric	Coefficient A
None	1.0
Mirafi® 140	1.9
Mirafi® 500X	2.0

3. Estimate required aggregate layer thickness.

Use 70-75% of aggregate thickness determined for unreinforced system.

4. Establish the rut geometry including width and maximum rut depth both on the aggregate surface and at the interface.

Subgrade rut depth, d , can for practical purposes be taken as the surface rut depth.

Subgrade rut width, W , can be estimated by the following equation:

$$W = B + 2X \quad (2.4)$$

where B = aggregate surface rut width

X = spreading effect of granular layer with and without fabric

Note: X varies from 0 mm up to 178-510 mm (7-20 in.), increasing with an increase in the amount the geotextile spreads out the rut.

5. Using assumed rut geometry, calculate the strain in the geotextile.

$$\theta = 2 \tan^{-1} \left(\frac{5d}{3W} \right) \quad (2.5)$$

$$R = \frac{3W}{8 \sin \theta} \quad (2.6)$$

$$\text{Percent Strain in Fabric, } \varepsilon_f = \left(\frac{4\pi R\theta}{135W} - 2 \right) \times 100\% \quad (2.7)$$

6. Taking the product of the fabric strain, ε_f , times the fabric modulus, K , calculate the tension in the fabric, t_f :

$$t_f = K\varepsilon_f \quad (2.8)$$

7. Calculate the differential normal stress across the fabric due to the uplifting effect of the fabric.

The differential normal stress is the normal stress difference between the top and bottom side of the fabric. The summation of the differential normal stress over the fabric in the loaded region is the portion of the applied load that is carried by the fabric. For practical purposes, only the differential stress needs to be calculated and added to the permissible stress on the subgrade to determine the permissible stress on the surface of the fabric.

$$\Delta\sigma_{z-f} = \frac{t_f}{R} \quad (2.9)$$

where $\Delta\sigma_{z-f}$ = differential normal stress across the fabric

t_f = tension in fabric

R = radius of circular deflected shape

8. Calculate the permissible vertical stress on the top of the fabric by summing the maximum permissible stress on the subgrade plus the differential normal stress due to the uplift by the fabric tension:

$$\sigma_{p-f} = \Delta\sigma_{z-f} + 3.2Ac_u \quad (2.10)$$

where $3.2Ac_u$ is the allowable stress given in Eq. 2.3

$\Delta\sigma_{z-f}$ is the differential stress across the fabric given in Eq. 2.9

9. Calculate the maximum vertical stress, σ_z , on the fabric using the Boussinesq theory. If the maximum vertical stress on the fabric is greater than the permissible vertical stress on the fabric, increase the thickness of the granular layer and return to step 4.

$$\sigma_z = p \left[1 - \left(\frac{1}{1 + \left(\frac{a}{z} \right)^2} \right)^{\frac{3}{2}} \right] \quad (2.11)$$

where P = total applied load

p = average contact pressure

z = aggregate layer thickness

a = radius of loaded area = $\sqrt{\frac{P}{\pi p}}$

Giroud and Noiray [4] developed a method that enables the engineer to calculate the required thickness of the aggregate layer and make the proper selection of the geotextile to be used. The results were presented in the form of design charts and are applicable only to purely cohesive subgrade soils and roads subjected to light - medium traffic (1-10,000 cycles).

The aggregate was assumed to have a CBR greater than 80. The subgrade soil was assumed to be saturated and to have low permeability and therefore, under quick loading, behave in an undrained manner. This means that the subgrade soil is incompressible, and in terms of total stresses, its friction angle is zero and its shear strength simply equals the undrained shear strength, c_u . It was assumed that the geotextile is rough enough to prevent sliding of the aggregate layer along the geotextile surface (that is, a *no slip* condition).

The design of an unpaved road without a geotextile was considered by comparing the maximum normal stress on the subgrade soil to the bearing capacity. Based on this analysis, charts were generated for the determination of aggregate thickness when the subgrade soil strength and the axle load are known. However, the charts were developed for unpaved roads with very light traffic.

Giroud and Noiray [4] found that for typical geotextiles, the reduction of aggregate thickness resulting from the use of a geotextile generally ranged from 20-60% for a subgrade soil with a CBR value of 1 and a number of passages between 1,000 and 10,000. An increase in the allowable rut depth caused a decrease in the required thickness of the aggregate layer with and without a geotextile. Furthermore, the smaller the geotextile tensile modulus, the larger the required thickness of the aggregate layer.

Giroud and Noiray [4] Design Procedure

1. Determine the axle load, P , and contact area, A_c :

$$P = 4 A_c p_c \quad (2.12)$$

where p_c = tire contact pressure.

For dual wheel axle configurations shown in Fig. 2.2:

contact area $\approx 2 A_c$

$$BL \approx 2 A_c \sqrt{2} \quad (2.13)$$

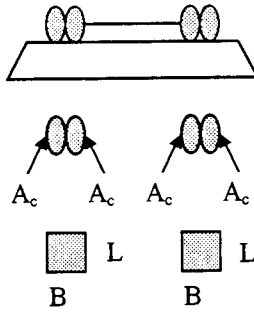


Figure 2.2: Dual wheel axle configuration

2. Set $p_c = p_{ec}$, where p_{ec} is the “equivalent contact pressure” between area $B \times L$ and the aggregate layer:

$$P = 2LBp_{ec} \quad (2.14)$$

$$p_{ec} = \frac{P_c}{\sqrt{2}} \quad (2.15)$$

3. Typical dual tire print geometry is such that for

$$\text{on-highway trucks: } L = \frac{B}{\sqrt{2}} \quad (2.16)$$

$$\text{off-highway trucks: } L = \frac{B}{2} \quad (2.17)$$

Note: We will look at on-highway trucks; the derivation for off-highway trucks follows the same procedure.

4. Using Eq. 2.15 and 2.16, L and p_{ec} can be eliminated from Eq.2.14:

$$B = \sqrt{\frac{P}{P_c}} \quad (2.18)$$

5. The relationship between normal stress on top of the aggregate, p_{ec} , with normal stress a distance h or h_o below is assumed to be pyramidal (Fig. 2.3):

$$\text{without geotextile: } p_{ec}LB = (B + 2h_o \tan \alpha_o)(L + 2h_o \tan \alpha_o)(p_o - \gamma h_o) \quad (2.19)$$

$$\text{with geotextile: } p_{ec}LB = (B + 2h \tan \alpha)(L + 2h \tan \alpha)(p - \gamma h) \quad (2.20)$$

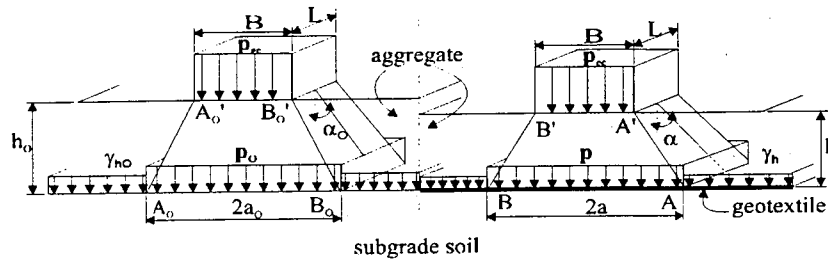


Figure 2.3: Pyramidal load distribution

6. An expression for stress on top of the geotextile can be generated using Equations (2.14) and (2.20):

$$p = \frac{P}{2(B + 2h \tan \alpha)(L + 2h \tan \alpha)} + \gamma h \quad (2.21)$$

Note: $\tan \alpha$ is typically taken as 0.5-0.7.

7. The stress at the plastic limit, q_p , was assumed to be

$$q_p = (\pi + 2)c_u \quad (2.22)$$

where c_u = undrained shear strength of the subgrade.

8. Due to the assumed failure mechanism with 45° angles in the plastic zone, the depth of the plastic zone, H_p , (Fig. 2.4) can be expressed as:

$$H_p = a\sqrt{2} \quad (2.23)$$

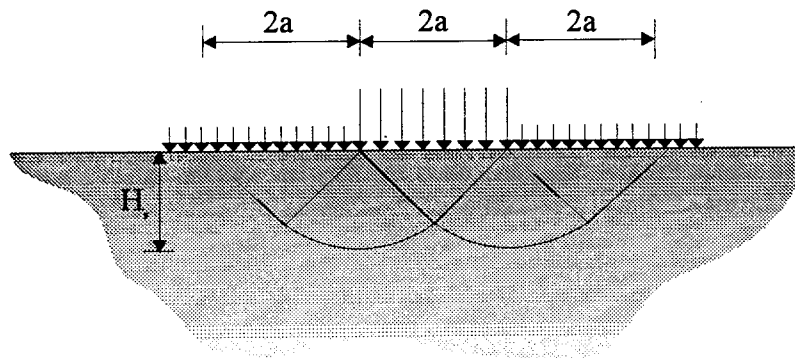


Figure 2.4: Plastic zone

From Fig. 2.2, $2a = B + 2h \tan \alpha$, so the plastic zone height can be rewritten as follows:

$$H_p = \frac{2a + 2h \tan \alpha}{2} \sqrt{2} = \frac{B + 2h \tan \alpha}{\sqrt{2}} \quad (2.24)$$

The actual stress on the subgrade, p^* , and the stress reduction due to the geotextile, p_g , is given by

$$p^* = p - p_g \quad (2.25)$$

At the limiting condition $p^* = q_p$:

$$p - p_g = (\pi + 2)c_u \quad (2.26)$$

Note: p_g is a function of the tension in the geotextile.

10. Determination of p_g :

Assume that the deformed shape of the geotextile consists of parabolas (Fig. 2.5) and that the subgrade is incompressible; thus, the volume of the subgrade displaced downwards equals the volume heaved upwards.

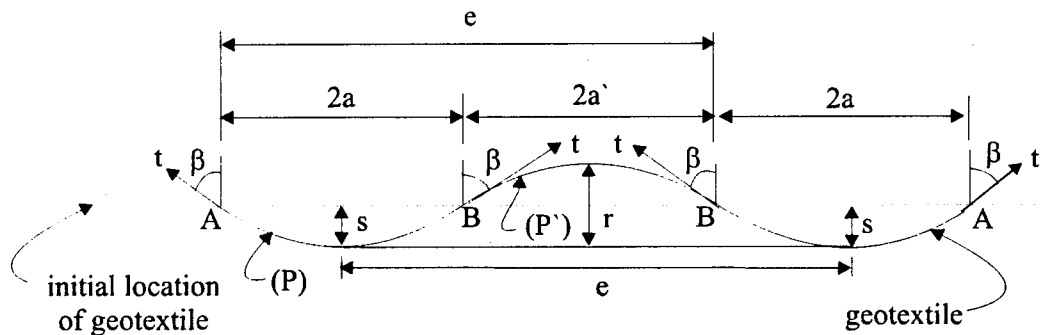


Figure 2.5: Geotextile deformed shape

There are two cases: (1) the parabola horizontal distance between the wheel loads is greater than that beneath the wheel load (i.e. $a' > a$); (2) the parabola horizontal distance underneath the wheel load is greater than that between the wheel load (i.e. $a > a'$). From the geometry of a curved geotextile:

$$2a = B + 2h \tan \alpha \quad (2.27)$$

$$2a' = e - B - 2h \tan \alpha \quad (2.28)$$

$$a' > a: \quad s = \frac{ra'}{a+a'} \quad (2.29)$$

$$a > a': \quad s = \frac{2ra^2}{2a^2 + 3aa' - a'^2} \quad (2.30)$$

Geotextile Elongation

$a' > a$: Equation (2.29) becomes $\frac{s}{a} > \frac{r-s}{a'}$ and tension in P is greater than in P' . P' is pulled towards P and uniform elongation, ε , is assumed:

$$\varepsilon = \frac{b+b'}{a+a'} - 1 \quad (2.31)$$

where a, a' = relative chord half-lengths

b, b' = half length of P and P'

$a > a'$: Equation (30) becomes $\frac{r-s}{a'} > \frac{s}{a}$ and tension in P' is greater than in P .

Geotextile does not move because of the high normal stresses on P due to the wheel load generated friction resulting in different amounts of elongation, ε , in P and P' . Elongation, ε , can be calculated directly using Eq. 2.33 because:

$$\varepsilon = \frac{b}{a} - 1 \quad (2.32)$$

Elongation, ε , can be calculated using Eq. 2.31 along with the following relationships between an arc of a parabola and subtended chord (Eq. 2.33 and 2.34) for the $a' > a$ conditions. For the $a > a'$ conditions, ε , is given directly by Eq. 2.33:

$$\frac{b}{a} - 1 = \frac{1}{2} \left[\frac{a}{2s} \ln \left(\frac{2s}{a} + \sqrt{1 + \left(\frac{2s}{a} \right)^2} \right) - 2 + \sqrt{1 + \left(\frac{2s}{a} \right)^2} \right] \quad (2.33)$$

$$\frac{b'}{a'} - 1 = \frac{1}{2} \left[\frac{a'}{2(r-s)} \ln \left(\frac{2(r-s)}{a'} + \sqrt{1 + \left(\frac{2(r-s)}{a'} \right)^2} \right) - 2 + \sqrt{1 + \left(\frac{2(r-s)}{a'} \right)^2} \right] \quad (2.34)$$

From Fig. 2.4 and 2.5, the following two expressions can be generated:

$$ap_g = t \cos \beta \quad (2.35)$$

$$\tan \beta = \frac{a}{2s} \quad (2.36)$$

where p_g = pressure reduction on the soil

Knowing the relationship between load, t , and strain, ε , for a geotextile:

$$t = K\varepsilon$$

the following expression for p_g can be derived:

$$p_g = \frac{K\varepsilon}{a\sqrt{1 + \left(\frac{a}{2s}\right)^2}} \quad (2.37)$$

11. Determination of aggregate layer thickness, h , using Eq. 2.20, 2.28, and 2.37:

$$\boxed{(\pi + 2)c_u = \frac{P}{2(B + 2h \tan \alpha)(L + 2h \tan \alpha)} + \frac{K\varepsilon}{a\sqrt{1 + \left(\frac{a}{2s}\right)^2}} \quad (2.38)}$$

By using Eq. (2.38), design charts can be generated for the required aggregate thickness, h , of a geotextile reinforced unpaved road.

Holtz and Sivakugan [18] used the Giroud and Noiray [4] design procedure to develop design charts for rut depths of 75, 100, 150, 200 and 300 mm (3, 4, 6, 8, and 12 in.). The modulus of the geotextile was found to not be as important for smaller rut depths (verses larger rut depths of 300 mm and larger). This finding was attributed to the small strains induced in the geotextile at smaller rut depths. It was explained that at smaller rut depths the membrane resistance assumed in the Giroud and Noiray [4] design procedure is not developed. So, for smaller rut depths it was claimed that the geotextile acts primarily as a separator between the gravel and subgrade.

Finally, the tire pressure was shown to have no influence on the required aggregate thickness when the undrained shear strength of the subgrade was less than about 50 kPa (0.5 tsf). Holtz and Sivakugan [18] found that for very low undrained shear strength values, a rapid

increase in required aggregate thickness occurred, irrespective of the rut depth and the geotextile modulus. Thus, a slight increase in the value of shear strength used for design could result in a significant reduction in the required aggregate thickness.

2.2.2 Shear Reinforcement

A general expression for evaluating the increased bearing capacity due to membrane action was presented by Espinoza [14]. Assuming the geometry of the deformed geotextile and a *no slip* condition, an expression was given for the horizontal and vertical forces at the interface. The shear stresses along the upper and lower sides of the interface were related by $\tau_{lower} = k\tau_{upper}$. For a subgrade composed of a soft soil and a base of cohesionless material, it was noted that the friction along the base-geotextile interface could be higher than the friction along the subgrade-geotextile interface. In such cases, it was found acceptable to assume $k = 0$ yielding $\tau_{lower} = 0$ and $\tau_{upper} = \tau$. Espinoza [14] derived expressions for a differential element, dl , of geotextile supporting applied vertical stresses and formulated a simple expression for the additional bearing capacity due to the membrane effect.

It was shown that in general, for small rutting factors, α ($\alpha = r/L$, where r is the rut depth and L is the effective horizontal length of the geotextile providing support), no significant differences for membrane support values were obtained when assuming a circular versus parabolic rut geometry. Also, for small α values, no significant differences were calculated for the additional bearing capacity assuming constant and variable strain. On the contrary, for large α values the choice of membrane support model significantly influenced the additional bearing capacity calculated. Espinoza [14] compared his model to other existing models, including Giroud and Noiray's [4] model and found that Giroud and Noiray's [4] model renders the most conservative results. An outline of the development of Espinoza's [14] expressions for determining additional bearing capacity for geotextile reinforced unpaved roads follows.

Espinoza [14] Bearing Capacity Equation

1. Development of expressions for the horizontal and vertical components of tension (Fig. 2.6):

$$\tan \beta(x) = \frac{dy}{dx} \quad (2.39a)$$

$$T_h = T(x) \cos \beta(x) \quad (2.39b)$$

$$T_v = T(x) \sin \beta(x) \quad (2.39c)$$

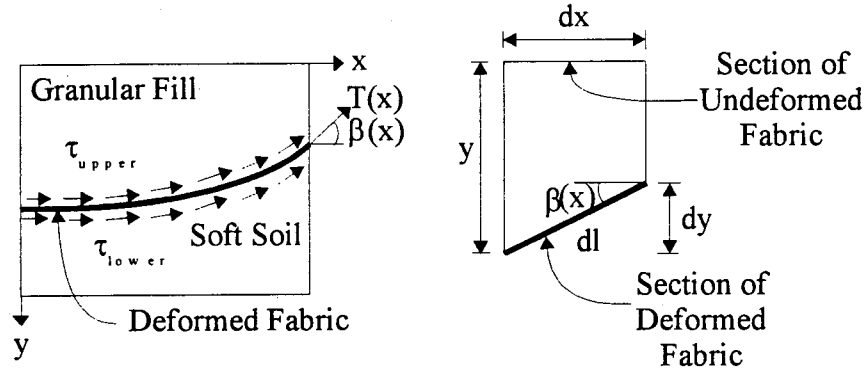


Figure 2.6: Section of stretched geotextile

Relationship between shear stresses on the upper and lower sides of the geotextile:

$$\tau_{lower} = k\tau_{upper} \quad (2.40)$$

Assuming that the friction is significantly larger on the geotextile's upper side:

$$k = 0$$

$$\tau_{lower} = 0$$

$$\tau_{upper} = \tau$$

3. Force equilibrium in the horizontal direction:

$$dT_h + \tau dl \cos \beta = dT_h + \tau dx = 0 \quad (2.41)$$

which yields:

$$\tau = -\frac{dT_h}{dx} \quad (2.42)$$

4. Force equilibrium in the vertical direction:

$$dT_v - (q_{ap} - q_s)dx + 2\tau dl \sin \beta = 0 \quad (2.43)$$

where q_{ap} = load intensity or stress at depth d
 q_s = soil reaction

5. Dividing Eq. 2.43 by dx and regrouping:

$$q_{ap} = \frac{dT_v}{dx} + q_s + \tau \tan \beta \quad (2.44)$$

6. Dividing Eq. 2.39b by 2.39c and taking the first derivative of the resulting expression:

$$\frac{dT_v}{dx} = \frac{dT_h}{dx} y'(x) + T_h y''(x) \quad (2.45)$$

7. Substituting Eq. 2.45 and 2.43 into 2.44 and using $q_{ap} = q_s + q_g$ where q_g is the additional bearing capacity due to the membrane effect, we get

$$q_g = T_h(x) \frac{d^2 y(x)}{dx^2} \quad (2.46)$$

8. A similar expression was developed by Sellmeijer et al. [18] using the theory of linear elasticity:

$$T(x) = E\varepsilon(x) \quad (2.47)$$

where E = fabric stiffness (Young's modulus)
 $\varepsilon(x)$ = fabric strain

9. Substituting Eq. 2.47 into 2.39b:

$$T_h = \varepsilon E \cos \beta \quad (2.48)$$

β can be written in terms of the first derivative of the fabric deflection:

$$\cos \beta = \frac{1}{\sqrt{1 + \left(\frac{dy}{dx}\right)^2}} \quad (2.49)$$

10. Substituting Eq. 2.49 into Eq. 2.48 and the resulting expression into Eq. 2.46, an equation for the additional bearing capacity due to membrane effect is obtained:

$$q_g(x) = \frac{E\varepsilon(x)y''(x)}{\sqrt{1 + (y'(x))^2}} \quad (2.50)$$

11. It is convenient to define an average membrane effect, q_{avg} , as follows:

$$q_{avg} = \frac{\int_{-\frac{L}{2}}^{\frac{L}{2}} q_g(x) dx}{L} = \frac{1}{L} \int_{-\frac{L}{2}}^{\frac{L}{2}} T_h(x) \frac{d^2 y(x)}{dx^2} dx \quad (2.51)$$

$$q_{avg} = \frac{2E}{L} \int_0^{\frac{L}{2}} \frac{\varepsilon(x) y''(x)}{\sqrt{1 + (y'(x))^2}} dx \quad (2.52)$$

Note: This expression holds true if *no slip* occurs along the soil-geotextile interface (i.e. tensile failure occurs first).

12. The fabric can be assumed to have *constant strain* or *variable strain*:

CONSTANT STRAIN

Integrating Eq. 2.52 assuming $\varepsilon(x)$ is constant:

$$\frac{q_{avg}}{2E} = \frac{\varepsilon \ln(\tan \beta_o + \sqrt{1 + \tan^2 \beta_o})}{L} \quad (2.53)$$

where β_o = deflection angle at $L/2$

Geotextile strain for an assumed *parabolic deformation*:

$$\varepsilon = \frac{1}{2} \left[\sec \beta_o + \frac{\ln(\tan \beta_o + \sec \beta_o)}{\tan \beta_o} \right] \quad (2.54a)$$

where $\tan \beta_o = 4\alpha$, $\sec \beta_o = \sqrt{1 + (4\alpha)^2}$, and α is the rutting factor defined as r/L . (2.54b)

Geotextile strain for an assumed circular deformation:

$$\varepsilon = \frac{1+(2\alpha)^2}{4\alpha} \tan^{-1} \beta_o - 1 \quad (2.55a)$$

$$\text{where } \tan \beta_o = \frac{4\alpha}{1-(2\alpha)^2}, \quad \sec \beta_o = \frac{1+(2\alpha)^2}{1-(2\alpha)^2} \quad (2.55b)$$

Note: Eq. 2.54 and 2.55 can be substituted into Eq. 2.52 to obtain an expression for average membrane support for a parabolic or circular geotextile deformation under constant strain.

VARIABLE STRAIN

Assuming that any point on the geotextile remains on the same vertical plane prior to deflecting:

$$\varepsilon = \frac{dl - dx}{dx} = -1 + \sqrt{\left(\frac{dy}{dx}\right)^2 + 1} \quad (2.56)$$

Substituting Eq. 2.56 into Eq. 2.52 and integrating an expression for average membrane support for a geotextile experiencing variable strain:

$$\frac{q_{avg}}{2E} = \tan \beta_o - \ln\left(\tan \beta_o + \sqrt{1 + \tan^2 \beta_o}\right) \quad (2.57)$$

$$\frac{L}{L}$$

If it is assumed that the geotextile is experiencing constant strain then, depending on the assumed geotextile deformed shape, either Eq. (2.54) or (2.55) can be substituted into Eq. (2.52) to determine the average membrane support. If it is assumed that the geotextile is experiencing variable strain, then Eq. (2.57) can be used to calculate the average membrane support (Eq. 2.56 has already been substituted into Eq. 2.52).

A procedure for evaluating the load capacity of single-layer reinforced soils was presented by Espinoza and Bray [15]. Slip between the reinforcement and the granular fill was considered. The analysis incorporated two important membrane support contributions, namely normal stress and interfacial shear stress membrane support. It was demonstrated that a significant membrane contribution could be developed even for cases in which proper anchorage was not provided.

Bearing capacity considerations often govern the design of these systems. The inclusion of a single geotextile within a two-layer soil system increases the bearing capacity due to three important soil-structure interaction effects:

1. Membrane support due to the deformed geotextile sustaining normal stresses.
2. Increased shear resistance due to the geotextile sustaining shear stresses.
3. Subgrade bearing capacity improvement due to reduction of shear stresses on the subgrade surface.

Many of the design procedures mentioned rely heavily upon the benefit of only one of these three effects, and this has often led to contradictory findings. Espinoza and Bray [15] introduced a bearing capacity equation that satisfies both vertical and horizontal force equilibrium and incorporates all three of the above mentioned effects. It was shown that the development of tensile forces in the membrane due to the transmission of shear stresses from the deforming fill to the underlying membrane (effect 2) is the main component of the membrane support contribution, and this effect does not require anchorage. In addition, the subgrade shear stress reduction (effect 3) is often the most significant benefit when including a single geotextile within a two-layer system.

A vertical surface traction, p , induces additional stresses to those created by the self-weight of the granular fill. The additional forces per unit area above the geotextile, q_{ap} , are balanced by the vertical soil reaction, q_s , and the support provided by the geotextile, q_g . From vertical force equilibrium of a differential geotextile element of unit area, it follows that the forces per unit area, $q_{ap}(x)$, $q_s(x)$, and $q_g(x)$ are related by $q_{ap}(x) = q_s(x) + q_g(x)$. The actual distribution of $q_s(x)$, $q_{ap}(x)$, and $q_g(x)$ depends on the geometric characteristics and material properties of the granular fill, subgrade soil and geotextile, and their interrelations. A number of design procedures have been proposed that are based on simplified deformation mechanisms that do not capture the interrelation between the different material components, that employ some empiricism, or that do not strictly satisfy equilibrium. The proposed design procedure was based on a closed form solution of the equilibrium equation that has less restrictive assumptions than existing designs, and incorporates all three primary benefits due to the inclusion of the geotextile [14].

The modified bearing capacity equation can be used to reconcile some contradictory findings that have been reported regarding the contribution of geotextile stiffness to single-layer reinforcement of granular road bases. It is generally believed that soils reinforced with high modulus geotextiles perform better. Yet, in a series of full-scale road section tests performed by Douglas and Kelly [20], results indicated that despite the large range in geotextile modulus, nearly identical performances were obtained for geotextiles that were fully anchored or completely free at the outside edges. Thus, a higher geotextile modulus was found to not necessarily result in higher road stiffness and, regardless of whether the geotextile edges are fixed or free, the geotextile should have similar performance. Furthermore, interfacial shear stress support depends on the applied load itself, q_{ap} , and the mobilized interface friction.

The interfacial shear stress was found to be independent of the conditions at the geotextile edges and the geotextile stiffness for typical fill and geotextile properties [20]. So, for the tests performed by Douglas and Kelly [20] it was likely that most of the bearing capacity improvement was due to interfacial shear stress support (effect 2) and the membrane induced reduction of applied shear stresses on the surface of the cohesive subgrade (effect 3). Moreover, the only tests that gave some differences in performance were those obtained using a polyethylene film separator. This type of material is likely to have smaller interface friction than woven and nonwoven materials and therefore, a difference in performance should be expected.

Similarly, Bakker [21] discussed the reinforcement of embankments and gravel roads and presented a model for the calculation of the bearing capacity of the subsoil underneath a layer of aggregate and geotextile. The bearing capacity equation was modified to take into account a geotextile. The friction at the geotextile-aggregate interface and at the geotextile-subsoil was neglected. Based on the modified bearing capacity equation and the geometry of the deformed subgrade, a relationship between the modulus of elasticity of the geotextile and the rut-depth for a set of given soil properties was calculated.

Espinoza and Bray [15] Bearing Capacity Equation

1. The expression for average membrane support (Eq. 2.52) was developed earlier by Espinoza [14]:

$$q_{avg} = \frac{\int_{-\frac{L}{2}}^{\frac{L}{2}} q_g(x) dx}{L} = \frac{1}{L} \int_{-\frac{L}{2}}^{\frac{L}{2}} T_h(x) \frac{d^2 y(x)}{dx^2} dx \quad (2.58)$$

This expression satisfies vertical and horizontal force equilibrium at the global level.

2. Derivation of an expression for the subgrade bearing capacity, \bar{q}_s , where the geotextile outside of the effective length (i.e. AB and DE in Fig. 2.7) exerts a vertical stress, \bar{q}_{lat} , due to membrane support, reducing the heave of the subgrade soil.

$$\bar{q}_s = cN_c + \gamma h + \bar{q}_{lat} \quad (2.59)$$

$$\bar{q}_{lat} = \frac{1}{L} \int_{-\frac{L}{2}}^{\frac{L}{2}} q_g(x) dx \quad (2.60)$$

$$N_c = 1 + \frac{\pi}{2} + a + \sin a \quad (2.61)$$

where $a = \cos^{-1} \left(\frac{\tau_c}{c_u} \right)$

τ_c = shear applied to the soft soil surface

c_u = undrained shear strength

N_c = bearing capacity factor

h = granular fill thickness

γ = aggregate unit weight

L_c = length of geotextile preventing heave

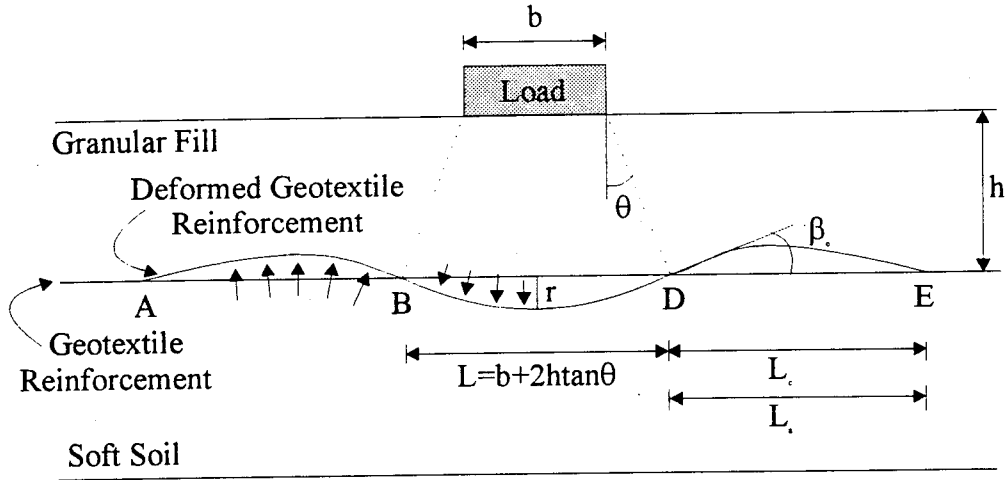


Figure 2.7: Geometry of deformed geotextile

3. An expression for the stress applied to the geotextile, \bar{q}_{ap} , can be developed by looking at the vertical stress within the aggregate layer, $\sigma_v(z)$:

$$\sigma_v(z) = \gamma z + \frac{pb}{b + 2z \tan \theta} \quad (2.62)$$

According to Eq. 2.62, the pressure applied to the geotextile can be expressed as:

$$\bar{q}_{ap} = \gamma h + a_b p \quad (2.63)$$

where $a_b = b/L$

$$L = b + 2h \tan \theta$$

4. By substituting Eq. 2.58, 2.59, and 2.63 into Eq. 2.46:

$$a_b = c_u N_c + \bar{q}_t \quad (2.64)$$

where \bar{q}_t = total membrane support, including both normal stress membrane support (effect 1) and interfacial shear stress support (effect 2).

$$\bar{q}_t = \frac{2}{L} \int_0^{\frac{L}{2}} q_g(x) dx + \frac{1}{L} \int_{\frac{L}{2}}^{L_c + \frac{L}{2}} q_g(x) dx \quad (2.65)$$

5. The shear stress along the interface, τ_x , equals $-\frac{dT_h}{dx}$. The extreme points A and E (Fig. 2.7) were chosen such that the geotextile is horizontal (i.e. $y'(L_c + L/2) = 0$). Assuming the shear stress, τ_x , is constant along BD, Eq. 2.65 becomes:

$$\bar{q}_t = \frac{1}{L} \left[T_o \sin \beta_o + 2 \int_{y(0)}^{y(\frac{L}{2})} \tau(x) dy \right] \quad (2.66)$$

$$\text{for } T_o \leq \min(\gamma h L_a \tan \psi, T_{\max}) \text{ and } \tau(x) \leq q_{ap} \tan \psi \quad (2.67)$$

where T_o = geotextile tensile force

β_o = angle of inclination at point D (Fig. 2.7)

ψ = interface friction angle

L_a = geotextile anchorage length

T_{\max} = geotextile maximum tension

Note: Eq. 2.66 allows for slip to be taken into consideration when the upper limits set by Eq. 2.67 are exceeded. The first term in Eq. 2.67 represents the membrane contribution obtained from outside the effective length (normal stress membrane support, effect 1) and depends on proper anchorage outside the effective length. The second term in Eq. 2.67 represents the interfacial shear stress support (effect 2) within the effective length and depends upon the applied load and the mobilized interface friction.

6. From limit equilibrium with a Mohr-Coulomb failure criterion, the shear stress along the effective length can be estimated as

$$\tau(x) = \bar{q}_{ap} \tan \psi_m = (\gamma h + \alpha_b p) \tan \psi_m \quad (2.68)$$

where ψ_m = mobilized interface friction angle

7. Assuming that ψ_m is constant along L , Eq. 2.67 reduces to

$$\bar{q}_t = \frac{1}{L} \left[T_o \sin \beta_o + 2r(\gamma h + \alpha_b p) \tan \psi_m \right] \quad (2.69)$$

where r = rut depth

8. Substituting Eq. 2.69 into Eq. 2.64, an expression for the admissible surface stress, p_{adm} , can be estimated:

$$P_{adm} = \frac{(c_u N_c + T_o \sin \beta_o / L + 2a_r \gamma h \tan \psi_m)}{a_b (1 - 2a_r \tan \psi_m)} \quad (2.70)$$

where $a_r = \alpha_r$ (from earlier) = r/L = rutting factor

Note: In many practical situations, proper anchorage cannot be ensured at all times. In such cases, $T_o = 0$ should be used to estimate the admissible stress. Even in cases where proper anchorage is provided, its effect will not be felt until large deformations are induced.

9. Using Eq. 2.62 to represent the vertical stresses and assuming that the horizontal stresses are proportional to the vertical stress ($\sigma_h = K\sigma_v$), the following derived expression can be used to compute the total horizontal force exerted on face HC in Fig. 2.8:

$$P_{HC} = \int_0^h \sigma_h dz = K \left(\frac{\gamma h^2}{2} + \frac{\eta p b}{2} \right) \quad \eta = \begin{cases} \ln(L/b) / \tan \theta & \theta \neq 0 \\ 2h/b & \theta = 0 \end{cases} \quad (2.71a)$$

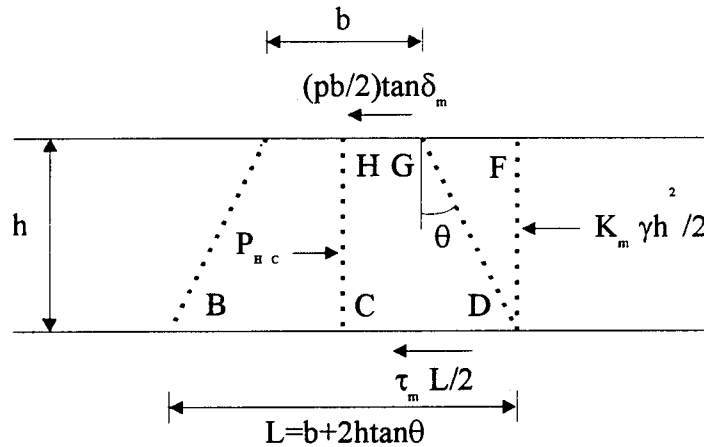


Figure 2.8: Load distribution through aggregate

10. Assuming that the applied load pushes the fill outward (Fig. 2.8), a passive pressure is developed on face DF. The corresponding force is computed as

$$\gamma K_{pm} h^2 / 2 \quad (2.71b)$$

where K_{pm} = the passive earth pressure coefficient

$$K_{pm} = \tan^2(\pi/4 + \phi_m/2)$$

ϕ_m = the soil friction angle

Allowing for friction force $(pb/2)\tan\delta_m$ on the footing base, where δ_m is the mobilized interface friction angle, the horizontal force equilibrium of the block CDFH yields:

$$\left(\gamma h + \frac{pb}{L}\right) \tan \psi_m \frac{L}{2} + \frac{1}{2} K_{pm} \gamma h^2 + \frac{pb}{2} \tan \delta_m = K \left[\frac{1}{2} \gamma h^2 + \eta \frac{pb}{2} \right] \quad (2.72)$$

Solving Eq. 2.72 for the interface mobilized friction, ψ_m gives

$$\tan \psi_m = \frac{\left[a_h (K - K_{pm}) + \frac{pb}{\gamma h L} (\eta K - \tan \delta_m) \right]}{\left(1 + \frac{pb}{\gamma h L} \right)} \quad (2.73)$$

where $a_h = h/L$ = dimensionless parameter

11. The mobilized friction angle on the base of the footing, δ_m , is expected to be quite small even for rough footings and, thus, it can be omitted from Eq. 2.73. Assuming that the fill tends to move outward from beneath the footing, the value of K in equation (2.71a) can be assumed to be equal to the active earth pressure coefficient (i.e. $K_{am} = \tan^2(\pi/4 - \phi/2)$). Replacing p in Eq. 2.73 with p_{adm} from 2.70, an expression of the mobilized interface friction, ψ_m , is

$$\tan \psi_m = \frac{\left[a_h (K - K_{pm}) + M_c (\eta K - \tan \delta_m) \right]}{\left(1 + M_c + 2a_r \left(a_h (K - K_{pm}) - \eta K + \tan \delta_m \right) \right)} \quad (2.74)$$

$$M_c = \frac{c_u N_c + T_o \sin \beta_o / L}{\gamma h} \quad (2.75)$$

Note: Eq. 2.72 and 2.74 have been derived based on equilibrium between the membrane and the sliding block above it, and are only valid for the situation shown in Fig. 2.8. The reinforcement should be checked for tension failure:

$$\frac{q_{ap} L \tan \psi_m}{2} < T_u \quad (2.76)$$

2.2.3 Factors Affecting Reinforced Unpaved Roads

Many factors affect how a geotextile performs in an SFA system:

- fabric stiffness
- fabric creep
- fabric location (placement somewhere other than the interface)
- fabric anchorage
- fabric texture
- aggregate type and shape
- subgrade and interface properties

The performance of an SFA system is greatly affected by so-called interface friction, which can be seen as a function of many of the above listed factors, including fabric stiffness and texture, aggregate type and geometry, and the subgrade properties. However, the interface properties are often expressed as a relationship between the aggregate and geotextile in reference to how the load is transferred. The information presented in this section pertains to research that has been performed to look specifically at one or more factors affecting the performance of an SFA system.

The effects of fabric stiffness, texture, creep, and location have been investigated. Some of the findings of the research pertaining to these issues are included in the following sections. The effects of fabric texture and aggregate type and shape on the interface friction properties and the overall effect of interface friction properties on the performance of the SFA system have not been closely examined. Subgrade properties are important to the performance of the SFA system; for example, for subgrades stronger than 90 kPa ($\text{CBR} > 3$), geotextiles are generally not required for reinforcement in unpaved roads, although geotextiles may provide other functions.

A small displacement finite element program was used by Burd and Brocklehurst [12] to investigate the reinforcement mechanisms in a geotextile reinforced unpaved road where large rutting *is not* permitted. The geotextile stiffness was varied. Results of the modeling showed that fabric stiffness has a modest effect on the load-deformation response of the road, but a substantial effect on the magnitude and nature of the shear stresses acting at the reinforcement-soil interface.

Work performed by and Milligan et al. [5] involved looking at the horizontal stresses that develop in the fill layer due to a vertical load. These horizontal stresses were found to generate shear stresses at the base of the fill layer. If reinforcement was absent, then these shear stresses

were sustained directly by the subgrade and in some instances were found to have a detrimental effect on the subgrade's bearing capacity. In the reinforced case, the shear stresses were sustained by the reinforcement. The presence of the reinforcement caused a reduction in the outward acting shear stresses on the surface of the subgrade and increased the bearing capacity of the subgrade.

Finite element studies of Zeevaert [23], Burd [24], and Burd and Houlsby [25] were based on calculations in which the only parameter that was varied was the reinforcement stiffness. It was assumed that *no slip* occurred at the soil/reinforcement interface. From these studies, it was clear that the reinforcement stiffness had little effect on the initial slope of the load-displacement response. But, in each case an approximate limit load was reached that increased with an increasing value of reinforcement stiffness (increased at most by 15%). It was shown that for each value of reinforcement stiffness, the shear stresses at the base of the fill reached a peak at a distance of about $0.7B$ from the footing centerline, where B is the footing width. As the reinforcement stiffness increased the magnitude of the shear stresses also increased. The shear stresses applied to the surface of the clay immediately beneath the reinforcement followed a similar pattern to the shear stresses at the fill base. Outward shear stresses were found to act underneath the footing and reached a peak value at a distance of about $0.7B$ from the footing centerline. The outward shear stresses decayed to zero at about $2.5B$ from the footing centerline. For the stiffest reinforcement, the direction of the shear stresses reversed and acted inwards. Lateral movement of the clay was thought to be restrained by the reinforcement.

The presence of outward shear stresses can reduce a soil's bearing capacity to as little as one-half of the value for purely vertical loading. If reinforcement is introduced, these shear stresses are picked up by the reinforcement, which is put into tension, and purely vertical forces are transmitted to the clay below, allowing the capacity of the clay to be realized. This helps explain why reinforcement is able to provide an improvement in road performance even at small rut depths.

The problem of soft subgrades, extremely heavy design axle loads, very low traffic volumes, and very low cost tolerances associated with access roads have led engineers to adopt designs using geotextiles. A number of design methods have been put forward, where the basis of

the method is the relationship between rut depth, traffic and geosynthetic characteristics. Douglas and Valsangkar [26] pointed out that overall transportation costs and efficiencies are linked to the relationship between roads and vehicles. Because of the impact that road stiffness has on fuel consumption and therefore vehicle operating costs, it was stated that stiffness rather than permanent rut depth should be adopted as the key design criterion for access roads. The range of road stiffness to be expected and how it is affected by geotextile inclusions was investigated by cycled-load testing of a large-scale model of a permanent structure consisting of different granular bases with various geotextiles placed on a peat subgrade. Surprisingly, the improvement in the stiffness of the model pavement over that for the subgrade itself was not great.

The scope of Douglas' test program included an investigation of the possible variation in pavement stiffness with cycled loading and a simulation of the low-frequency load cycling appropriate to slow-speed travel of heavy vehicles on low-volume roads. The tests were carried out in a 3 m x 4 m x 2 m pit with the loads applied through a 300 mm diameter plate. The loads were cycled at a frequency of 0.5 Hz, corresponding to a steady stream of axles spaced at 4 m, traveling at about 7 km/h. The subgrade CBR was much less than one; the gravel was a pit run gravel and crushed greywacke. Two geotextiles were used: a nonwoven geotextile at the interface in all cases and in some cases a geogrid was placed at the mid-depth of the gravel base. Sinusoidal loading was applied with peak to trough loads of 4.5 kN (1012 lb) and 0.1 kN (22.5 lb). The test ran up to 30,000 cycles and it was shown that the stiffness continued to gradually increase with cycled loading. The stiffness for a compacted, crushed rock model road with a depth ratio $H/D=0.5$ and a geogrid inclusion at the mid-depth, was approximately 3.6 times that of the peat subgrade itself for the same number of cycles at a peak stress of 62 kPa (9 psi).

Fatigue tests were performed using an SFA system and a soil-aggregate system [20]. The reinforcement was placed at the base-subgrade interface and in other cases at both the interface and the base mid-depth. The lateral anchorage was also varied between a long lateral anchorage (7.0 m geotextile width) and a short lateral anchorage (4.5 m geotextile width). The clay subgrade had an undrained shear strength of between 30 and 50 kPa (0.3 and 0.5 tsf). The subbase used was a crushed limestone with zero cohesion and a friction angle of 47°. Four types of geotextiles were used: Bidim[®] U 24, Bidim[®] U 34, Scotlay[®] (100 g) and the Scotlay[®] (200 g).

The loading system consisted of a truck with an axle weight of 130 kN (29,000 lb) moving at 20 km/hr (12.5 miles/hr).

The rut evolution confirmed the following. (1) Rutting was less for the stiffer geotextile. (2) Anchorage of 7 m resulted in better conditions than an anchorage of 4.5 m. (3) The use of two geotextiles, one at the interface the other at the base mid-depth, provided better behavior than the use of one geotextile for unpaved roads with small strains.

2.3 Separation in Unpaved Roads

There are many factors that affect the amount of pumping at the gravel-subgrade interface of unpaved roads. These factors include the number of cycles, mean stress, stress amplitude, standing water, frequency, aggregate thickness, over-consolidation ratio, confining pressure, and size of gravel particles. A laboratory assessment of the ability of fabrics to prevent soil migration under conditions of dynamic loading was performed by Hoare [28].

The effects of varying the volume of water used to simulate the effects of the ponded water on the subgrade surface seemed to have little effect on the amount of subgrade contamination in the gravel (soil contamination value, SCV), provided there was sufficient moisture available for the soil. The SCV was found to increase linearly with the logarithm of the number of applied cycles. The soil was found to migrate through the fabric at points where the gravel particles were in contact with the subgrade. The moisture content of the soil at the points of contact with a gravel particle increased to a value close to its liquid limit. This was thought to possibly be a result of soil suction and local shearing caused by the high stresses at the contact points. The phenomenon of clay pumping was thought to be caused by the wet (and hence soft) soil on the surface of the subgrade squeezing through the fabric.

The SCV may be reduced by decreasing the stresses at the contact points of the gravel particles on the subgrade. This may be achieved by either reducing the applied stress levels or by using a gravel with a finer grading or higher fines content, which will increase the number of contact points and hence reduce the stresses at each point of contact. The SCV was found to be

insignificantly reduced by the use of a heavier needle-punched fabric rather than a light melt-bonded fabric.

Alobaidi and Hoare [29] performed a laboratory investigation into the factors that have an important influence on the pumping phenomenon in an SFA system. One specific subgrade soil and geotextile were chosen for the tests. Alobaidi and Hoare [29] found that the amount of pumping was directly related to the cyclic deformation of the system and it suggested that this finding would be of great significance in the design and development of materials to minimize pumping.

Tests showed that the rate of pumping could be determined from the rate of permanent deformation. Tests also indicated that the rate of pumping decreased with the number of cycles. Factors that may have caused this decrease in the pumping rate included the formation of a self-induced filter at the back of the geotextile, decreased contact stress, clogging of the geotextile, and increased viscosity of the slurry. Tests were performed where the stress amplitude remained constant and the mean stress was varied. Results showed that the increase in mean stress led to a decrease in cyclic deformation.

Tests also showed that an increase in the stress amplitude led to (1) an increase in the rate of permanent deformation, (2) an increase in the cyclic deformation of the system, and (3) a consequent rise in the amount of pumping at every stage in the pumping test. The amount of pumped fines increased with the amount of standing water on top of the subgrade. The effect of frequency was more pronounced in the series with the greater amount of standing water. The ELT (equivalent loss of thickness from the subgrade surface) due to pumping was affected to a large extent by the concentration of fines in the standing water. The cyclic history seemed to have no effect on the ELT (this conclusion must be restricted to the particular materials used in this test). The ELT decreased significantly with increase of the over-consolidation ratio. Finally, the permanent deformation of the system decreased with an increase in the confining pressure during all stages of a pumping test and the amount of pumped fines was less for small-size particles.

Bell et al. [30] found that subbase clay pumping in model tests under dynamic cyclic loading was dependent mainly on stress level, soil moisture content, and clay content of the subgrade soil. Geotextiles with effective opening sizes of less than 100 μm reduced clay pumping

significantly when used as separating membranes between the clay subgrade and stone subbase. The mechanism of clay pumping was found to arise mainly from slurry filled depressions formed by stone penetration into the clay subgrade surface. The thick geotextiles were most successful in reducing clay pumping over a wide range of moisture contents and soils. The cushioning effect of the geotextiles thickness seemed to reduce stone point penetration into the subgrade. Slurry penetration through the fabric was found to only occur between the stone-point depressions, where the fabric was relatively uncompressed. The thin geotextiles were found to not perform as well as the thicker geotextiles in reducing clay pumping. However, all the geotextiles tested performed a useful separating function in reducing the stone penetration down into the soft clay subgrades and in preventing the plastic flow of the clay up into the stone interstices. Subbase contamination and geotextile clogging were found to be related to the ratio between the geotextile equivalent opening size, O_{95} , and the subgrade particle size, D_{85} .

Lafleur and Rollin [31] noted that geotextiles must satisfy two criteria. The first relates to its punching resistance: it must be able to contain the individual coarse particles without tearing, in the range of the applied stresses. The second criterion bears on its filtering capacity: it must be able to prevent fine subgrade particles from migrating upward into the subbase. Under dynamic stresses, the filtering conditions are more severe since alternating flow can take place at the subgrade-geotextile interface, preventing the development of self-filtration and arching of the particles.

Nishida and Nishigata [32] investigated the relationship between the reinforcement and separation functions in road construction. A distinct relationship was found between the opening size of woven geotextiles and the total weight of the soil mass through the geotextile. However, for the nonwoven geotextiles, this relationship was unclear. The excess pore pressure in each case increased as the number of loadings increased. Separation was found to be the primary function when $\sigma/c_u < 8$ and reinforcement was the primary function when $\sigma/c_u > 8$, where σ is the vertical stress on the subgrade and c_u is the subgrade's undrained shear strength.

2.4 Case Studies

Austin and Coleman [33] presented the results of a full-scale field study conducted to evaluate the effectiveness of various geosynthetics as the primary reinforcement in aggregate layers placed over very soft subgrades. A test road containing several test sections was constructed. Each test section contained a different geosynthetic with three unreinforced sections as controls.

A two-axle dump truck was used with a rear axle of 80 kN (18,000 lb). The tires were inflated to 550 kPa (80 psi). The test road was cycled with traffic until a 75 mm (3 in.) rut occurred. This rut depth was considered failure. All failed sections exhibited similar characteristics of severe rutting with adjacent upheaval. Contamination of the subbase was apparent where geotextile separators were not used. The results of the field evaluation were compared with the theoretical design procedures proposed by Giroud et al. [34] and the results correlated fairly well. The number of axle load passes actually achieved for a given thickness of a geosynthetic-reinforced aggregate subbase over soft subgrade soils was less than the expected number of passes calculated. It was believed that the difference was due to the fact that higher in-place aggregate strengths are assumed in the theoretical design procedure than those actually achieved during the construction of haul roads.

The long-term separation and drainage performance of 22 geotextile separators installed between 1978 and 1991 and exhumed from permanent roadways in Washington state was evaluated [35]. The geotextiles exhumed consisted of heat-bonded nonwovens, needle-punched nonwovens, and woven slit films. The exhumed geotextile pieces showed that the short-term separation and drainage functions were more critical to the pavement system than their long-term performance, due to consolidation and subsequent strength gain of the subgrade soils. It also appeared that geotextile retention might not be as critical in separation applications as previously thought.

Several of the sites had very soft subgrades upon installation of the geotextile. However, upon exhuming the geotextiles, the subgrade was found to be consolidated and strong with no free water, where if today the subgrade were being built on, no geotextile would be necessary; the soil was fully competent. It was noted that even if the geotextile separators become somewhat

blinded or clogged in the short-term but were still capable of separating materials and dissipating excess pore pressures until the subgrade consolidated, there was little need for a functioning separator for the remainder of the roadway design life.

The primary purpose of the geotextile separator is to prevent mixing of aggregate and subgrade materials. However, in order for the geotextile to be an effective separator during the life of the pavement system, it is generally recognized that the geotextile must also provide secondary functions of filtration and drainage at the soil/geotextile interface. A geotextile can prevent migration, but it can be adversely affected by soil particles blocking and clogging/caking pore openings.

Page [36] reported on eight sites that involved exhuming geotextiles from existing roadways. It was noted that the required strength needed to maintain separation over the design life of a project was relatively small compared to the strength required to resist damage during construction. Of the eight sites chosen for the investigation, five were considered useful for further study. Four sites utilized a woven slit film material with mass per area of approximately 135 g/m^2 (4 oz/yd^2) and one site utilized a nonwoven needle punched material with a mass per area of 180 g/m^2 (5.3 oz/yd^2). Minor puncture damage was found at all locations. This damage, however, did not seem to affect the geotextile's performance as a separator. Grain size distributions were determined for the base material at different heights above the geotextiles, showing slightly higher fines content directly above the geotextile. Index strength tests were performed on the exhumed geotextile and indicated that all the geotextiles appeared to have survived reasonably well with an average percent of strength retained for the grab tensile test, trapezoidal tear test, puncture test and burst test between 72-99%.

It was pointed out that the increase in the amount of fines in the base course was so small in all cases that it was hard to say with certainty that the fines migrated up from the subgrade. Blinding was observed in varying degrees, with the worst blinding observed in the woven slit film. It was apparent from the tests performed that, for the woven slit film geotextiles, only a small amount of contamination of the material by fine-grained soil particles was required to cause a significant drop in permittivity.

Slit film woven geotextiles would be adequate for separation applications over most subgrade soils. However, they tend to become blinded more readily than the nonwovens when used over clayey-slit subgrades. The use of a heavier geotextile with large grab elongation would help to minimize the damage during installation. Lightweight (120 g/m^2) nonwoven geotextiles should not be used for any separation application regardless of the subgrade type or initial base course lift thickness. Puncture holes were present in many of the woven slit film geotextiles, where gravel-sized particles were present on the subgrade surface. The use of a heavier geotextile (270 g/m^2), which meets the high survivability strength criteria and has a high grab elongation, would help to minimize damage during installation. However, the heavier geotextiles are more expensive and there was no evidence from this study that the presence of moderate construction damage to the geotextile separator significantly affected the performance of the roadway.

2.5 Summary

A summary table has been prepared from the literature review of geotextiles for reinforcement and separation in unpaved roads. Included in the summary table are condensed procedures, key findings, and assumptions.

Table 2.1: Summary of literature review findings

Author(s) and Reference Number	Overview of Work and Findings	Key Assumptions
Barenberg [1]	<ul style="list-style-type: none"> • Developed reinforced unpaved road design criteria • Found geotextile properties have a significant effect on behavior of SFA system—specifically, the geotextile modulus • Permissible values for allowable subgrade stress were found to be: <i>with geotextile:</i> $\sigma = 6c_u$ <i>without geotextile:</i> $\sigma = 3.2c_u$ 	<ul style="list-style-type: none"> • Deflected shape of geotextile was a circular arc • No slip
Kinney [2]	<ul style="list-style-type: none"> • Developed the fabric tension model (FTM) • Included methods for determining geotextile shear and normal stresses and geotextile strain energy • FTM was basis for Barenberg's (1980) revised SFA design procedure 	<ul style="list-style-type: none"> • No slip

Author(s) and Reference Number	Overview of Work and Findings	Key Assumptions
<p>Barenberg [3]</p>	<p>Developed procedure using Kinney's (1979) FTM <i>Procedure:</i></p> <ol style="list-style-type: none"> 1. $\sigma_{all} = 3.2 A c_u$ $A = 1.0-2.0$ 2. Estimate gravel thickness 3. Establish rut geometry: depth, d, chosen width, W: $W=B+2X$ B = gravel rut width X = spreading effect 4. Geotextile strain: $\epsilon_f = \left(\frac{4\pi R\theta}{135W} - 2 \right) \times 100\%$ $R = \frac{3}{8} \frac{W}{\sin \theta}, \theta = 2 \tan^{-1} \left(\frac{5}{3} \frac{d}{W} \right)$ 5. Fabric tension, t_f: $t_f = K \epsilon_f$ 6. Differential stress across fabric, $\Delta\sigma_{z-f}$: $\Delta\sigma_{z-f} = t_f / R$ 7. Permissible stress on fabric: $\sigma_{p-f} = \Delta\sigma_{z-f} + 3.2 A c_u$ 8. Using Boussinesq equation, calculate vertical stress on fabric and check to see if less than permissible. 	<ul style="list-style-type: none"> • Developed for Mirafi[®] 140 and 500X • Deflected shape of geotextile was a circular arc • No slip

Author(s) and Reference Number	Overview of Work and Findings	Key Assumptions
Bell et al. [30]	<ul style="list-style-type: none"> • Performed laboratory tests to investigate subbase contamination • Found relatively thick geotextiles with small pore sizes to be effective in limiting contamination • High pore water pressure dissipation rates were associated with high contamination and low dissipation rates with low contamination • Nonwoven geotextiles found to be ineffective in preventing clayey fines contamination but more successful in preventing subbase penetration • Geotextiles with effective opening sizes less than 100 mm reduced clay pumping significantly • Cushioning effect of thick geotextiles reduced stone penetration into soil • All geotextiles tested performed a useful separation function 	<ul style="list-style-type: none"> • Separation function only
Giroud and Noiray [4]	<ul style="list-style-type: none"> • Developed an equation to determine the required aggregate layer thickness, h, as a function of loading, subgrade undrained shear strength, and geotextile properties. <p><i>Analytic expression:</i></p> $(\pi + 2)c_u = \frac{P}{2(B + 2h \tan \alpha)(L + 2h \tan \alpha)} + \frac{K\varepsilon}{a \sqrt{1 + \left(\frac{a}{2s}\right)^2}}$	<ul style="list-style-type: none"> • No slip of geotextile relative to aggregate and subgrade • <10,000 cycles • Aggregate CBR of 80 • Purely cohesive subgrade soils • Membrane action

Author(s) and Reference Number	Overview of Work and Findings	Key Assumptions
Hoare [28]	<ul style="list-style-type: none"> • Performed lab tests to investigate subgrade pumping • Used soil contamination value, SCV (weight of subgrade soil passing the fabric per unit area of fabric) to measure pumping • Soil found to migrate through fabric at contact points between subbase and subgrade • SCV found to be insignificantly reduced by the use of a heavier needle-punched fabric rather than a light melt-bonded fabric 	<ul style="list-style-type: none"> • Separation function only
Haliburton and Barron [11]	<ul style="list-style-type: none"> • Investigated effect of fabric location on SFA performance • Optimum placement depth found to be 1/3 the width of the loaded area • At large deformations, membrane support (even for high modulus fabrics) was small compared to total load capacity • Separation seen as allowing pore pressure dissipation and consolidation 	<ul style="list-style-type: none"> • Observations from field and lab tests
Douglas and Kelly [20]	<ul style="list-style-type: none"> • Performed fatigue tests on SFA systems • Rutting found to be less for stiffer geotextiles • More anchorage resulted in better conditions • Use of two geotextiles-one at the interface the other at the base middepth-performed better than one geotextile at interface 	<ul style="list-style-type: none"> • Based on performance tests

Author(s) and Reference Number	Overview of Work and Findings	Key Assumptions
Page [36]	<ul style="list-style-type: none"> Reported on 8 sites where geotextiles were exhumed Worst blinding was observed in the woven slit films It was recommended that lightweight (3.5 oz/yd²) nonwoven geotextiles not be used for separation 	<ul style="list-style-type: none"> Findings based on tests and observations
Espinoza [14]	<ul style="list-style-type: none"> Developed an expression for evaluating the increase in bearing capacity due to membrane action. Allowable applied stress, q_{ap}: $q_{ap} = q_s + q_{avg}$ $q_s = \text{soil reaction}$ $q_{avg} = \text{additional capacity due to geotextile}$ $q_{avg} = \frac{2E}{L} \varepsilon \ln(\tan \beta_o + \sqrt{1 + \tan^2 \beta_o})$ <p><i>Parabolic Deformation:</i></p> $\varepsilon = \frac{1}{2} \left[\sec \beta_o + \frac{\ln(\tan \beta_o + \sec \beta_o)}{\tan \beta_o} \right]$ <p><i>Circular Deformation:</i></p> $\varepsilon = \frac{1 + (2\alpha)^2}{4\alpha} \tan^{-1} \beta_o - 1$ 	<ul style="list-style-type: none"> No slip $\tau_{lower} = 0, \tau_{upper} = \tau$ Constant strain
Nishida and Nishigata [32]	<ul style="list-style-type: none"> Investigated relationship between reinforcement and separation in geotextile reinforced unpaved roads Separation found to be primary function when $\sigma/c_u < 8$ and reinforcement found to be primary function when $\sigma/c_u > 8$ σ = vertical stress on subgrade c_u = subgrade undrained shear strength 	<ul style="list-style-type: none"> Results not applicable to nonwovens

Author(s) and Reference Number	Overview of Work and Findings	Key Assumptions
Espinoza and Bray [15]	<ul style="list-style-type: none"> • Developed procedure for evaluating the load capacity of reinforced soils • Analysis incorporated two important membrane support contributions: normal stress and interfacial shear stress support • An expression for admissible surface stress, p_{adm}, was developed based on a modified bearing capacity equation $p_{adm} = \frac{(c_u N_c + T_o \sin \beta_o / L + 2a_r \eta \tan \psi_m)}{a_b (1 - 2a_r \tan \psi_m)}$ <p>where:</p> $\tan \psi_m = \frac{[a_h (K - K_{zm}) + M_c (\eta K - \tan \delta_m)]}{(1 + M_c + 2a_r (a_h (K - K_{zm}) - \eta K + \tan \delta_m))}$	<ul style="list-style-type: none"> • Slip considered
Metcalfe et al. [35]	<ul style="list-style-type: none"> • Investigated the performance of 22 geotextile separators installed between 1978 and 1991 • Short-term separation and drainage functions were found to be more critical than their long-term performance due to subgrade strength gain due to consolidation • Subgrades of excavated sites found to be consolidated and strong • Even if geotextiles became blinded or clogged in short-term still able to perform while subgrade consolidated • Found to be little need for long-term separation 	<ul style="list-style-type: none"> • Separation function only

Chapter 3

Direct Shear Tests

It has been widely recognized and accepted that interface friction is a very important parameter in designing geotextile reinforced unpaved roads. Shear stress, τ_r , develops at the base of a gravel layer under a wheel load (Fig. 3.1). Due to this shear stress, the interface friction of the soil-fabric-aggregate (SFA) system becomes a critical design parameter.

Assuming similar stiffness characteristics, it is anticipated that larger interface friction will be associated with better performance, as the shear stress applied to the subgrade may be reduced if slip does not take place. To quantify interface friction and deformation behavior, 18 direct shear tests were performed on SFA systems. Three types of geotextiles were used: a lightweight slit film, heavyweight woven, and a nonwoven. The soil was a clay material with a plasticity index of 11, liquid limit of 34, and plastic limit of 23. The aggregate was a crushed gravel material with a significant amount of fines and a diameter at 85% passing of 19 mm (0.75 in.). For each normal load used, the test was performed twice, once with the geotextile attached to the top box (clay sliding relative to the geotextile), the other with it attached to the bottom box (gravel sliding relative to the geotextile).

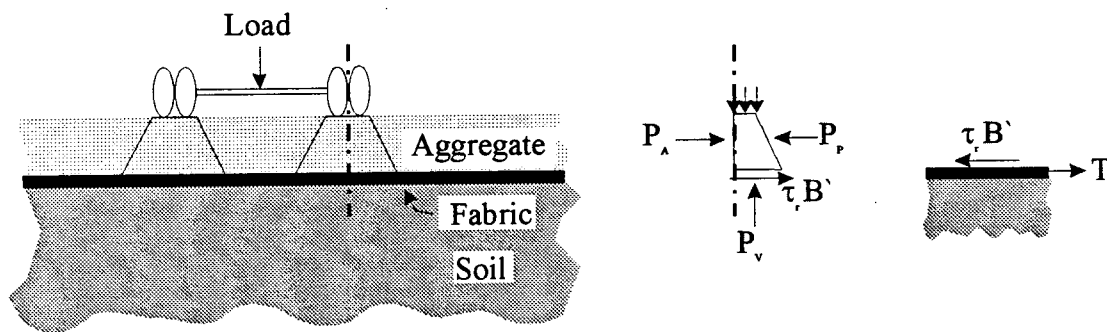


Figure 3.1: Section of reinforced unpaved road

3.1 Apparatus and Setup

3.1.1 Apparatus Description

The large-scale direct shear tests were performed using a Brainard-Kilman™ LG-113 direct shear machine (Fig. 3.2). The top box dimensions were 305 x 305 x 102 mm deep (12 x 12 x 4 in.). The bottom box dimensions were 406 x 305 x 102 mm deep (16 x 12 x 4 in.) allowing for a maximum of 102 mm (4 in.) of travel by the lower box. The overall dimensions of the machine were 965 x 609 x 660 mm (38 x 24 x 26 in.) weighing 272 kg (600 lb). The bottom box could move at a rate varying from 0.127-6.35 mm/min (0.0001-0.20 in./min).

The direct shear machine generated normal load through a bladder connected to an air pressure line. Pressure within the bladder produced movement of a piston and loaded the 19 mm (0.75 in.) thick rigid load platen (Fig. 3.2). The maximum normal load and corresponding pressure the bladder could provide was 45 kN (10,000 lbf) and 689 Pa (100 psi) with a maximum shear force of 45 kN (10,000 lbf).

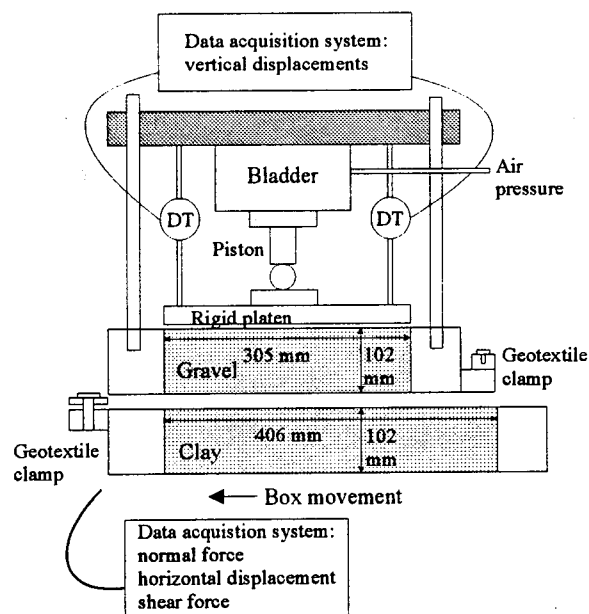


Figure 3.2: Direct shear box

3.1.2 Apparatus Setup

The direct shear machine was placed on a firm surface and leveled by adjusting feet attached to the base of the machine. The gap between the top and bottom box was set at 19 mm (0.75 in.). This gap was set according to ASTM D 5321, which calls for the distance between the upper surface of the geosynthetic specimen and the lower surface of the upper box to be at least equal to the D_{85} of the upper soil.

A pressure line was connected directly to the bladder. The pressure in the line was monitored by a pressure gauge. The direct shear machine digital readout provided corresponding load values. Before conducting any tests, the bladder loading system was calibrated (Fig. 3.3). A linear variable differential transformer and a load cell were attached to the bottom box to measure horizontal displacement and shear force.

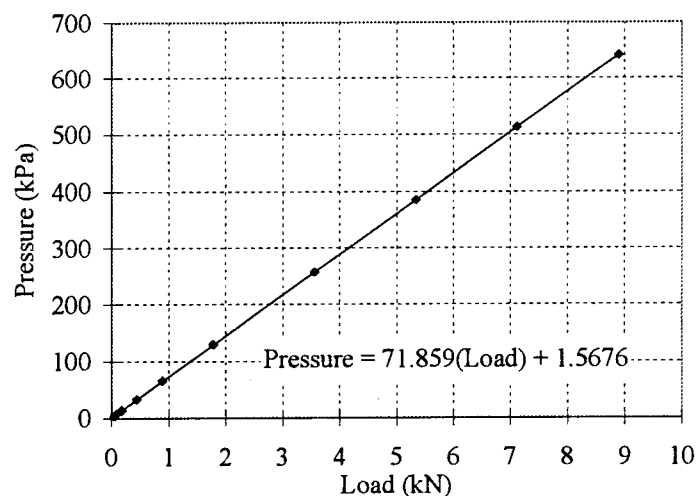


Figure 3.3: Bladder calibration curve

Vertical displacement of the rigid load platen was monitored during the tests by two displacement transducers (DT in Fig. 3.2) so as to record any volume change or rotation of the load platen during testing. Readings were recorded at a two second interval by a data acquisition system.

3.2 Test Materials and Test Setup

3.2.1 Test Materials

The bottom box was filled with a silty-clay subgrade material taken from Sibley County, Minnesota. The optimum moisture content, w_{opt} , was 20% (Fig. 3.4), with a maximum dry unit weight, γ_{dmax} , of 16.5 kN/m³ (105 pcf); the soil was classified according to AASHTO as A-6 (9). The plasticity index was 11, with a liquid limit of 34 and plastic limit of 23.

Class 5 gravel, according to the Minnesota Department of Transportation specifications, was placed in the top box. The crushed gravel contained a significant amount of fines (Fig. 3.5) and had a uniformity coefficient of 16 and coefficient of curvature of 0.24. The diameter of the gravel at 85% passing was 19 mm (0.75 in.) with a friction angle, found using the direct shear apparatus of about 42° (Fig. 3.6).

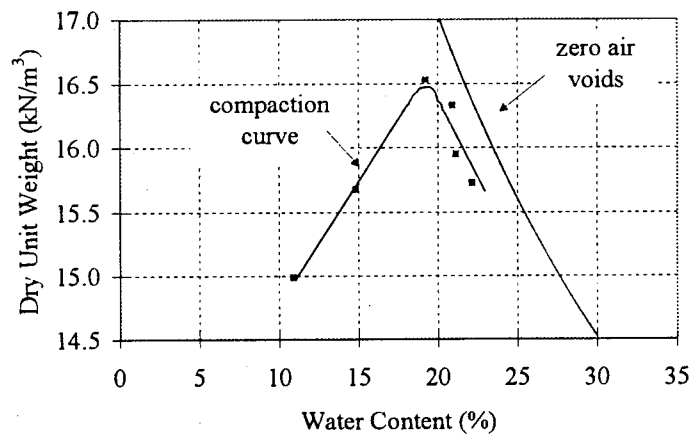


Figure 3.4: Silty-clay compaction curve

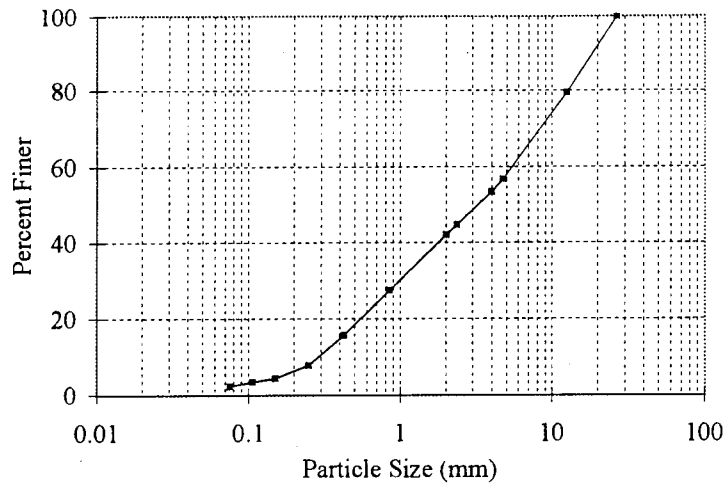


Figure 3.5: Gravel gradation curve

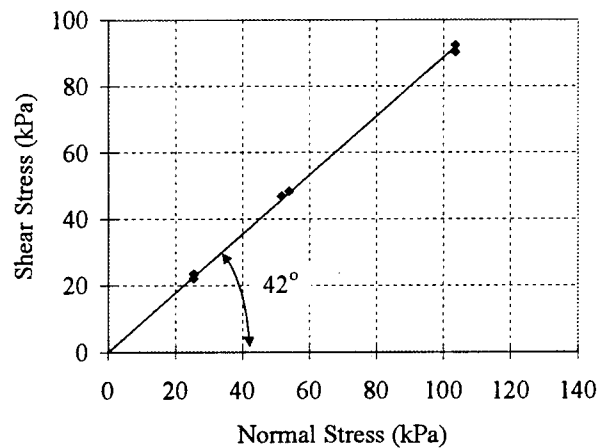


Figure 3.6: Results of gravel direct shear tests

A geotextile was placed on the subgrade material at the interface of the direct shear box. By either clamping the geotextile to the top or bottom box, the material in the top box or bottom box moved relative to the geotextile. To examine the potential effects of the clamping configuration on test results, all tests were performed twice: first with the silty-clay sliding relative to the geotextile (geotextile clamped to the top box) and then with the gravel sliding relative to the geotextile (geotextile clamped to the bottom box) (Fig. 3.2).

Three different geotextiles were used: Synthetic Industries Inc. Geotex 200ST lightweight woven slit film, Amoco Fabrics & Fibers Co. 4553 nonwoven and 2016 heavyweight woven. All three fabrics are polypropylene based. Physical and mechanical properties of these fabrics can be found in Table 3.1.

Table 3.1: Physical and mechanical properties of the geotextiles

Properties \ Geotextile	lightweight slit film	heavyweight woven	nonwoven
mass (g/m ²)	150	270	340
apparent opening size ¹ (mm)	0.425	0.425	0.15
Permittivity ² (sec ⁻¹), flow rate (l/min/m ²)	0.07/240	0.55/1625	1.5/4470
puncture ³ (kN)	0.445	0.530	0.575
mullen burst ⁴ (kPa)	3100	5510	2750
trapezoid tearing ⁵ (kN)	0.330	0.53	0.355
grab tensile/elongation ⁶ (kN/%)	0.890/15	1.4/15	0.9/50
Notes: 1. ASTM D 4751, 2. ASTM D 4491, 3. ASTM D 4833, 4. ASTM D 3786 5. ASTM D 4533, 6. ASTM D 4632			

3.2.2 Test Setup

The normal stress that could be applied to the direct shear box was controlled by the maximum amount of pressure that could be generated through the line (about 690 kPa), which generated a normal stress of 103 kPa (15 psi). This maximum normal stress corresponded well with the normal stress applied to an unpaved road by a typical dual-wheel load. Since this value represented the high end of the normal stresses used for the direct shear tests, two other normal stresses were chosen for the tests by using three-quarters and one-half the maximum pressure, corresponding to a normal stress of 76 and 52 kPa (11 and 7.5 psi). By performing three direct shear tests, one at each normal stress, three different values for the shear stress at failure were obtained.

3.3 Test Matrix

3.3.1 Clay Placement

The weight of clay needed to fill the box at 95% of modified Proctor was determined knowing the volume of the bottom box. At 95% Proctor, $\gamma_d = 15.7 \text{ kN/m}^3$ (99.9 pcf). The volume of the bottom box was calculated to be 0.0125 m^3 (0.44 ft^3). Therefore, the weight of soil needed to fill the bottom box was 0.196 kN (44.0 lb) and 39.2 N (8.8 lb) of water was mixed with the dry soil to achieve a 20% moisture content.

The mixed clay was placed in two lifts. Each lift was compacted with 100 blows of a Marshall stability hammer. To aid in the compaction process, a wood frame was built to fit over the bottom box such that the inside walls of the box and frame were flush with respect to one another. The compacted clay specimen appeared to experience only minor surface scratching after each test. Due to the significant amount of work required to remove, remix, replace, and compact the clay specimen, only two clay specimens were used in the series of tests with the first being replaced when cracking/tearing appeared at the clay surface. Tests 1-12 were conducted using the first clay specimen, which had a moisture content of 23.5%. The second clay specimen had a moisture content of 23.6% and was used for tests 13-18 (Table 3.2).

3.3.2 Geotextile and Gravel Placement

The geotextile could either be clamped to the top or bottom box (Fig. 3.7). For each test a geotextile approximately 400 x 500 mm (16 x 20 in.) was used. One of the shorter ends of the geotextile was cut such that it would easily fit into the clamp (Fig. 3.8). For this series of tests it was decided to place the clay in the bottom box and the gravel in the top box. When the geotextile is clamped to the bottom box the gravel is sliding relative to the geotextile. It was decided to run all tests twice; once with the geotextile clamped to the top box and once with it attached to the bottom box. A new section of fabric was used for each test.

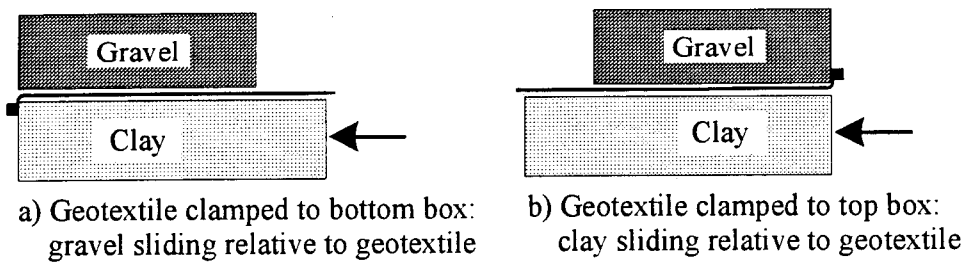


Figure 3.7: Geotextile clamping and sliding schematic

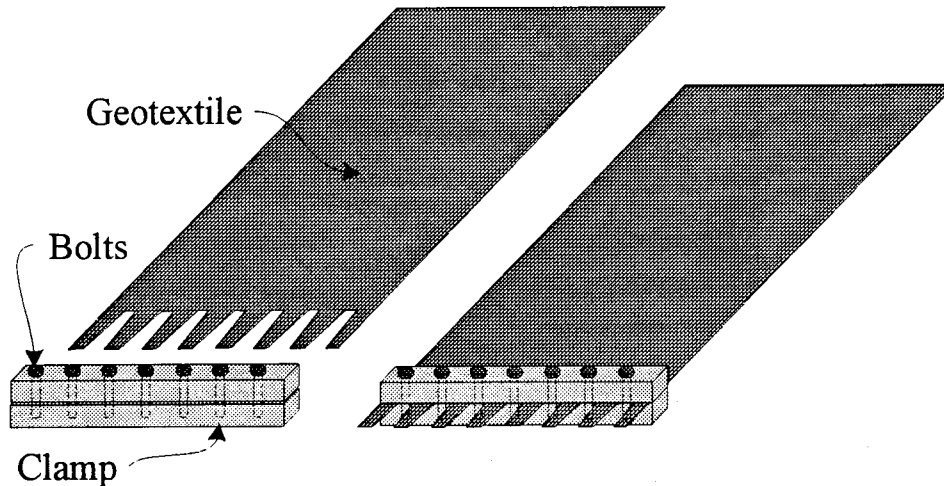


Figure 3.8: Geotextile clamping system on the direct shear machine (Fig. 3.2)

For the first test, the lightweight slit film geotextile was used. The geotextile was clamped to the top box causing the clay to slide relative to the geotextile. The top box was then placed in position, the geotextile was held taut and approximately 76 mm (3 in.) of gravel was placed in the top box. The gravel was placed using a small scoop to assure that the gravel stayed properly graded. Once the gravel was placed the surface was smoothed using a trowel and the 19 mm (0.75 in.) thick load platen was placed upon the gravel.

With the load platen in place, a distance of approximately 6.5 mm (0.25 in.) existed between the top of the rigid load platen and the top of the shear box. This allowed for corner measurements to be taken with a caliper to verify that the rigid platen was seated level relative to the shear box. Upon satisfactory seating of the load platen, the load cell was fastened by four bolts to the top box of the direct shear apparatus. The bolts were tightened and a level was used

to make sure that the plate attached to the top of the load cell was horizontal. The valve connecting the air hose to the bladder was closed and the air pressure increased to the required amount.

For the first test in each series, a normal stress of 52 kPa (7.5 psi) was used. Once the correct pressure was reached the valve was opened and the normal stress was applied to the direct shear box compressing the SFA system. When the vertical digital displacement transducers attached to the rigid load platen remained constant, the two data acquisition systems were activated and the direct shear apparatus was set for a shear displacement of 51 mm (2 in.) at a rate of 5 mm/min (0.2 in./min). A total displacement of 51 mm (2 in.) was chosen because practice tests indicated that the maximum shear stress was achieved at this displacement. The displacement rate of 5 mm/min. (0.2 in./min) was chosen simply because it was the fastest rate possible by the machine.

During the test the load platen was closely monitored to make sure that it stayed relatively horizontal. With the shearing motion of the bottom box, some gravel was lost through the 19 mm (0.75 in.) gap at the interface of the two boxes. The amount of loss was reduced by careful placement of the gravel so as to create a wall of gravel at the gap. Also, the amount of gravel loss was significantly reduced for the tests where the clay was sliding relative to the geotextile versus the tests where the gravel was sliding.

Upon completion of the test, the data acquisition systems and pressure were turned off. With the pressure off, the system unloads allowing the load cell to be unbolted and removed. The gravel was scooped out of the top box and weighed to record the amount of gravel lost during the test. The geotextile was then unclamped and removed from the apparatus leaving the clay surface exposed. Both the geotextile and clay surfaces were inspected for any damage caused during testing. For all of the tests performed, the amount of damage (i.e. tearing/ripping) to the geotextile was negligible. After completing 12 direct shear tests, tearing/cracking of the clay surface was noticed. Because of this, the clay was removed and the bottom box was refilled with clay following the same procedure as followed for the initial placement of clay.

This procedure was followed for 18 tests. The first test was performed as described, using the lightweight slit film geotextile attached to the top box, allowing the clay to slide relative to the

geotextile with a normal stress of 52 kPa (7.5 psi). The second test was the same as the first except that the nonwoven geotextile was used. For the third test the slit film geotextile was attached to the bottom box, allowing the gravel to slide relative to the geotextile. The normal stress remained the same. The tests continued in a similar pattern and are listed in Table 3.2 as 1, 2, and so on in test order.

Table 3.2: Direct shear test order

Test No.	Geotextile ¹	Normal Stress (kPa)	Material Sliding ²	Test No.	Geotextile ¹	Normal Stress (kPa)	Material Sliding ²
1	slit film	52	clay	10	nonwoven	103	clay
2	nonwoven	52	clay	11	slit film	103	gravel
3	slit film	52	gravel	12	nonwoven	103	gravel
4	nonwoven	52	gravel	13	woven	52	clay
5	slit film	77	clay	14	woven	52	gravel
6	nonwoven	77	clay	15	woven	77	clay
7	slit film	77	gravel	16	woven	77	gravel
8	nonwoven	77	gravel	17	woven	103	clay
9	slit film	103	clay	18	woven	103	gravel

Notes:

1. Slit film corresponds to Synthetic Industries Inc. Geotex 200ST, nonwoven to Amoco Fabric & Fibers Co. 4553, and woven to Amoco Fabric & Fibers Co. 2016.
2. When the geotextile is clamped to the top box the *clay* slides relative to the geotextile. When clamped to the bottom box, the *gravel* slides relative to the geotextile.

3.4 Results

For each direct shear test, a plot of the shear stress verses shear displacement was generated displaying a maximum shear stress for that test (Fig. 3.9). By performing three direct shear tests at three different normal stresses for each SFA system, three points could be plotted on a shear stress verses normal stress diagram (Mohr's stress plane) allowing for a range of interface friction values to be determined. The results of the 18 direct shear tests are given in Table 3.3. The corresponding shear stress verses normal stress diagrams are shown in Figures 3.10a, b, and c. The failure envelopes were forced through the origin (zero cohesion/adhesion) because a soil-fabric-aggregate system has no tensile strength.

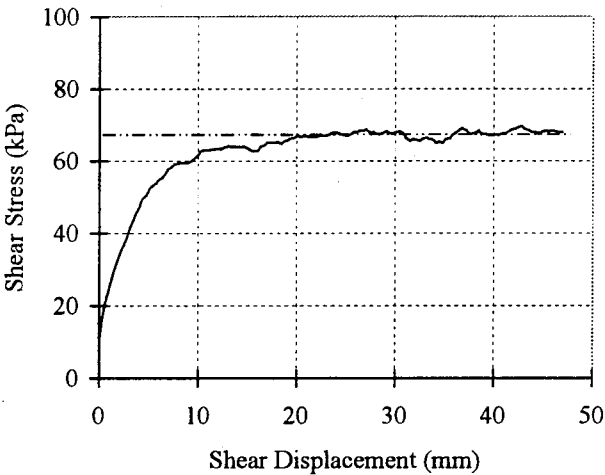
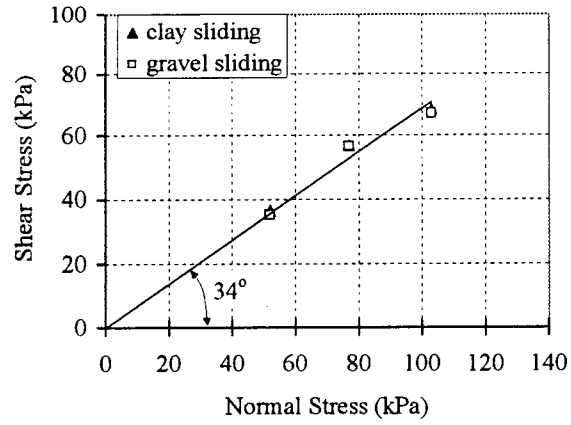
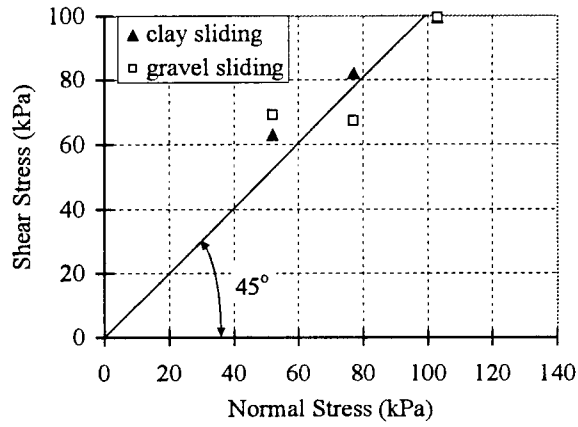


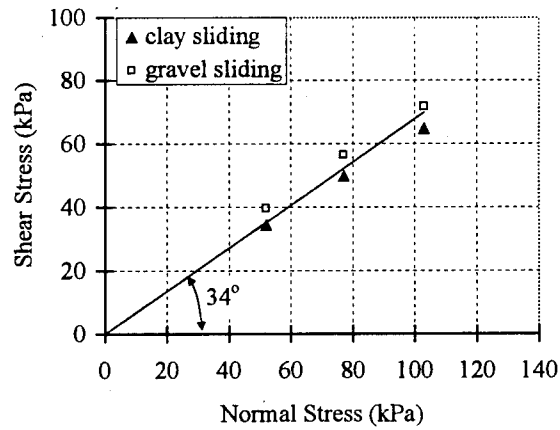
Figure 3.9: Results from slit film sliding on gravel (test number 11)



(a) lightweight slit film



(b) nonwoven



(c) heavyweight woven

Figure 3.10: Results from direct shear tests on the SFA systems

Table 3.3: Summary of shear tests

Lightweight slit film-clay sliding		Nonwoven-clay sliding		heavyweight woven-clay sliding	
normal stress (kPa)	shear stress (kPa)	normal stress (kPa)	shear stress (kPa)	normal stress (kPa)	shear stress (kPa)
52	37	52	63	52	35
77	57	77	82	77	50
103	68	103	99	103	65
lightweight slit film-gravel sliding		nonwoven-gravel sliding		heavyweight woven-clay sliding	
normal stress (kPa)	shear stress (kPa)	normal stress (kPa)	shear stress (kPa)	normal stress (kPa)	shear stress (kPa)
52	35	52	69	52	40
77	57	77	67	77	57
103	67	103	99	103	72

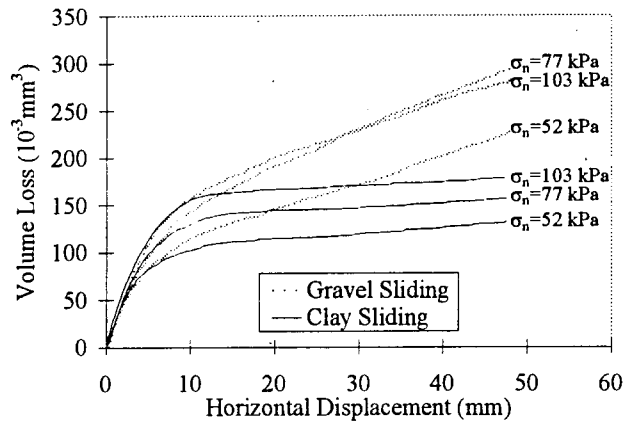
The results show that the best-fit line gives a 45° interface friction angle for the nonwoven geotextile system, and a 34° best-fit interface friction angle for the slit film and woven geotextile systems (Table 3.4). The gravel for the SFA system tests may have been placed at a greater unit weight than the tests run on the gravel alone. This could result in a friction angle for the nonwoven reinforced systems greater than the 42° generated by running tests on the systems with gravel alone (Fig. 3.6). Nevertheless, it may be stated that the interface friction angle for the nonwoven geotextile system is similar to the friction angle of the gravel alone. The texture of the nonwoven geotextile may allow for interlocking at the interface. The woven materials tended to decrease the friction of the system to a value less than that of the gravel alone.

Table 3.4: Interface friction angles

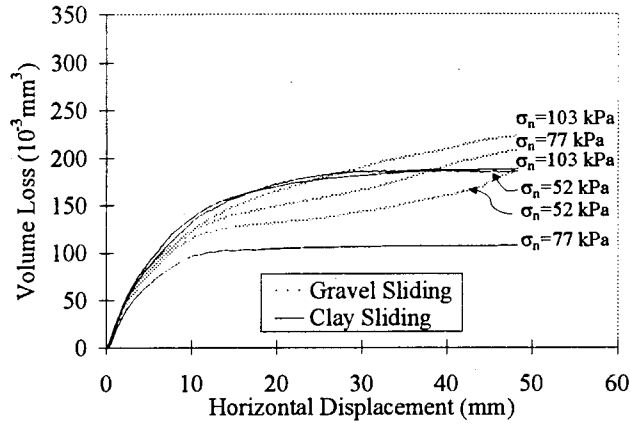
Geotextile	$\phi_{\text{best-fit}}$
Lightweight slit film	34°
Nonwoven	45°
Heavyweight woven	34°

Although the tensile strength of the woven geotextile is much larger than that of the slit film (Table 3.1), both the lightweight woven (slit film) geotextile and the heavyweight woven geotextile are similar in that they are both relatively thin and incompressible. The inability of these materials to be compressed under the gravel load may result in less ability of the gravel to interlock with the geotextile resulting in the similar results for system interface friction for these fabrics.

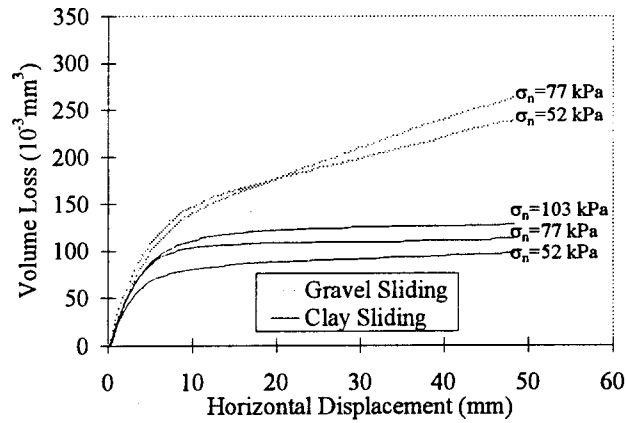
The two digital displacement transducers attached to the rigid load platen (Fig. 3.2) were primarily used to access whether or not the load remained uniformly distributed. However, the displacement transducer data gathered by the attached data acquisition system was also used to monitor the loss of gravel during testing. For each test, the gravel was compacted by the application of the normal load prior to starting the direct shear test. As the bottom box moved horizontally a small amount of aggregate was lost due to the 19 mm (0.75 in.) gap between the top and bottom box. In most of the normal load cases, the tests with the clay sliding relative to the geotextile generated the least amount of aggregate loss with the aggregate volume loss actually decreasing to close to zero as each test progressed (Fig. 3.11). In all cases where the gravel was sliding relative to the geotextile the volume loss continued to occur throughout the tests.



a) lightweight slit film



b) nonwoven



c) heavyweight woven

Figure 3.11: Change in aggregate volume for three geotextiles: gravel and clay sliding

3.5 Summary

Interface friction in a geotextile reinforced unpaved road allows for the transfer of shear stresses from aggregate to geotextile, relieving the subgrade of these potentially damaging stresses. By performing direct shear tests on soil-fabric-aggregate systems, interface friction values were obtained for three different geotextiles: lightweight slit film, heavyweight woven, and nonwoven.

For the direct shear test series, two tests were performed at each of three normal loads: one with the geotextile attached to the top box, the other with it attached to the bottom box resulting in either the clay or gravel sliding relative to the geotextile. Little difference was seen in the values for interface friction for these two testing scenarios. However, the aggregate loss through the box gap decreased to close to zero as the clay sliding tests progressed, while the aggregate loss during the tests with the gravel sliding continued to occur throughout the duration of the test.

The direct shear test series performed on the soil-fabric-aggregate systems indicated that the nonwoven geotextile developed an interface friction comparable to that of the gravel alone, while the lightweight and heavyweight woven geotextiles generated 20% lower interface friction angles. The results showed that the best-fit line (assuming zero cohesion) gives a 45° interface friction angle for the nonwoven geotextile system and a 34° interface friction angle for the lightweight slit film and heavyweight woven geotextile systems. The higher interface friction of the nonwoven geotextile may be a result of its texture and compressibility, which could result in interlocking between the gravel and geotextile.

Chapter 4

Model Tests

Geotextile reinforced unpaved roads were modeled in the laboratory to evaluate the performance of an unpaved road with and without geotextile at the subgrade-geotextile interface. A series of 11 model tests along with 2 practice tests were conducted. Both geotextile type and gravel thickness were varied. The moisture content of the clay subgrade was monitored so as to remain 3-7% above optimum ($w = 23-27\%$).

The model test apparatus consisted of a 560 mm (22 in.) diameter thin-walled steel cylinder that was filled with clay. The inside cylinder wall was covered with plastic foam to reduce the effects of the boundaries by allowing displacement at the cylinder wall. Two types of geotextiles were used in the model tests: a woven slit film (150 g/m^2) and a nonwoven (340 g/m^2). The geotextile was placed unanchored on the clay surface and covered with either 100, 150, or 200 mm (4, 6, or 8 in.) of gravel. Approximately 10,000 cycles were applied to each modeled system; due to large deformation some tests experienced fewer cycles.

4.1 Apparatus and Setup

A full-scale geotextile reinforced unpaved road design was performed in order to model the soil-fabric-aggregate (SFA) system in the laboratory. The full-scale design was then scaled down for the laboratory model tests. Finally, the cylindrical model test apparatus was designed to minimize boundary effects.

4.1.1 Determination of SFA System

A geotextile reinforced unpaved road was designed for an 80 kN (18,000 lb) dual tire axle load, P , following the suggestion of Giroud and Noiray [4]. A typical tire pressure, p_c , of 480 kPa (70

psi) was used resulting in an effective tire contact pressure, p_{ec} (Eq. 4.1a), of 339 kPa (49.2 psi). The area, LxB , was calculated according to Eq. 4.1b to be 0.118 m² (183 in.²). The contact area, A_c , was determined by calculating L and B (substitute 4.1c into 4.1b) to be 0.122 m² (189 in.²). An area this size would produce a circle with a 0.40 m (15.5 in.) diameter. Knowing p_{ec} and A_c , an effective dual tire load, F_{ec} , of 41.4 kN (9300 lb) was calculated.

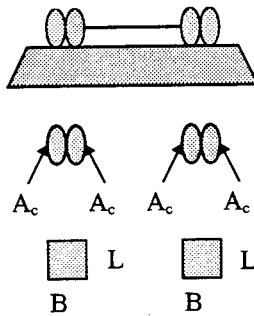


Figure 4.1: Tire print configuration

$$p_{ec} = \frac{\sqrt{2}}{2} p_c \quad \Rightarrow \quad P = 2LBp_{ec} \quad (4.1a)$$

knowing: $P = 4A_c p_c \quad A_c = \frac{LB}{2\sqrt{2}}$

$$LB \approx 2A_c \sqrt{2} \quad (4.1b)$$

$$L = B/\sqrt{2} \quad (4.1c)$$

The undrained shear strength, c_u , of the subgrade material to be used in the model tests was conservatively taken as 40 kPa (5.8 psi). Knowing the effective dual tire load and contact area, the Federal Highway Administration [22] design procedure was used to complete the geotextile reinforced unpaved road design. The design procedure recommended a bearing capacity factor of five for the reinforced unpaved road design when the permissible rutting would be less than 50 mm (2 in.). A factor of six was recommended if rut depths greater than 100 mm (4 in) were permitted. The average of these two factors was used resulting in a required gravel thickness of 200 mm (8 in.).

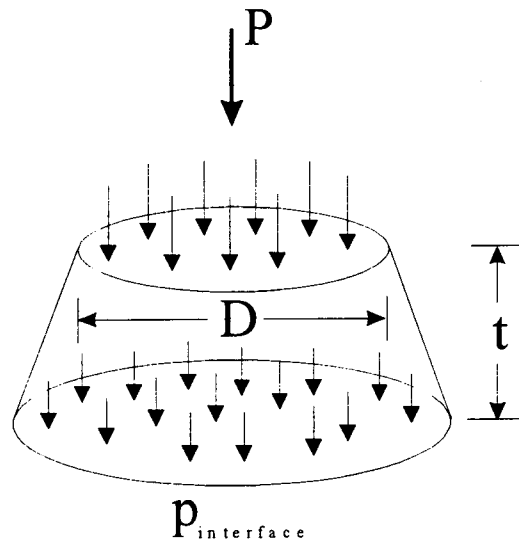


Figure 4.2: Interface pressure

Assuming a circular tire print of 0.40 m (15.5 in.) and a 31° load distribution angle (the 2:1 approximation) through the gravel, 200 mm (8 in.) of gravel and a 41.4 kN (9300 lb) dual tire load would produce a 130 kPa (18.8 psi) vertical stress at the gravel-geotextile interface over a 0.64 m (25.1 in.) diameter area (Fig. 4.2). However, the size of the model test apparatus was controlled by the testing machine, which could only handle an apparatus 0.61 m (24 in.) wide. Considering the potential boundary effects, the loading area at the clay surface was too large for the size of the test apparatus. Because the conditions at the geotextile interface were of interest, it was decided to keep the vertical stress at the base of the gravel layer constant during scaling.

By reducing the load to 7.34 kN (1650 lb), the aggregate layer thickness to 100 mm (4 in.), and the load-plate diameter to 146 mm (5.75 in.), the vertical stress at the interface remained at 130 kPa (18.8 psi) but over a smaller diameter area of 0.27 m (10.6 in.). This smaller diameter area minimized the effects of the apparatus boundaries.

Pressure isobars (Fig. 4.3) for a square footing were used to determine what the subgrade layer thickness should be for the model tests [37]. Assuming that all the vertical stress is transferred to the clay surface (a frictionless interface), the area of the distributed pressure at the clay surface of the scaled model was determined to be 270 mm (10.6 in.). A container 600 mm

(24 in.) in diameter and 600 mm (24 in.) in height encompassed the 13 kPa (1.88 psi) pressure isobar (Fig. 4.3), which represented 10% of the vertical stress.

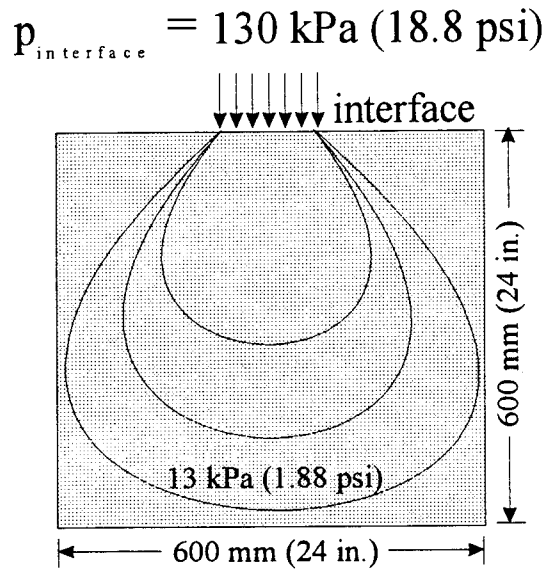


Figure 4.3: Pressure isobar

4.1.2 Cylinder Design

The average radial displacement, u_r , and radial stress, σ_r , along the proposed cylinder wall boundary were determined using the CIRCLY program [38]. Values for the modulus of elasticity, E , and Poisson's ratio, ν , were estimated for the granular material as 35 MPa (5000 psi) and 0.3, and for the clay material as 7.8 MPa (1125 psi) and 0.5 [39]. The average values for σ_r and u_r along the cylinder wall were determined to be 159 kPa (23 psi) and 5.3 mm (0.21 in.).

A 560 mm (22 in.) diameter-55 gallon steel drum was an inexpensive solution for the model test apparatus. Knowing the average radial stress and displacement values at the proposed apparatus wall, an attempt was made to design the walls such that this displacement could take place. In addition, to evaluate the structural integrity of the steel drum, it was simply treated as a pressure vessel (Fig. 4.4) and the minimum wall thickness was estimated.

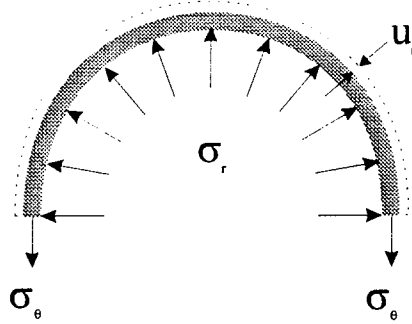


Figure 4.4: Loading of a cylindrical pressure vessel

In performing this analysis, Eq. 4.2 and 4.3 were used assuming an E of 207 GPa (30,000 ksi), ν of 0.285, and an ultimate strength of 248 MPa (36 ksi) for steel. A 55-gallon steel drum has an approximate thickness of 0.8 mm (0.03125 in.). A cylinder this thick easily meets the strength requirements. However, walls this thick would be extremely stiff relative to the field conditions. Little wall displacement would occur.

$$\varepsilon_\theta = \frac{u_r}{r} \quad \Rightarrow \quad \varepsilon_\theta = \frac{\sigma_\theta}{E} + \frac{\nu}{E}(-\sigma_r - \sigma_z) \quad (4.2)$$

$$\sigma_\theta = \frac{P_i r}{t} \quad (4.3)$$

To allow for continuous displacement of the clay subgrade material at the cylinder wall, two layers of 6.4 mm (0.25 in.) thick plastic sheet foam were glued to the wall using a spray adhesive. These sheets were removed and replaced between tests if they lost their compressibility. The final cylinder design is depicted schematically in Figure 4.5.

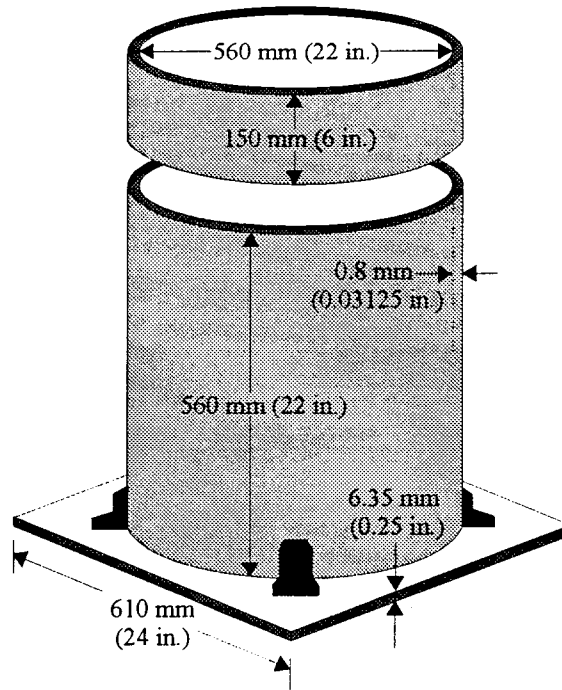


Figure 4.5: Schematic of cylinder design

4.1.3 Testing System and Configuration

A closed-loop, servo-controlled testing machine was used for the experiments (Fig. 4.6). An existing test program was modified to produce a haver-sine loading within a specified load range. The program input parameters included upper and lower load limits, loading frequency, sleep time (time between cycles), number of cycles, number of cycles between data acquisition, and time between data samples. The data file generated for each test included time, load, and displacement information.

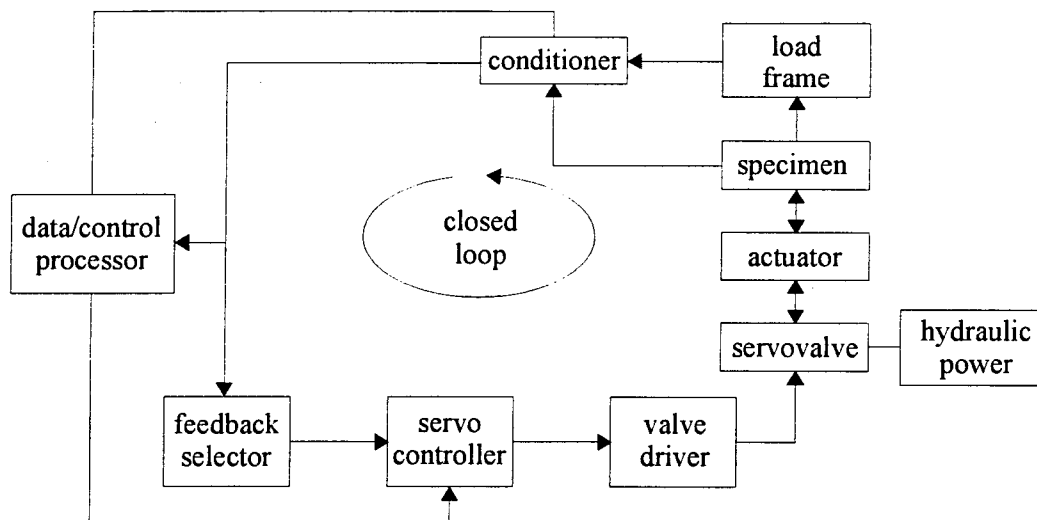


Figure 4.6: Operation of closed-loop, servo-controlled testing machine

To accommodate the scaled tire load of 7.34 kN (1650 lb) to be used for the model test, an upper load limit of 8.9 kN (2,000 lb) was used. Since problems can occur if the load plate loses contact with the apparatus, 10% of the upper load limit, 0.89 kN (200 lb), was specified as the lower load limit.

At higher frequencies the testing machine was unable to follow the specified load path. Therefore, a frequency of 0.2 Hz was used. Even with this low frequency the machine had difficulty keeping up with the specified load path prior to stiffening of the soil-fabric-aggregate system. A sleep time of 5 seconds was used for the tests. This time length was chosen for symmetry: haversine loading over 5 seconds with a seating load of 0.89 kN (200 lb) over the 5 second sleep time (Fig. 4.7).

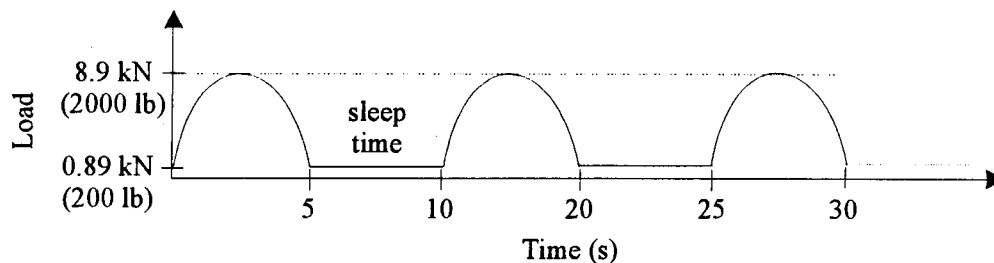


Figure 4.7: Loading history

All tests were programmed for 10,000 cycles. To obtain information over a load step, five data samples at a one second time interval were taken per cycle. With 10,000 cycles, data could only be recorded every 50th cycle due to limitations of the data file size. Initially, 10-20 cycles were applied to each soil-fabric-aggregate system with data taken every other cycle. This procedure provided information about the initial deformation of the SFA system. After completing the initial cycles, the test was started again and programmed for 10,000 cycles.

4.2 Materials

As in the direct shear tests, the SFA system model tests were performed using a silty-clay subgrade material taken from Sibley County, Minnesota. The optimum moisture content was 20% (Fig. 3.4), with a maximum dry unit weight of 16.5 kN/m³ (105 pcf). The soil plasticity index was 11, with a liquid limit of 34 and plastic limit of 23 and could be classified according to AASHTO as A-6 (9). The moisture content of the silty-clay during all 11 model tests varied from 3.4% to 7.1% over optimum, with moisture content values between 23.4 % and 27.1%.

Class 5 gravel, according to the Minnesota Department of Transportation specifications, was used. The crushed gravel contained a significant amount of fines (Fig. 3.5) and had a uniformity coefficient of 16 and coefficient of curvature of 0.24. The friction angle of this material was tested using the direct shear apparatus (Fig. 3.2) and found to be 42° (Fig. 3.6).

Because the interface friction angles of the lightweight slit film and heavyweight woven were similar, it was decided to eliminate the heavyweight woven from the model tests resulting in the use of Synthetic Industries Geotex 200ST lightweight woven slit film and Amoco Fabrics & Fibers 4553 nonwoven. Both fabrics are polypropylene based. Physical and mechanical properties of these fabrics can be found in Table 3.1.

The bottom portion of the cylinder was designed to hold the clay subgrade; the removable top contained the gravel, with the geotextile resting at the (gravel-subgrade) interface between the two cylinders (Fig. 4.8). The bottom cylinder had volume of 0.14 m³ (4.83 ft³). However, there was not enough silty-clay to fill this volume. Therefore, fill materials were used in the bottom half of the cylinder. The fill placed at the bottom was a silty-sand with an optimum moisture content

and dry unit weight of 10% and 21 kN/m³ (134 lb/ft³) (Fig 4.9). The soil was classified according to AASHTO as an A-2-4 material with 32% passing the #200 sieve, 28% silt, and 3% clay. The top fill material was a low plasticity clay with an optimum moisture content and dry unit weight of 18.5% and 15 kN/m³ (96 lb/ft³) (Fig. 4.10). The top fill was classified according to AASHTO as an A-6 material with 62% passing the #200 sieve: 41% silt and 22% clay.

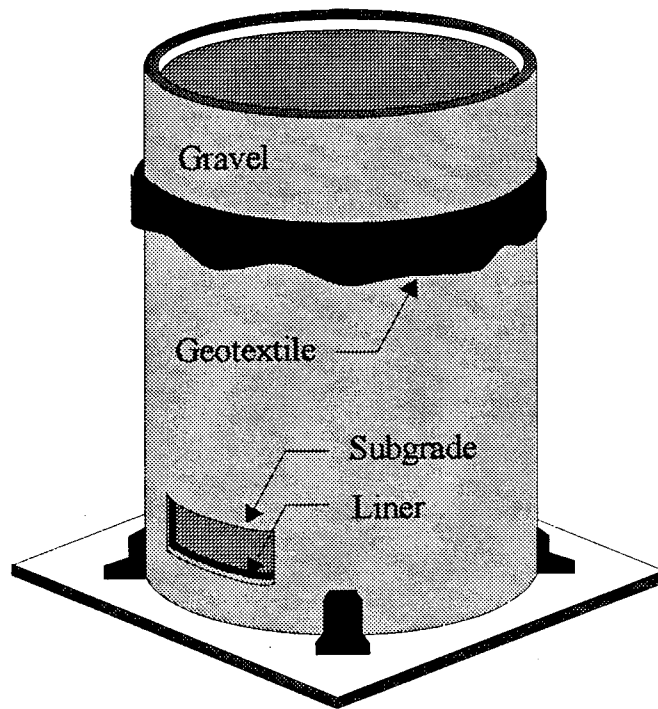


Figure 4.8: Geotextile location for model tests

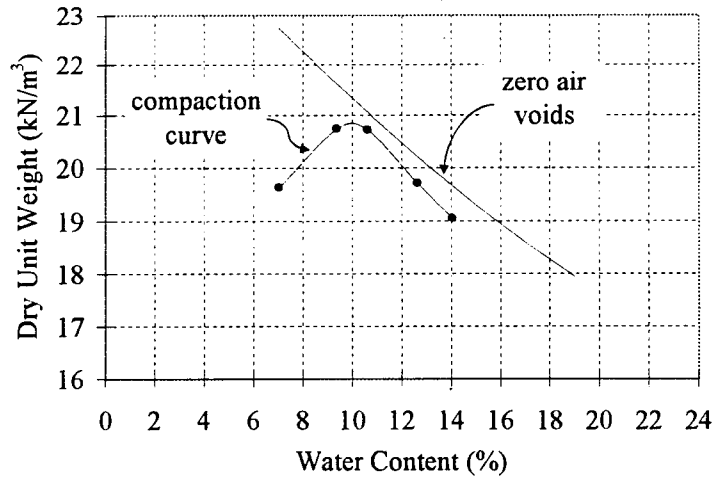


Figure 4.9: Bottom fill compaction curve

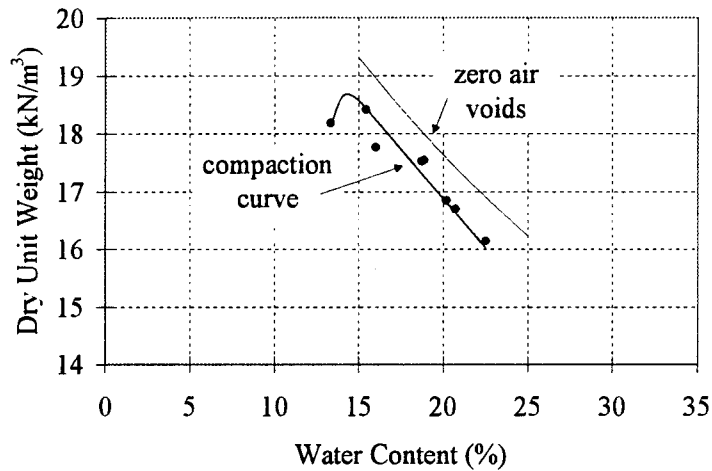


Figure 4.10: Top fill compaction curve

A total of 460 N (110 lb) of the silty-sand plus 71 N (15.8 lb) of water were mixed to create a fill with a 14% moisture content. This material was placed in the bottom of the cylinder. This fill could be classified as a low-strength subgrade material due to its 14% moisture content. A total of 400 N (89 lb) of the low plasticity clay plus 110 N (24.6 lb) of water were mixed to create a fill with a 27.7% moisture content. This low plasticity clay was placed on top of silty-sand and could be classified as a low-strength subgrade material due to its large (27.7%) moisture content. Neither fill material could be compacted due to their extremely weak conditions.

The silty-clay comprised the top third of the subgrade soil profile. The optimum moisture content of this material was estimated to be around 20% (Fig. 3.4). To generate a weak subgrade it was determined that a moisture content approximately 5% over optimum be used. The material was then placed in the apparatus in three lifts. Each lift was compacted with 80 blows of a Proctor hammer allowing each lift to be compacted without overlapping the compaction blows. The silty-sand plus the low plasticity clay filled the bottom 400 mm (1.3 ft) or 71% of the cylinder. The silty-clay material filled the top 160 mm (0.5 ft) or 29% of the cylinder.

Before and after each test, the moisture content of the silty-clay was checked. If necessary, more water was added so that the material would remain at about 2-5% above optimum. Between model tests the silty-clay was removed and remixed due to compaction from the load cycles. When the material was removed, an effort was made to avoid any mixing of the fill material with the silty-clay.

With the clay subgrade in-place a 1 m² (12 ft²) square piece of geotextile was placed directly on the subgrade and the top cylinder rested on the geotextile and bottom cylinder. The gravel was placed in the top portion of the cylinder. The top cylinder was not clamped to the bottom cylinder. Three different gravel thicknesses were used: 100, 150, or 200 mm (4, 6, or 8 in.). For tests with 100 and 150 mm (4 and 6 in.) of gravel, compaction was performed by applying 2 rounds of 22 blows with the Marshall stability hammer (44 blows total) to the gravel surface. With 200 mm (8 in.) of gravel, 22 additional blows were applied.

After completing the model test series, compaction tests were rerun on the silty-clay (Fig. 4.11). This test was performed to evaluate whether the amount of mixing that occurred between the silty-clay and the underlying fill material was significant. The compaction curve for the silty-clay showed no apparent change relative to the compaction curve generated prior to the model tests. Therefore, any mixing that occurred can be interpreted as minor.

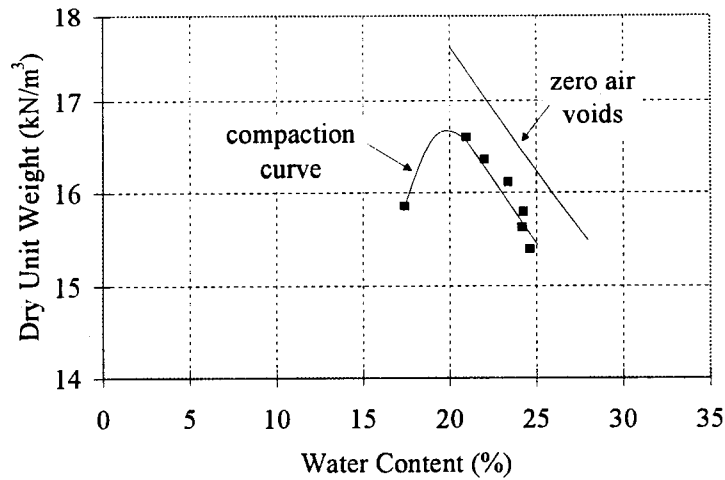


Figure 4.11: Compaction curve for silty-clay after completion of model tests

4.3 Practice Tests

Two practice tests were performed prior to beginning the series of 11 model tests. One test was performed with the slit film geotextile reinforcement located at the subgrade-gravel interface and the other with the nonwoven reinforcement. The practice tests were performed to make sure that the apparatus functioned properly and to investigate geotextile anchorage. Two anchorage scenarios were considered: constant stiffness and constant force (Fig. 4.12).

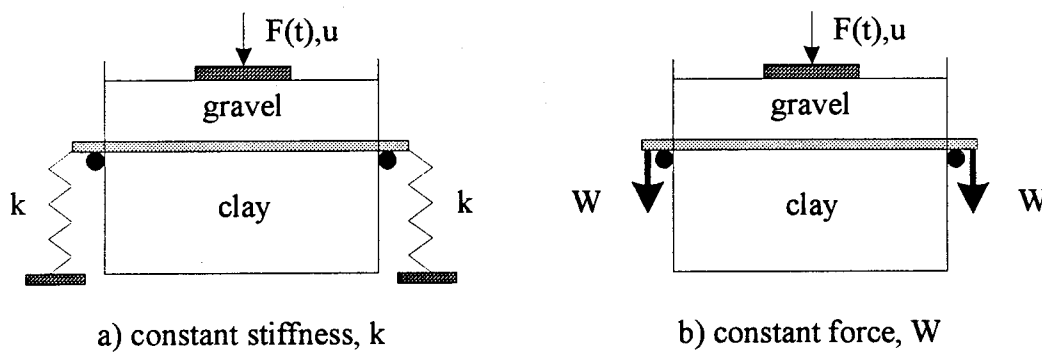


Figure 4.12: Anchorage scenarios

4.3.1 Anchored Slit Film Reinforcement

The first practice test was performed using the slit film geotextile reinforcement and 100 mm (4 in.) of gravel. The gravel was not compacted. The geotextile was clamped to the outer circumference of the bottom barrel using a large hose clamp. The silty-sand was placed in the bottom of the cylinder with a 14% moisture content and the low plasticity clay was placed on top with a 28% moisture content. Neither fill material was compacted because of their extremely weak states. The silty-clay was placed on top of the clay so that it would be the material in contact with the geotextile. The silty-clay was mixed to a 40% moisture content so as to produce saturated conditions.

The test was programmed to run 5,000 cycles at a frequency of 0.1 Hz with a 3 second sleep time cycles. A set of 10 data was taken every 50th cycle in order to capture the full loading and unloading sequence. The upper and lower load range limits were specified as 8.9 kN (2,000 lb) and 0.89 kN (200 lb).

The test ran 600 cycles before it was terminated. The upper load plate, which was 254 mm (10 in.) in diameter, punched into the gravel during the test causing the gravel layer to fail. The final rut depth at the clay surface was 89 mm (3.5 in.). The clay was pushed down under the load area and moved up outside this area seemingly the result of a bearing capacity failure (the clay subgrade was extremely weak for this test). The geotextile was fully tensioned, anchored by the hose clamp. Moisture traveled through the geotextile, into the gravel, and could be seen within a 38 mm (1.5 in.) thick gravel region directly above the geotextile. The average moisture content of the gravel in this region was 4.7% (the gravel was initially dry).

4.3.2 Unanchored Nonwoven Reinforcement

The moisture content of the silty-clay was decreased prior to the second practice test as a result of the performance of the first practice test. The silty-clay material was removed from the apparatus and allowed to dry in bins. It was determined that the clay material should be approximately 5-8% above optimum ($w_{opt} = 20\%$). The clay was dried to a 30% moisture content; then dry material was mixed in to obtain the desired moisture content of 26%. This material was placed in

the apparatus in three lifts. Each lift was compacted by approximately 70 blows with the compaction hammer. Nonwoven geotextile and 100 mm (4 in.) of gravel were used in the second practice test. The geotextile was left unanchored but marked so as to monitor any movement of the geotextile relative to the cylinder wall.

The test was programmed to run 10,000 cycles at a frequency of 0.2 Hz with a 5 second sleep time between cycles. A set of 10 data was taken every 50th cycle. The upper and lower load range limits were specified as 8.9 kN (2,000 lb) and 0.89 kN (200 lb). The total running time for this test was approximately 27.8 hours. Again, the gravel was not compacted.

During testing the geotextile did not move relative to the cylinder wall—the geotextile was not “pulled-in” by the 140 mm (5.5 in.) deep and 292 mm (11.5 in.) rut diameter that formed. By inspecting the geotextile, it appeared that the geotextile stretched only within the distributed load area at the geotextile interface. No water movement occurred from the clay through the geotextile and into the gravel.

Due to punching failures that seemed to occur within the gravel for both practice tests, the gravel for all future model tests was compacted prior to testing. The first model test performed was similar to the practice test just discussed in that the clay material had the same moisture content and nonwoven reinforcement was used along with 100 mm (4 in.) of gravel. The model test experienced 58 mm (2.3 in.) of rutting relative to the 140 mm (5.5 in.) that occurred in the practice test with uncompacted gravel. Compaction reduced the rutting by approximately 89 mm (3.5 in.).

4.4 Test Matrix

Eleven model tests were performed. The variables of the model tests were the gravel thickness (100, 150, 200 mm) and geotextile type (slit film and nonwoven). The moisture content of the silty-clay varied from test to test by a range of 3.4-7.1% over the optimum moisture content (Fig. 3.4, Table 4.1).

The 11 model tests are listed in Table 4.1. The tests are named according to the type of geotextile reinforcement used, if any (S=slit film, N=nonwoven, and X=no geotextile

reinforcement), gravel thickness (100, 150, 200 mm), and a digit representing the number of tests run with the same reinforcement and gravel thickness configuration (1,2, or 3). Italicized tests in Table 4.1 are those with lower moisture contents. Because of the seemingly low moisture contents for these tests (S42 and S81), moisture was added to the silty-clay and these tests rerun (S43 and S82). The tests S41 and N41 were the practice tests previously discussed.

Table 4.1: Eleven model tests and their moisture contents

Test Name	Moisture Content, %	Test Name	Moisture Content, %
X41	27.0	<i>S42</i>	24.2
X61	26.3	S43	25.6
X81	25.7	S61	26.3
N42	25.9	<i>S81</i>	23.4
N61	24.6	S82	25.0
N81	24.2		

The moisture content of the silty-clay was monitored closely during the model test series. After each test, the clay was removed, remixed, and the moisture content checked. If the moisture content was acceptable the silty-clay was placed back in the cylinder for the next test. The clay was always placed in three lifts, each lift receiving approximately 90 blows with the compaction hammer. After placing all of the clay in the cylinder, ridges left in the surface by the hammer were leveled. The geotextile was placed on top of the clay unanchored. The top cylinder was then placed on the bottom cylinder and the geotextile marked so as to monitor any movement. Finally, the gravel was placed in one lift. For 100 or 150 mm (4 or 6 in.) of gravel, compaction was performed by covering the surface with 22 blows of the Marshall Hammer two times (a total of 44 blows). For 200 mm (8 in.) of gravel, the same compaction procedure was followed, although this procedure reduced the gravel thickness to something less than 200 mm (8 in.). Therefore, more gravel was added and 22 more blows applied such that a 200 mm (8 in.) of gravel thickness existed.

After completion of a test, the gravel and top cylinder were removed along with the geotextile. The geotextile was inspected for movement along the cylinder circumference as well

as for stretching and damage. The geotextile did not move relative to the cylinder circumference for any of the tests. However, it did appear to have stretched in the approximate region of the distributed load area at the gravel-geotextile interface.

The rut depths for the slit film reinforced models were always greater than those for the nonwoven reinforced models. However, the slit film geotextile appeared to deform more elastically than the nonwoven. The nonwoven fibers, which are random in orientation, seemed to have stretched inelastically and appeared restructured. For each test, a new section of geotextile was used. No damage occurred to any of the geotextile test sections.

The clay surface was mapped after testing by removing the geotextile and partitioning the surface into eight wedges so as to take the following surface measurements (Fig. 4.13):

1. rut depth
2. rut diameter
3. rut curve length
4. distance from cylinder wall to the start of the rut

After mapping the rutted clay surface, three core samples were taken near the rut center. The cores were tested under uniaxial compression to obtain an estimate of the (final) undrained shear strength.

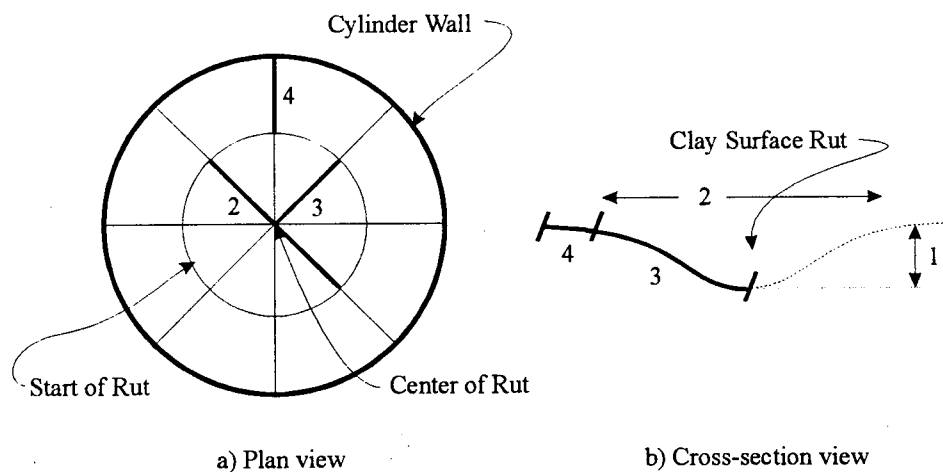


Figure 4.13: Rut mapping measurements

4.5 Results

4.5.1 Test Parameters and Final Rut Depths

As mentioned earlier, the moisture contents varied slightly from one model test to another. This is important to keep in mind when analyzing the test data. Other test parameters varied, including the number of cycles applied to the model and the maximum load achieved. In general, the number of cycles was approximately 10,000. However, for the tests with 100 and 150 mm (4 in. and 6 in.) of gravel and no geotextile reinforcement (X41, X61), the number of cycles was less. Only 330 cycles were applied to the model with 100 mm (4 in.) of gravel and only 2,200 cycles to the model with 150 mm (6 in.). The number of cycles was less due to rutting close to the capacity of the testing machine.

The maximum load was near the specified value (8.9 kN or 2,000 lb), but some tests actually surpassed the maximum load value (X81, S81, S82, and N81). The maximum load achieved was a function of the model properties such as gravel thickness, presence of geotextile reinforcement, and moisture content (system stiffness) and the gain setting of the servo-hydraulic load frame. The tests with 200 mm (8 in.) of gravel were exposed to the highest loads.

A summary of the final rut depth of the clay subgrade, moisture content, number of cycles, maximum load, and final undrained shear strength for each test are shown in Figure 4.14. The rut depth values for X41 and X61 were extrapolated for 10,000 cycles (Fig. 4.15). The actual rut depths for X41 and X61 after 330 cycles and 2200 cycles were 90 mm (3.5 in.) and 100 mm (4 in.).

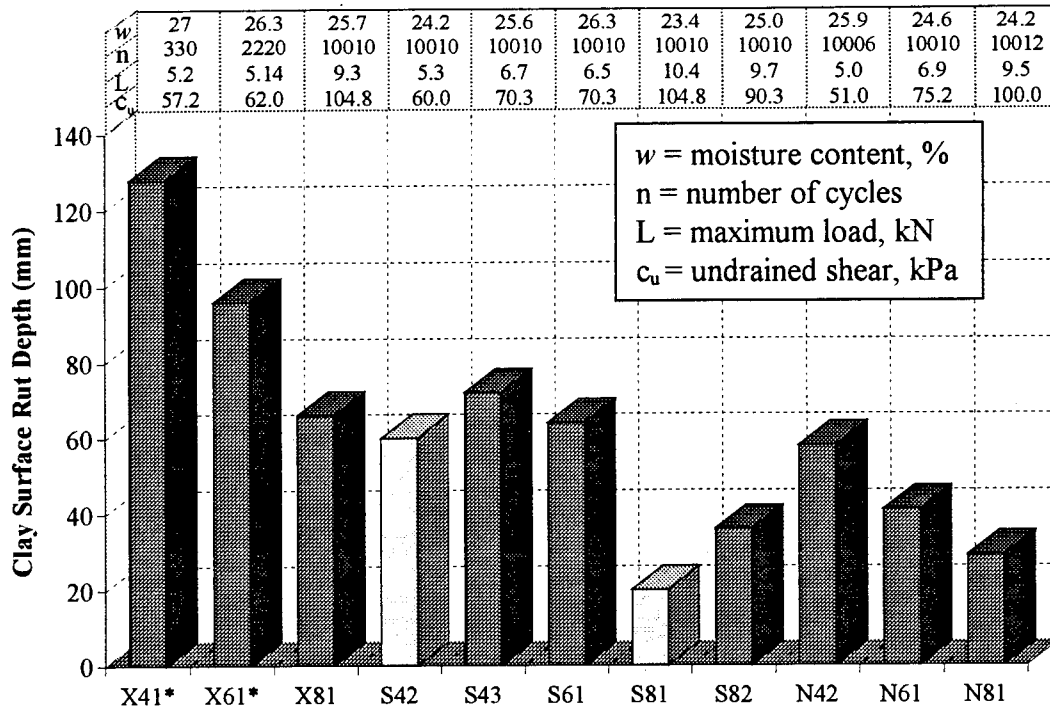


Figure 4.14: Rut depth histogram with table of test parameters
 (* extrapolated rut depth values)

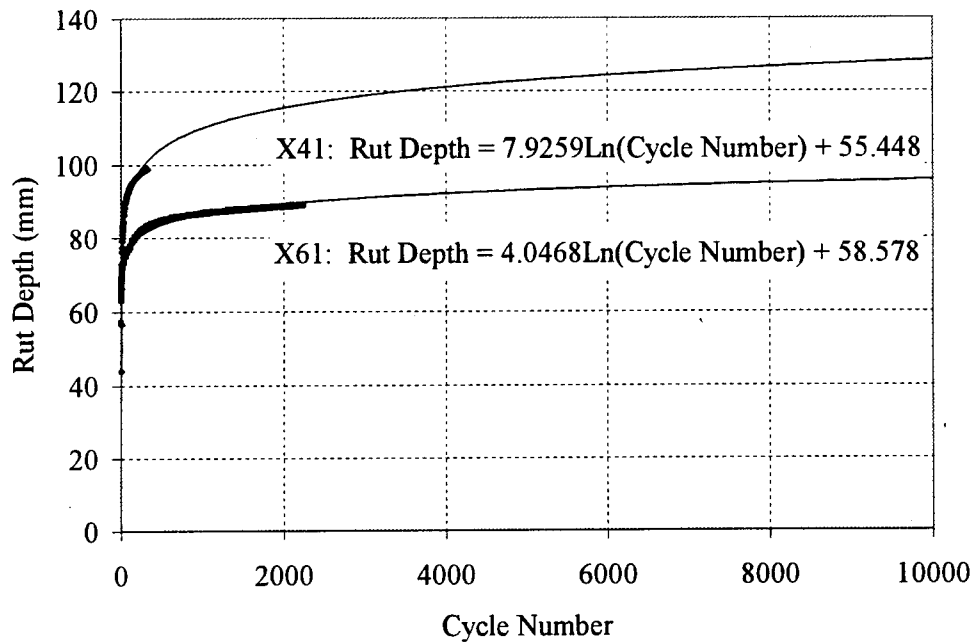


Figure 4.15: Extrapolated rut depths for X41 and X61

4.5.2 Shape of Rut

The shape of the rut was observed to be cubic in character and symmetric about the base. The following expression was used to plot the (half) geometry of the rut's cross-section (Fig 4.16) and was based on the parameters and coordinate system shown in Figure 4.17:

$$y = -\frac{2H}{R^3}x^3 + \frac{3H}{R^2}x^2 \quad (4.4)$$

with boundary conditions $y'(0) = 0$, $y'(R) = 0$, $y(0) = 0$, and $y(R) = H$. Eight measurements of the rut curve length, S (Fig. 4.17), were taken for each test along with four diameter ($2R$) and four rut depth (H) measurements. The recorded values for S , R , and H were averaged to arrive at one value for each. The value S was calculated in a piecewise linear fashion for every 2.5 mm (0.1 in.) in the horizontal direction (x). The calculated value for S corresponded well with the measured value (Table 4.2). The rut geometries were plotted using Eq. 4.4 and are shown in Fig. 4.18 and 4.19.

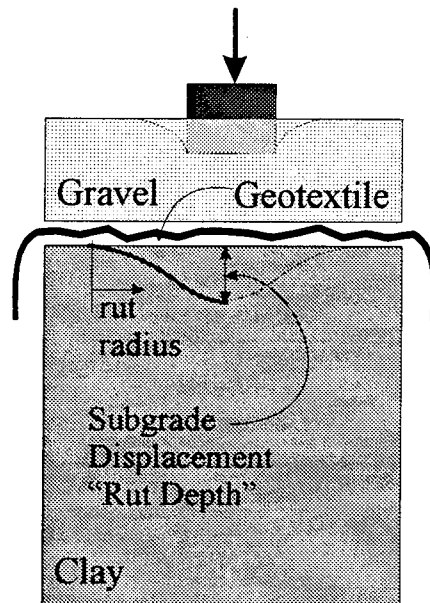


Figure 4.16: Rut geometry interpretation



Figure 4.17: Coordinate system used to develop Eq. 4.4

Table 4.2: Comparison of measured and calculated values for S

Test Name	Measured S values, cm	Calculated S values, cm	% Difference
X41	15.2	15.6	2.4
X61	16.2	16.6	2.5
X81	15.2	15.5	1.6
S42	13.1	13.5	2.7
S43	13.6	14.0	3.1
S61	14.6	14.7	0.7
S81	12.6	12.0	4.9
S82	14.6	14.9	2.5
N42	13.5	13.8	2.1
N61	12.3	12.3	0.3
N81	12.3	12.1	1.3

From Fig. 4.19, it is apparent that for all gravel thicknesses the model tests with nonwoven reinforcement out-performed the slit film reinforced and unreinforced model tests in terms of rut depths (excluding S42 and S81 due to their lower moisture contents). For the reinforced model tests, an increased load-spread angle through the gravel was observed by comparing the rut diameters for the different model tests at a certain rut depth value (Fig. 4.19). It is apparent that the reinforced models tended to have larger rut diameters, indicating an increase in the load-spread angle through the gravel most likely due to geotextile-gravel interlock.

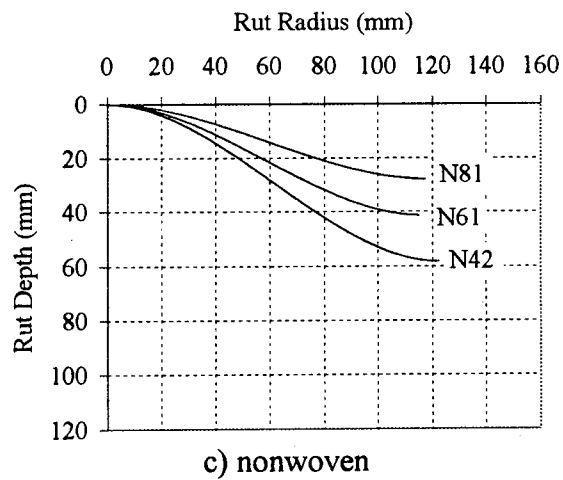
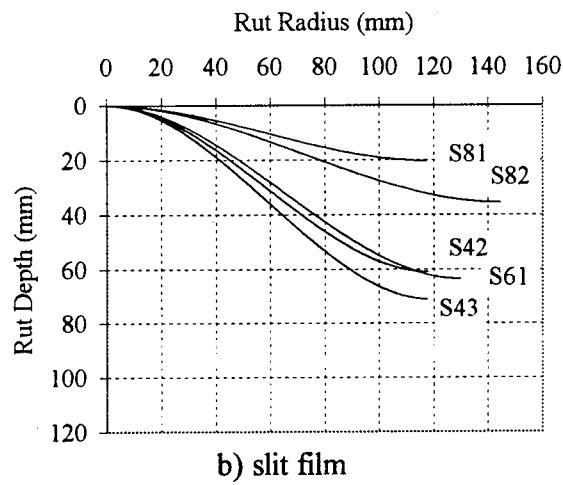
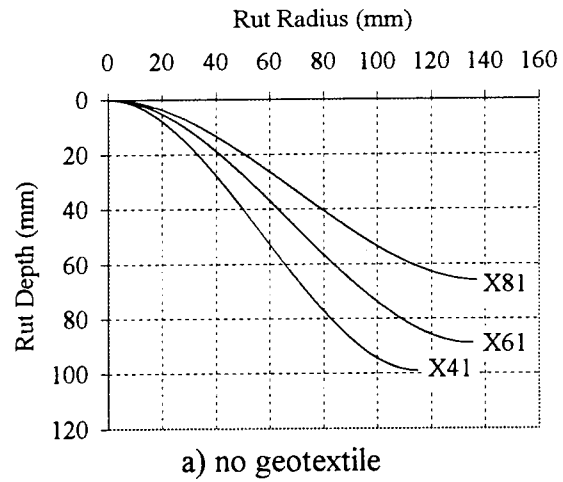


Figure 4.18: Rut geometry as a function of reinforcement

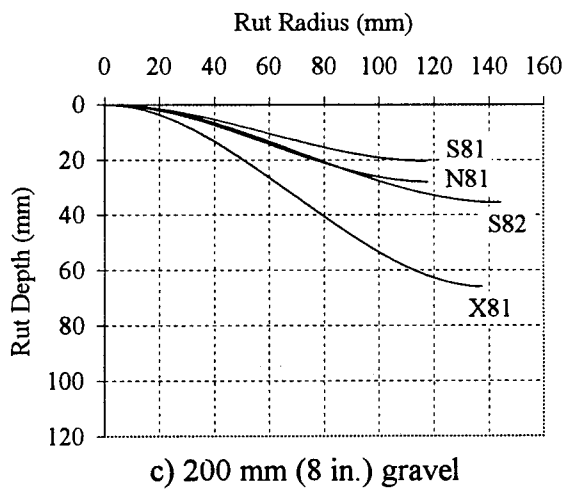
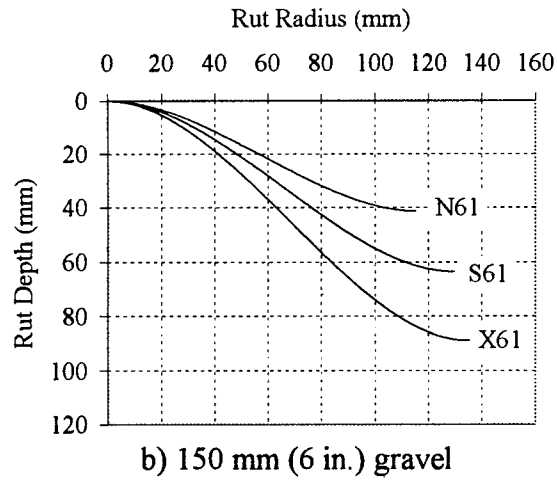
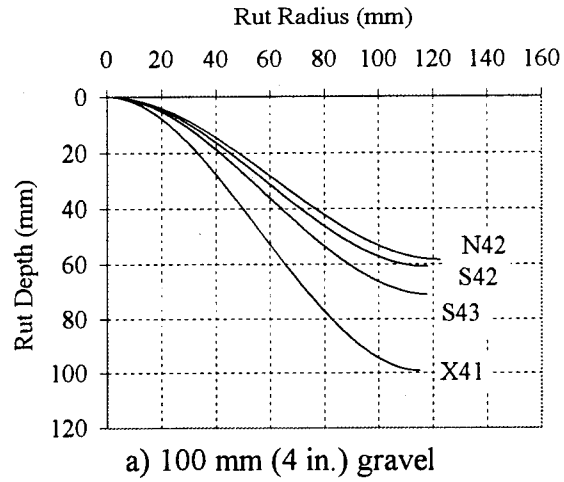


Figure 4.19: Rut geometry as a function of gravel thickness

4.5.3 Equivalency Charts

Time, displacement, and load values were recorded during testing. For approximately the first 20 cycles, data was collected every other cycle. For the rest of the test, data was collected every 50th cycle. A seating load equivalent to the lower load range value of 0.89 kN (200 lb) was applied to the soil-fabric-aggregate system prior to testing. Depending on the model being tested, sometimes the displacement was quite large for the seating load. The initial displacement information was not acquired, resulting in differences between the acquired and measured values for final displacement. In all cases, the measured values of the rut depth were greater than the displacement recorded by the data acquisition system due to this initial deformation. To determine the rut geometry at any load, it was assumed that the gravel thickness remained constant during testing and that the recorded displacement, or stroke, equaled the measured rut depth at the clay surface. A correction was applied to the stroke value such that these values would be equal for each test. The corrections are shown in Table 4.3.

Table 4.3: Correction for stroke

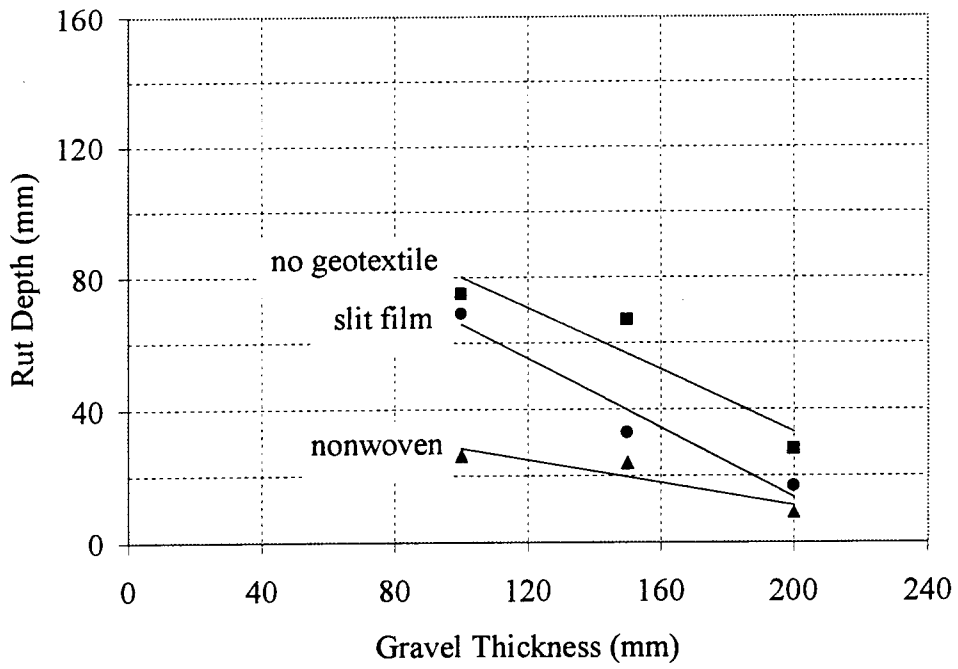
Test Name	Rut Depth, mm (in.)	Stroke, mm (in.)	Stroke Correction, Mm (in.)
X41	99 (3.9)	26 (1.0)	73 (2.9)
X61	89 (3.5)	24 (0.9)	65 (2.6)
X81	66 (2.6)	58 (2.3)	8 (0.3)
S43	72 (2.8)	5 (0.2)	67 (2.6)
S61	64 (2.5)	35 (1.4)	29 (1.1)
S82	36 (1.4)	30 (1.2)	6 (0.2)
N42	58 (2.3)	44 (1.8)	14 (0.6)
N61	41 (1.6)	33 (1.3)	8 (0.3)
N81	29 (1.1)	14 (0.5)	15 (0.6)

The values for the rut depth at different cycles are shown in Table 4.4 and are plotted versus gravel thickness for each system tested (Fig. 4.20). These plots are referred to as equivalency charts because, for a certain rut depth the gravel thickness can be determined. Using the equivalency chart at 10,000 cycles (Fig. 4.20d), the system with nonwoven reinforcement and 100 mm (4 in.) of gravel generated the same amount of rutting as the slit film system with 150 mm (6 in.) of gravel and the unreinforced system with 200 mm (8 in.) of gravel. In terms of rut depths, the nonwoven reinforcement resulted in a 50% aggregate saving. It is important to note that these equivalency charts are performance-based charts for specific conditions with initial subgrade undrained shear strengths estimated to be between 40 and 50 kPa (5.8-7.25 psi).

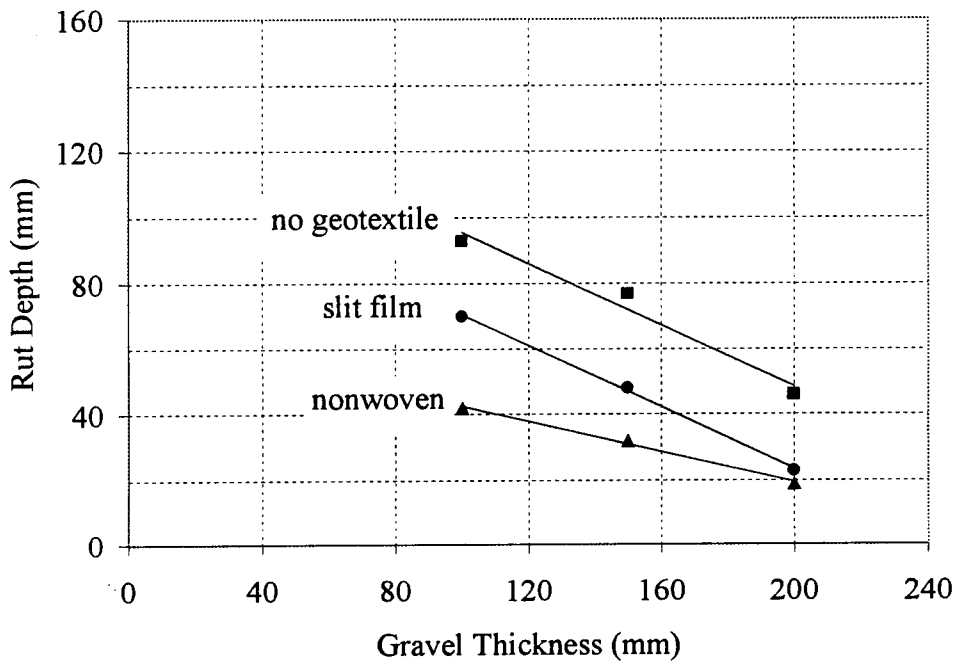
From Table 4.4, it is observed that the nonwoven and slit film geotextile reinforced systems tended to stiffen at the same rate with 86-91% of the total deformation occurring by the 1,000th cycle. The system with 100 mm (4 in.) of gravel and reinforced with the slit film geotextile achieved 99% of its total deformation by the 1,000th cycle. The system stabilized with 72 mm (2.8 in.) of deformation.

Table 4.4: Rut depths at different cycle intervals

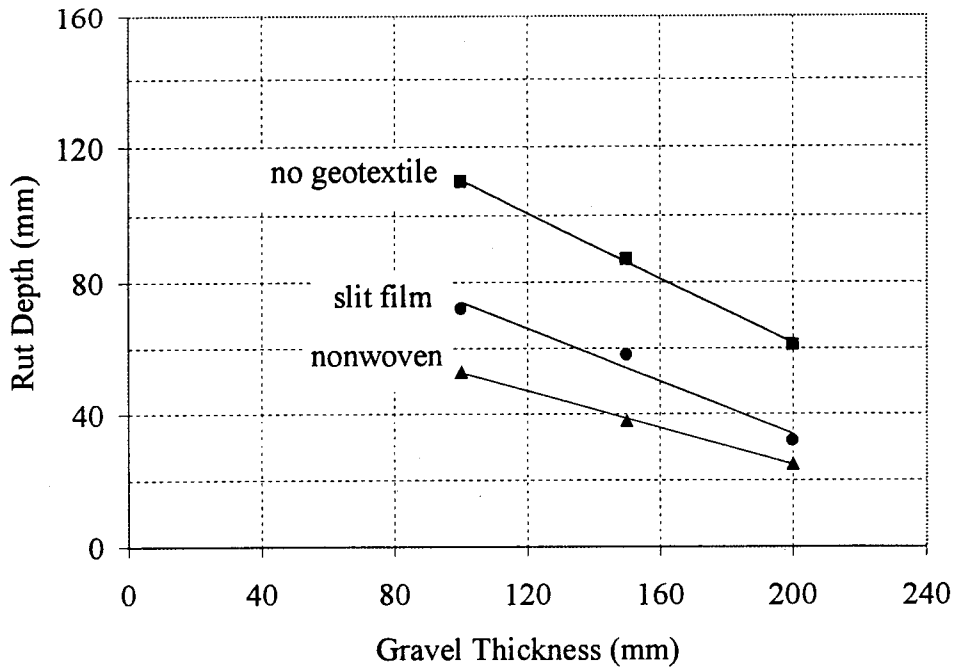
Test Name	Rut Depth After, mm (in.)...			
	10 cycles	100 cycles	1,000 cycles	10,000 cycles
X41	75 (3.0)	93 (3.7)	110 (4.3)	128 (5.0)*
X61	67 (2.6)	77 (3.0)	87 (3.4)	96 (3.8)*
X81	28 (1.1)	46 (1.8)	61 (2.4)	66 (2.6)
S43	69 (2.7)	70 (2.8)	72 (2.8)	72 (2.8)
S61	33 (1.3)	48 (1.9)	58 (2.3)	64 (2.5)
S82	17 (0.7)	23 (0.9)	32 (1.3)	36 (1.4)
N42	26 (1.0)	42 (1.7)	53 (2.1)	58 (2.3)
N61	24 (0.9)	32 (1.3)	38 (1.5)	41 (1.6)
N81	9 (0.4)	19 (0.75)	25 (1.0)	29 (1.1)
* extrapolated values				



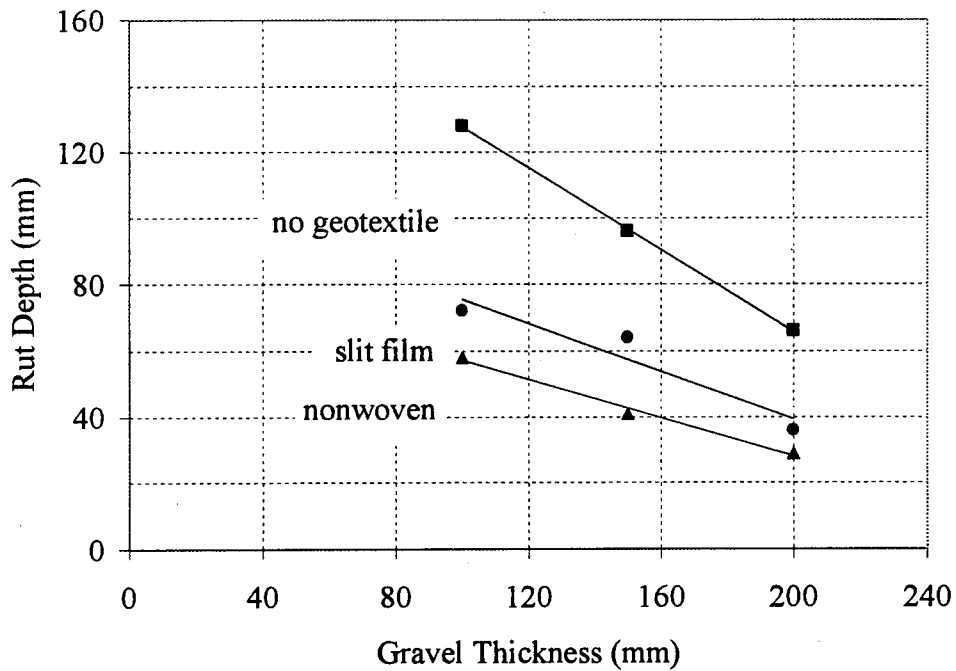
a) 10 cycles



b) 100 cycles



c) 1,000 cycles



d) 10,000 cycles

Figure 4.20: Equivalency charts after 10, 100, 1,000, and 10,000 cycles for subgrade with average (final) shear strength of 75 kPa

4.5.4 Bearing Capacity

A bearing capacity factor for a footing resting on a saturated clay (undrained behavior) is simply the ratio between the maximum applied normal stress and the undrained shear strength. For the design of an unpaved road, a similar factor can be defined. For a given gravel thickness, a bearing capacity factor, N_c , was calculated for each model test, where N_c equaled the maximum applied stress (the bearing capacity) divided by the final shear strength. The bearing capacity was assumed to occur at 40 mm (1.6 in.) of deformation, so the stress at this rut depth was used. The undrained shear strength was conservatively taken as the final shear strength. For different gravel thicknesses, the ratio of N_c^{rein} for reinforced systems versus $N_c^{no\ rein}$ for the systems with no fabric are plotted (Fig. 4.21). According to Fig. 4.21, a bearing capacity factor approximately 1.6 times that used for designing unpaved roads with no reinforcement can be used for design.

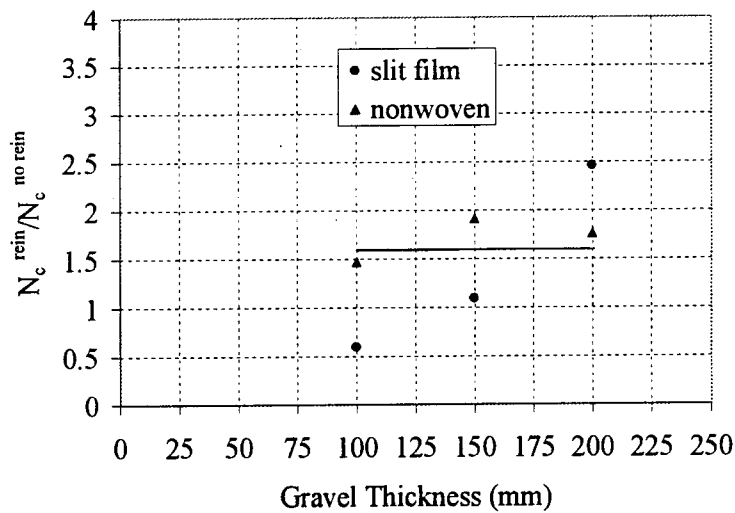


Figure 4.21: Bearing capacity factors for the unreinforced, slit film reinforced, and nonwoven reinforced tests

Rigorous solutions for computing the bearing capacity of a strip footing in a $\phi = 0$ condition can be expressed as:

$$q_{ult} = (2 + \pi)c_u \quad c_u = \text{undrained shear strength} \quad (4.5)$$

Equation 4.5 was modified by Skempton [41] to account for geometric loading and depth influence factors:

$$q_{ult} = (2 + \pi)c_u [1 + 0.2(\text{width}/\text{length})] \quad (4.6)$$

Similarly, Rodin [42] found that the ultimate bearing capacity for a static circular or square footing resting on clay is given by

$$q_{ult} = 6.2c_u \quad (4.7)$$

The ultimate bearing capacity is the stress condition necessary to produce plastic flow in a soil without a surcharge or other constraint. At a stress less than that required for complete failure, however, local over-stressing may occur and cause a localized shear failure. According to Rodin [42], plastic deformation of a flexible loaded area begins when the stress, q , reaches the level:

$$q = \pi c_u \quad (4.8)$$

Barenberg [3] found that the allowable stress on an unreinforced system was $3.3c_u$ or approximately πc_u , which is the value at which Rodin [42] suggested that localized plastic strains were initiated. For the reinforced systems, Barenberg [3] found that the allowable stress was $6c_u$, which is the level at which plastic flow would normally occur. Steward et al. [7] drew very similar conclusions for allowable stress values for unreinforced and reinforced systems as to those generated by the model tests (Table 4.5). Giroud and Noiray [4] suggested allowable stress levels for unreinforced and reinforced systems of $3.13c_u$ and $5.14c_u$, and De Groot et al. [43] found levels of $3c_u$ and $5c_u$. These allowable stress levels would result in a ratio of bearing capacity factors for reinforced versus unreinforced systems ratios of approximately 1.6-2.0, the range of values similar to that determined from the model tests.

The increase in the bearing capacity factor for gravel roads with reinforcement is directly related to the interaction of shear stress and normal stress existing at the surface of the subgrade. If shear stress is absent, then the full value of the bearing capacity (the maximum normal stress) can be realized. If shear stress is then added to the loading, a reduction in bearing capacity

occurs. With the maximum shear stress of the undrained shear strength present, the bearing capacity factor reduces to one half of the value for purely vertical loading. Thus, if reinforcement is introduced, these shear stresses can be carried by the fabric, which is put into tension, and the full bearing capacity of the clay can be mobilized.

Table 4.5: Results from Steward et al. [7]

Traffic Level	Allowable Stress	Performance	
High	$2.8c_u$	Very little rutting	Without Fabric
Low	$3.3c_u$	Deep rutting	Without Fabric
High	$5c_u$	Very little rutting	With Fabric
Low	$6c_u$	Deep rutting	With Fabric
High traffic level: >1,000 passes of an 18 kip (80 kN) axle load; low traffic: <100 passes.			

4.6 Summary

The results of a series of 13 model tests with and without geotextile reinforcement at the gravel-subgrade interface showed that, in terms of rut depths, the nonwoven geotextile performed better than the slit film for all gravel thicknesses. The nonwoven reinforced system with 100 mm (4 in.) of gravel was equivalent to the slit film reinforced system with 150 mm (6 in.) of gravel and the unreinforced system with 200 mm (8 in.) of gravel in terms of rut depths, which was 60 mm (2.4 in.). Obviously, a gravel thickness of 100 mm (4 in.) is insufficient for most practical applications and other factors would need to be considered before extrapolating the conclusion to the field. The improved performance on the part of the nonwoven geotextile was most likely due to the nonwoven's frictional characteristics.

The bearing capacity factor for the model tests reinforced with the nonwoven fabric was 1.6 times greater than that for the model tests without reinforcement. These results agreed well

with the results of previous work performed by Steward et al. [7], Barenberg [3], Giroud and Noiray [4], and De Groot et al. [43]. The bearing capacity factor for the slit film reinforced systems changed with gravel thickness.

The rut diameters for the slit film and nonwoven geotextile reinforced systems tended to be larger than those of the unreinforced systems, indicating that interlocking of the gravel and geotextile produced confinement on the gravel resulting in an increased load-spread angle through the gravel. Other significant observations were that geotextile anchorage was unimportant, as the geotextile appeared to only be stretched and pulled within the distributed load area at that location. Outside of this area, no stretching of the geotextile was observed. It was shown from practice tests that gravel compaction was important for developing interlock between the gravel and geotextile. For the nonwoven reinforced system with 100 mm (4 in.) of gravel, a rut reduction of 89 mm (3.5 in.) was recognized by performing gravel compaction. Finally, no damage to the geotextile was observed in any of the tests.

Chapter 5

Conclusions

When a vertical load from a vehicle is applied to an unpaved road involving a gravel aggregate-clay subgrade system, horizontal and vertical stresses are generated. The horizontal stresses in the aggregate result in outward shear stresses on the surface of the subgrade. These shear stresses reduce the bearing capacity of the clay to as little as one half the value for purely vertical loading. If fabric is present, these shear stresses can possibly be carried by the reinforcement (depending on interface friction), allowing the full bearing capacity of the clay to be mobilized.

A series of 18 direct shear tests and 13 unpaved road model tests were performed to evaluate how system properties such as interface friction affect performance. Interface friction values were obtained for three different geotextile types—lightweight slit film (150 g/m^2), heavyweight woven (270 g/m^2), and nonwoven (340 g/m^2)—by performing direct shear tests on soil-fabric-aggregate systems. The nonwoven geotextile developed an interface friction comparable to that of the gravel alone (42°), while the lightweight and heavyweight woven geotextiles generated 20% lower interface friction angles (around 34°). The interface friction of the nonwoven geotextile may be a result of its texture, which could generate increased interlock between the gravel and geotextile, when compared to the slit film and woven geotextile systems. Little difference was seen in the values for interface friction for the clay sliding relative to the geotextile and the gravel sliding relative to the geotextile.

Results of the unpaved road model test series performed with and without geotextile reinforcement at the gravel-subgrade interface showed that in terms of rut depths, the nonwoven performed better than the slit film geotextile for all gravel thicknesses. The nonwoven reinforced system with 100 mm (4 in.) of gravel was equivalent to the slit film reinforced system with 150 mm (6 in.) of gravel and the unreinforced system with 200 mm (8 in.) of gravel, although a significant rut depth of approximately 60 mm (2.4 in.) was observed. The improved performance

on the part of the nonwoven geotextile was most likely due to the nonwoven's frictional characteristics shown by the direct shear tests.

Allowable stress levels for the unreinforced and nonwoven reinforced systems were determined to differ by a factor of about 1.6. These results agreed well with the results of previous work. The load-spread angle through the gravel tended to be larger for the reinforced systems than for the unreinforced systems indicating that interlocking of the gravel and geotextile produced confinement on the gravel resulting. Other significant observations were that geotextile anchorage was unimportant, as the geotextile appeared to only be stretched and pulled within the distributed load area at that location. Outside of this area, no stretching of the geotextile was observed as present. Finally, no damage to the geotextile was observed in any of the tests.

A simple design procedure that could be followed is contained in section A.1 of the Appendix. The procedure is that outlined in the FHWA Geosynthetic Design and Construction Guidelines, and is basically that adopted by the U.S. Forest Service Guidelines for Use of Fabrics in Construction and Maintenance of Low-Volume Roads. The procedure is simple to follow and it does not rely on a particular mechanism or an assumed rut geometry. The bearing capacity factors suggested are reasonable, but the gravel thicknesses may be unconservative (the Forest Service allows large rutting). In fact, the design method states that separation is the primary function.

References

- [1] Barenberg, E.J., Dowland, J.H. Jr., and Hales, J.H. (1975). Evaluation of soil aggregate systems with Mirafi[®] fabric. Civil Engineering Studies, Department of Civil Engineering, University of Illinois, Champaign-Urbana, Illinois. August.
- [2] Kinney, T.C. (1979). Fabric induced changes in high deformation soil-fabric-aggregate systems. Ph.D. thesis, University of Illinois, Champaign-Urbana, Illinois. January.
- [3] Barenberg, E.J. (1980). Design procedures for soil-fabric-aggregate systems with Mirafi[®] 500X fabric. Civil Engineering Studies, Department of Civil Engineering, University of Illinois. October.
- [4] Giroud, J.P. and Noiray, L. (1981). Geotextile-reinforced unpaved roads. Journal of the Geotechnical Engineering Division, American Society of Civil Engineers. 107(GT 9): 1233-1254, September.
- [5] Milligan, G.W.E., Jewell, R.A., Houlsby, G.T., and Burd, H.J. (1989). A new approach to the design of unpaved roads. Ground Engineering. 22(3), 22(8).
- [6] ASTM (1994). Annual Books of ASTM Standards. American Society for testing and Materials, Philadelphia, Pennsylvania.
- [7] Steward, J., Williamson, R., and Mohny, J. (1977). Guidelines for the use of fabrics in construction and maintenance of low-volume roads. US Department of Agriculture, Forest Service. Portland, Oregon. Also published as Report No. FHA-TS-78-205 (1978).
- [8] Douglas, R.A. and Kelly, M.A. (1986). Geotextile reinforced unpaved logging roads: the effect of anchorage. Geotextiles and Geomembranes. 4(2): 93-106.
- [9] Yoder, E.J. (1959). Principles of pavement design. John Wiley and Sons, Inc. New York. 21-32.
- [10] Brorsson, I. and Eriksson, L. (1986). Long-term properties of geotextiles and their function as a separator in road construction. Proceedings of the Third International

- Conference on Geotextiles. Vienna, Austria. April 7-11, 1986. Industrial Fabrics Association International, St. Paul, Minnesota. 1: 93-98.
- [11] Haliburton, T.A. and Barron, J.V. (1983). Optimum-depth method for design of fabric reinforced unsurfaced roads. National Research Council and Transportation Research Board. Washington, D.C. Report No. 916: 26-32.
- [12] Burd, H.J. and Brocklehurst, C.J. (1990). Finite element studies of the mechanics of reinforced unpaved roads. Proceedings of the Fourth International Conference on Geotextiles, Geomembranes, and Related Products. The Hague, Netherlands. May 28-June 2, 1990. Industrial Fabrics Association International, St. Paul, Minnesota. 217-221.
- [13] Houlsby, G.T. and Jewell, R.A. (1990). Design of reinforced unpaved roads for small rut depths. Proceedings of the Fourth International Conference on Geotextiles, Geomembranes, and Related Products. The Hague, Netherlands. May 28-June 2, 1990. Industrial Fabrics Association International, St. Paul, Minnesota. 171-176.
- [14] Espinoza, R.D. (1994). Soil-geotextile interaction: evaluation of membrane support. Geotextiles and Geomembranes. Elsevier Applied Science. 13(5): 281-293.
- [15] Espinoza, R.D. and Bray, J.D. (1995). An integrated approach to evaluating single-layer reinforced soils. Geosynthetics International. Industrial fabrics Association International, St. Paul, Minnesota. 2(4): 723-739.
- [16] Bender, D.A. and Barenberg, E.J. (1978). Design and behavior of soil-fabric-aggregate systems. National Research Council and Transportation Research Board. Washington, D.C. Report No. 671: 64-75.
- [17] Ahlvin, R.G. (1962). Flexible pavement design criteria. Journal of the Aerospace Transport Division. Proceedings of the American Society of Engineers. 88(AT 1).
- [18] Holtz, R.D. and Sivakugan, N. (1987). Design charts for roads with geotextiles. Geotextiles and Geomembranes. Elsevier Applied Science. 5: 191-199.
- [19] Sellmeijer, J.B., Kenter, C.J., and Van Den Berg, C. (1982). Calculation method for a fabric reinforced road. Proceedings of the Second International Conference on Geotextiles. Las Vegas, Nevada. August 1-6, 1982. Industrial Fabrics Association International, St. Paul, Minnesota. 2: 393-398.

- [20] Douglas, R.A. and Kelly, M.A. (1986). Geotextile 'reinforced' unpaved logging roads: the effect of anchorage. *Geotextiles and Geomembranes*. Elsevier Applied Science. 4(2): 93-106.
- [21] Bakker, J.G. (1977). Mechanical behavior of membranes in road foundations. *Proceedings of the First International Conference on Geotechnics*. Paris, France. April. 1: 139-142.
- [22] Holtz, R.D. Christopher, B.R., and Berg, R.R. (1995). Geosynthetic design and construction guidelines. FHWA, NHI and USDOT Publication No. FHWA HI 95-038. May.
- [23] Zeevaert, A.E. (1980). Finite element formulation for the analysis of interfaces, nonlinear and large displacement problems in geotechnical engineering. Ph.D. thesis, Georgia Institute of Technology, Atlanta, Georgia.
- [24] Burd, H.J. (1986). A large displacement finite element analysis of a reinforced unpaved road. D.Phil thesis, University of Oxford, Oxford, England.
- [25] Burd, H.J. and Houlsby, G.T. (1986). A large strain finite element formulation for one dimensional membrane elements. *Computers and Geotechnics*, 2(1): 3-22.
- [26] Douglas, R.A. and Valsangkar, A.J. (1992). Unpaved geosynthetic-built resource access roads: stiffness rather than rut depths as the key design criteria. *Geotextiles and Geomembranes*. Elsevier Applied Science. 11(1): 45-59.
- [27] Douglas, R.A. (1993). Stiffness of geosynthetic-built unpaved road structures: experimental programme, analysis and results. *Proceedings of Geosynthetics '93*. Vancouver, British Columbia, Canada. Industrial Fabrics Association International, St. Paul, Minnesota. 1: 21-32.
- [28] Hoare, D.J. (1982). A laboratory study into pumping clay through geotextiles under dynamic loading. *Proceedings of the Second International Conference on Geotextiles*. Las Vegas, Nevada. August 1-6, 1982. Industrial Fabrics Association International. St. Paul, Minnesota. 2: 423-428.

- [29] Alobaidi, I. and Hoare, D. (1994). Factors affecting the pumping of fines at the subgrade subbase interface of highway pavements: a laboratory study. Geosynthetics International. Industrial Fabrics Association International. St. Paul, Minnesota. 1(2): 221-225.
- [30] Bell, A.L., McCullough, L.M., and Snaith, M.S. (1982). An experimental investigation of sub-base protection using geotextiles. Proceedings of the Second International Conference on Geotextiles. Las Vegas, Nevada. August 1-6, 1982. Industrial Fabrics Association International. St. Paul, Minnesota. 2: 435-440.
- [31] Lafleur, J., Rollin, A.L., and Mlynarek, J. (1990). Clogging of geotextiles under pumping loads. Proceedings of the Fourth International Conference on Geotextiles, Geomembranes, and Related Products. The Hague, Netherlands. May 28-June 2, 1990. Industrial Fabrics Association International. St. Paul, Minnesota. 189-192.
- [32] Nishida, K. and Nishigata, T. (1994). The evaluation of separation function for geotextiles. Proceedings of the Fifth International Conference on Geotextiles, Geomembranes, and Related Products. Singapore. Sept. 5-9, 1994. Industrial Fabrics Association International. St. Paul, Minnesota. 1: 139-142.
- [33] Austin, D.N. and Coleman, D.M. (1993). A field evaluation of geosynthetic-reinforced haul roads over soft foundation soils. Proceedings of Geosynthetics '93. Vancouver, British Columbia, Canada. Industrial Fabrics Association International. St. Paul, Minnesota. 1: 65-80.
- [34] Giroud, J.P., Ah-Line, C., and Bonaparte, R. (1984). Design of unpaved roads and trafficked areas with geogrids. Polymer Grid Reinforcement. Conference Proceedings. Thomas Telford Limited. London. 116-127.
- [35] Metcalfe, R.C., Holtz, R.D., and Allen, T.M. (1995). Field investigation to evaluate the long-term separation and drainage performance of geotextile separators. Proceedings of Geosynthetics '95. Nashville, Tennessee. Industrial Fabrics Association International. St. Paul, Minnesota. 3: 951-962.
- [36] Page, M.W. (1990). Performance of geotextile separators." Master Thesis. University of Washington, Seattle, Washington.

- [37] Cernica, J.N. (1995). Geotechnical engineering: soil mechanics. John Wiley & Sons. 206.
- [38] Wardle, L.J. (1976). Program CIRCLY-a computer program for the analysis of multiple complex circular loads on layered anisotropic media-user's manual. Geomechanics Computer Program No.2, CSIRO Division of Applied Geomechanics.
- [39] Das, B.M. (1990). Principles of foundation engineering. Second Edition. PWS Publishing Company. Boston. 161.
- [40] Prandtl, L. (1921). Penetrating strengths of plastic construction materials. Mathematical Mechanics. 1: 15-20.
- [41] Skempton, A.W. (1951). The bearing capacity of clays. Proceedings of the British Building Research Congress. 1: 180-189.
- [42] Rodin, S. (1965). Ability of a clay fill to support a construction plant. Journal of Terramechanics. 1(4): 51-68.
- [43] De Groot, M., Janse, E., Maagdenberg, T.A.C., and Van den Berg, C. (1986). Design method and guidelines for geotextile applications in road construction. Proceedings of the Third International Conference on Geotextiles. Vienna, Austria. 3: 741.

Appendix A
Vendor Recommended Design Procedures

Vendor Recommended Design Procedures

In unpaved road design, a geotextile can be included to reinforce the aggregate-subgrade system and/or to separate the aggregate from the subgrade. An unpaved road with a geotextile is commonly referred to as a soil-fabric-aggregate (SFA) system due to the three main components. When designing an SFA system, it is necessary to obtain product information from the geotextile vendor. Some vendors include a procedure for designing SFA systems with their products. The following three design procedures were predominately recommended by vendors:

1. FHWA Geosynthetic Design and Construction Guidelines [22]
 - Amoco Fabrics and Fibers Company
 - Contech Construction Products Inc.
 - Synthetics Industries
2. U.S. Forest Service Guidelines for Use of Fabrics in Construction and Maintenance of Low-Volume Roads [7]
 - Linq Industrial Fabrics, Inc.
3. Design Procedure for SFA Systems with Mirafi[®] 500X [3]
 - Mirafi[®]

Included in this report is a brief outline of these three design procedures. When permitted, design charts were reproduced and included in this report. Both the Holtz et al. [22] and Steward et al. [7] design procedures assume the separation function as the primary function in SFA systems. Barenberg's [3] design procedure assumes that there is significant rutting in the road and assumes a rut geometry so as to determine the vertical force carried by the geotextile.

A.1 FHWA Geosynthetic Design and Construction Guidelines [22]

FHWA sponsored the development of a manual that included a procedure for the design of unpaved roads with geotextile [22]. The procedure is widely used and is recommended by Amoco Fabric and Fibers Company, Contech Construction Products Inc., and Synthetic Industries when designing with their geotextile products. The procedure assumes that the geotextile's main function is as a separator; no geotextile tensile reinforcing mechanism is considered. If a tensile reinforcing mechanism is generated then an additional benefit will exist. Simply considering the separation function is deemed conservative and acceptable.

The use of a geotextile in an unpaved road is recommended for the following subgrade conditions according to the FHWA manual:

- poor soils
 USCS: SC, CL, CH, ML, MH, OL, OH, and PT
 AASHTO: A-5, A-6, A-7-5, and A-7-6
- low undrained shear strength
 $c_u < 90 \text{ kPa (13 psi)}$ $c_u = \text{undrained shear strength}$
 CBR < 3
 resilient modulus $\approx 30 \text{ MPa (4350 psi)}$
- high water table

Similarly, the following geotextile functions are considered appropriate for the following subgrade strengths:

Undrained Shear Strength, kPa	Subgrade CBR	Functions
60 – 90	2 -3	filtration and possibly separation
30 –60	1 -2	filtration, separation, and possibly reinforcement
< 30	< 1	all functions including reinforcement

For a geotextile to perform its intended function, it is first necessary for the geotextile to survive the construction operations. The FHWA manual includes a survivability criteria (Tables

A.1 and A.2) developed by Task Force 25 [46]. Table A.1 relates the elements of construction such as equipment, aggregate characteristics, subgrade preparation, and subgrade shear strength to the severity of the loading imposed on the geotextile. The geotextile strength required to survive the most severe conditions anticipated during construction can then be determined using Table A.1.

Table A.1: Construction survivability ratings [Task Force 25, 46]

Site Soil CBR at Installation ¹	< 1		1 to 2		> 3	
Equipment Ground Contact Pressure (kPa)	> 350	< 350	> 350	< 350	> 350	< 350
Cover Thickness ² (compacted, mm)						
100 ^{3,4}	NR ⁵	NR	H ⁵	H	M ⁵	M
150	NR	NR	H	H	M	M
300	NR	H	M	M	M	M
450	H	M	M	M	M	M
Notes:						
1. Assume saturated CBR unless construction scheduling can be controlled.						
2. Maximum aggregate size not to exceed one-half the compacted cover thickness.						
3. For low-volume, unpaved roads (ADT<200 vehicles).						
4. The 100 mm minimum cover is limited to existing road bases and is not intended for use in new construction.						
5. NR = not recommended; M = moderate; and H = high.						

Table A.2: Physical property requirements¹

Survivability Level	Grab Strength ⁴ , (N) ASTM D 4632		Puncture Resistance ⁴ , (N) ASTM D 4833		Tear Strength ⁴ , (N) ASTM D 4533	
	< 50 % Geotextile Elongation	> 50 % Geotextile Elongation	< 50 % Geotextile Elongation	> 50 % Geotextile Elongation	< 50 % Geotextile Elongation	> 50 % Geotextile Elongation
Moderate	801	512	311	178	311	178
High	1201	801	445	334	445	334
Additional Requirements:					<u>Test Method</u>	
<i>Apparent Opening Size</i>					ASTM D 4751	
1. < 50 % soil passing 0.075 mm sieve, AOS < 0.6 mm						
2. > 50 % soil passing 0.075 mm sieve, AOS < 0.3 mm						
<i>Permeability</i>					ASTM D 4491	
k of the geotextile > k of the soil						
<i>Ultraviolet Degradation</i>					ASTM D 4355	
At 150 hours of exposure, 70% strength retained						
<i>Geotextile Acceptance</i>					ASTM D 4759	
Notes:						
1. For the index properties, the first value of each set is for geotextiles that fail at less than 50% elongation, while the second value is for geotextiles that fail at greater than 50% elongation. Elongation is determined by ASTM D 4632.						
2. Values shown are minimum roll average values. Strength values are in the weakest principal direction.						
3. The values of the geotextile elongation do not relate to the allowable consolidation properties of the subgrade soil. These must be determined by a separate investigation.						
4. Numeric values are hard conversions of English units.						

The following design method considers the separation function as the primary function. The method was developed by Steward et al. [7] for the U.S. Forest Service and allows the designer to consider vehicle passes, equivalent axle loads, axle configurations, tire pressures, subgrade strengths, and rut depths. It is assumed in the method that the aggregate is cohesionless and has a CBR of 80, the number of vehicle passes is less than 10,000, and the subgrade undrained shear strength is less than 90 kPa (13 psi, CBR < 3).

Procedure

1. Determine subgrade undrained shear strength, c_u .

empirical relationships:

$$c_u = 30 * \text{CBR}$$

$$c_u = \text{the WES cone penetrometer index divided by 10}$$

2. Determine wheel loading for design period.

- maximum single wheel load
- maximum dual wheel load
- maximum dual tandem wheel load

3. Estimate maximum amount of traffic anticipated for each design vehicle class.

4. Establish amount of tolerable rutting during the road's design life.

50 - 75 mm (2-2.5 in.) of rutting is generally acceptable during construction

5. Obtain the appropriate bearing capacity factor (Table A.3).

Table A.3: Bearing capacity factors

	Ruts (mm)	Traffic (Passes of 80 kN axle equivalents)	Bearing Capacity Factor, N_c
Without Geotextile	< 50	> 1000	2.8
	>100	< 100	3.3
With Geotextile	< 50	> 1000	5.0
	>100	< 100	6.0

6. Determine the required aggregate thickness for each maximum loading (Fig. A.1, A.2, A.3).
7. Select design thickness. The thickness should be given to the next higher 25 mm (1 in.)
8. Check geotextile drainage and filtration requirements (Table A.4).

Table A.4: Drainage and filtration requirements

Requirements:	Definitions:
$AOS \leq D_{85}$ (wovens) $AOS \leq 1.8D_{85}$ (nonwovens) $k_{\text{geotextile}} \geq k_{\text{soil}}$ $\psi \geq 0.1 \text{ sec}^{-1}$	AOS = apparent opening size of geotextile (specified by geotextile manufacturer) D_{85} = gravel diameter for 85% passing $k_{\text{geotextile}}$ = geotextile permeability (specified by geotextile manufacturer) k_{soil} = soil permeability ψ = geotextile permittivity (specified by geotextile manufacturer)

9. Check survivability requirements (Table A.1).
10. Specify geotextile properties such that they meet or exceed survivability requirements.

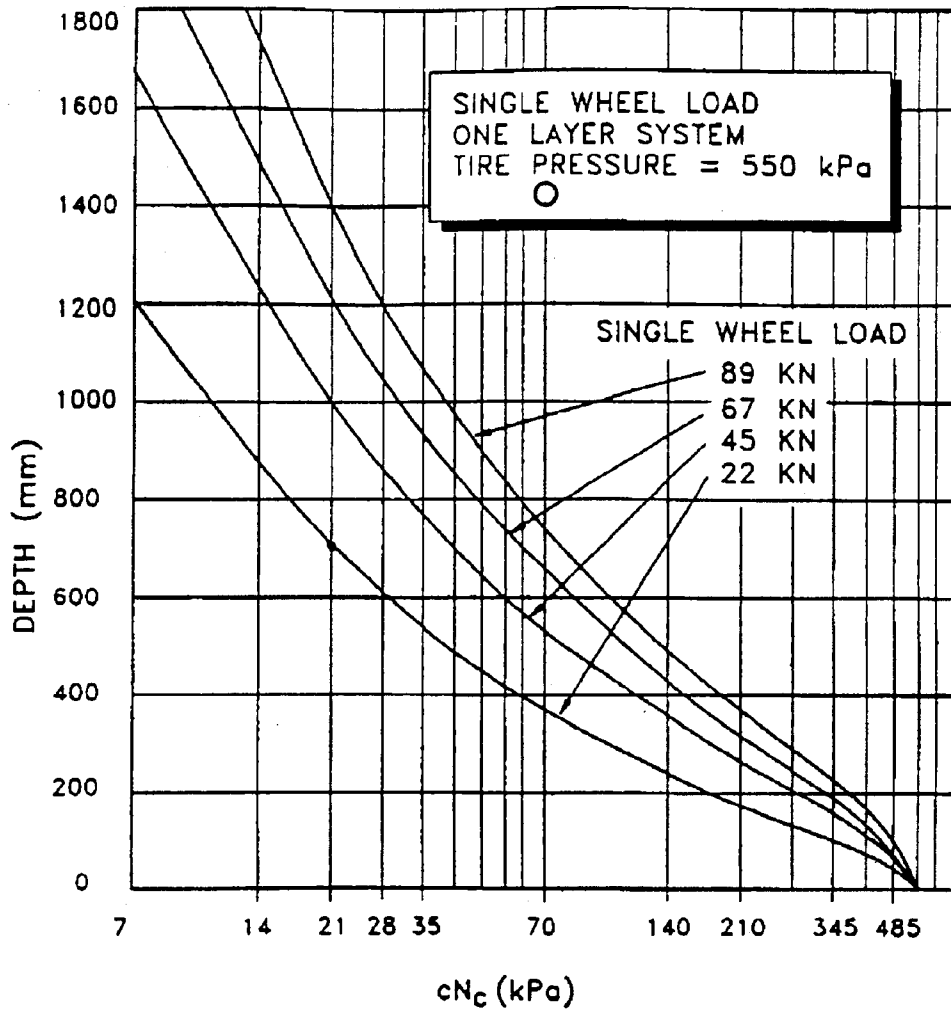


Figure A.1: Thickness design curve for single wheel loads [7]

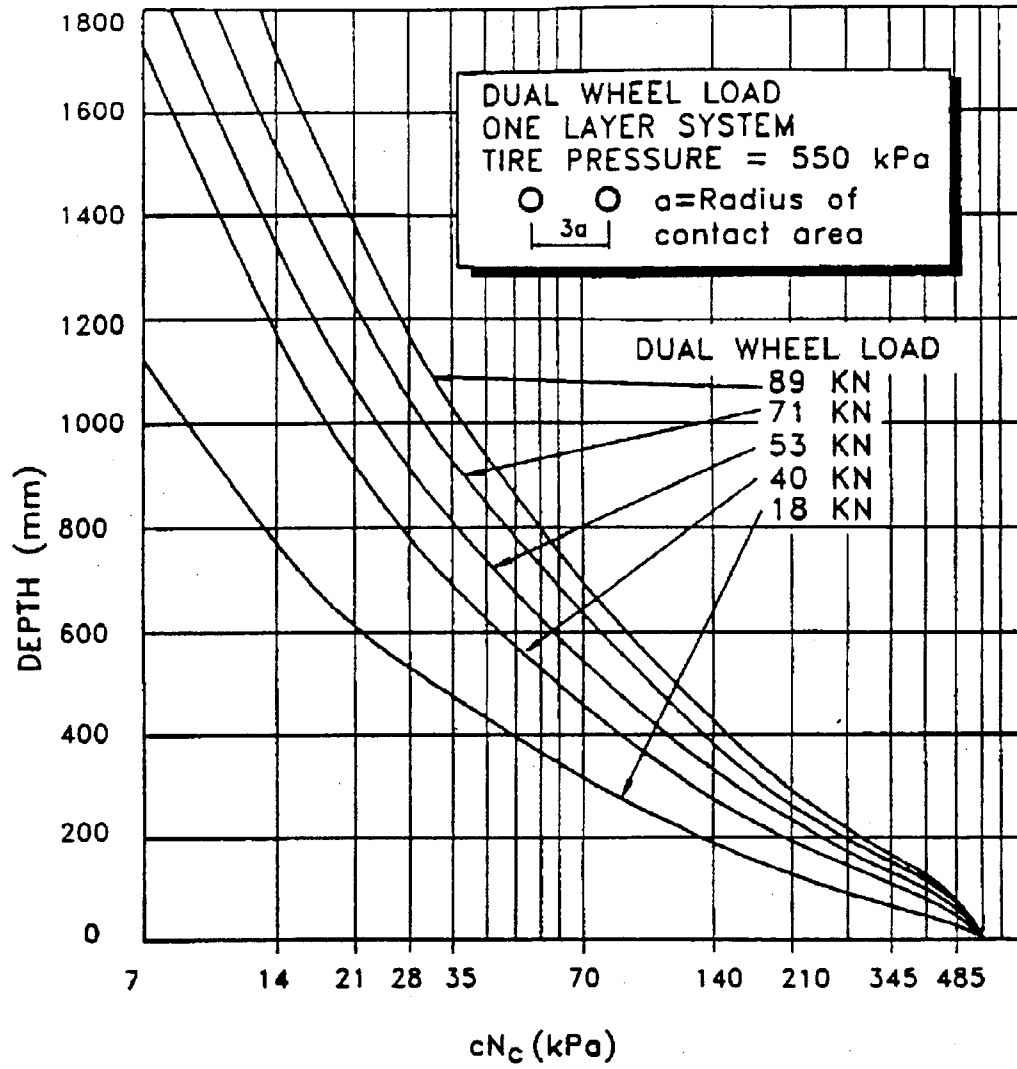


Figure A.2: Thickness design curve for dual wheel loads [7]

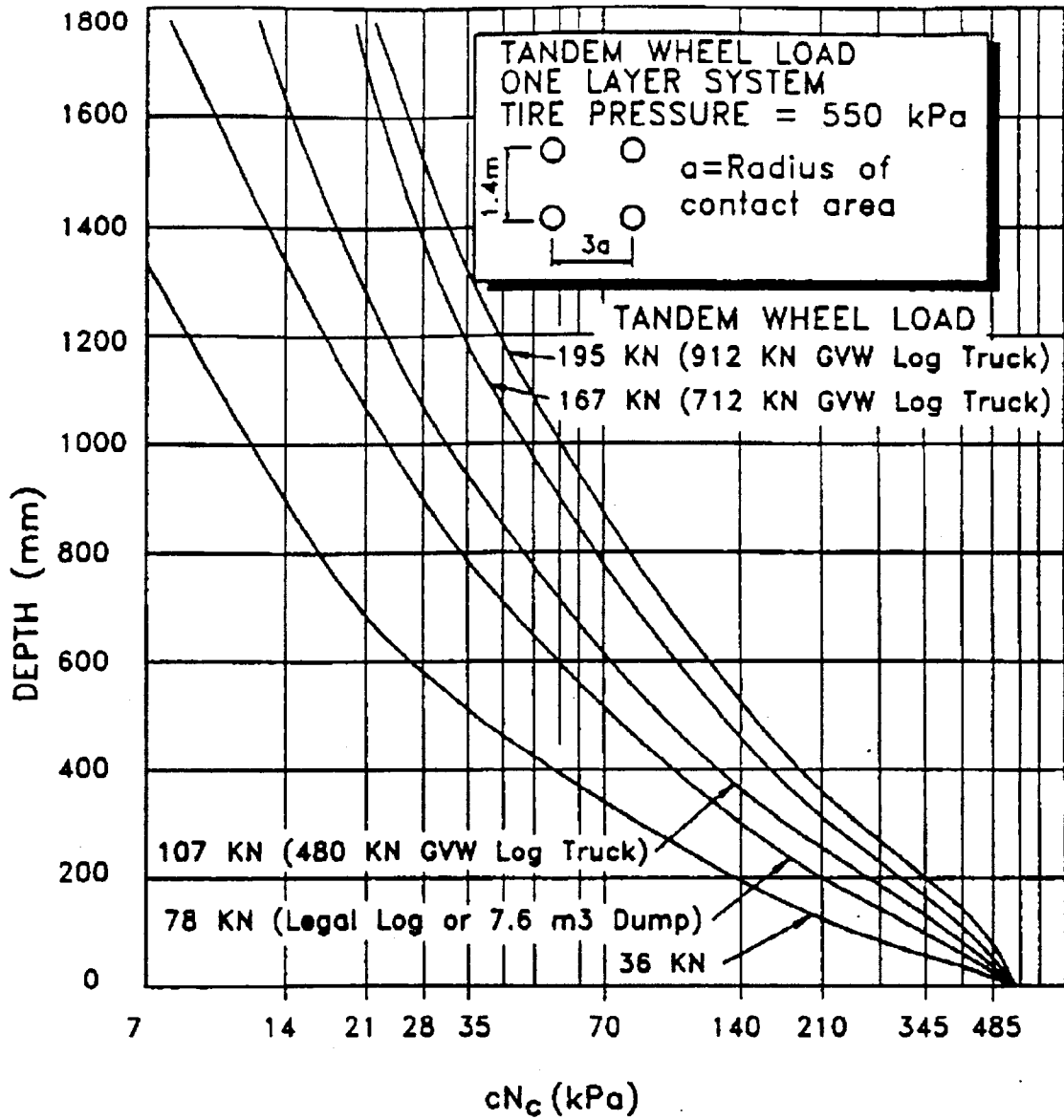


Figure A.3: Thickness design curve for tandem wheel loads [7]

A.2 U.S. Forest Service [7]

The U.S. Forest Service [7] developed guidelines for the use of geotextiles in the construction and maintenance of low-volume roads. The guidelines included a procedure for unpaved low-volume road design with geotextiles for separation or reinforcement. This design procedure is recommended by Linq Industrial Fabrics, Inc. for use when designing unpaved roads with their geotextile products.

The design procedure developed by Steward et al. [7] was based on work by Barenberg [1], who later developed a design and installation procedure for the use of Mirafi® 500X and 600X [3]. The design procedure developed by Steward et al. [6] for the use of geotextiles in low-volume unpaved roads is the basis for the procedure generated by Holtz et al. [22]. Therefore, to avoid redundancy, the procedure developed by Steward et al. will not be outlined.

Steward et al. [7] also developed a procedure for estimating the cost effectiveness of fabric as a separation layer. By placing the geotextile at the subgrade-gravel interface, the geotextile can prevent the migration of small subgrade particles into the gravel as well as the pushing of the gravel down into the subgrade. By preventing this “mixing”, the geotextile may be cost effective. The procedure for estimating geotextile cost-effectiveness is as follows.

Procedure

1. Estimate contamination zone thickness.

Make test excavations in existing roads with similar construction, soils, and traffic to the project being designed.

2. Assign a structural value (“a” value) to the contaminated and uncontaminated layers.
3. Calculate the required structural section thickness with and without contamination.
4. Calculate the structural cost of the contamination, C_c :

C_c = thickness difference between the system with and without contamination

5. Include in conventional design the additional aggregate thickness required by contamination as either subbase or base material.

6. Assume in the geotextile design that 75% of contamination is prevented. Geotextile system consists of geotextile plus 25% additional subbase/base and the originally designed structural section.
7. Perform a cost analysis of system with and without geotextile.

An unpaved road can be designed with geotextile according to the method developed by Steward et al. [7] as presented in the FHWA manual [Holtz et al., 22]. This design can be compared to a conventionally designed unpaved road without geotextile. By performing this comparison, savings can often times be recognized when designing over poor subgrades where drainage and filtration at the aggregate-subgrade interface are important.

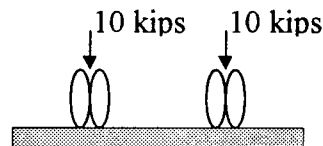
A.3 Barenberg [3]

Barenberg [3] developed a design procedure for using Mirafi® 500X and 600X to reinforce unpaved roads. This procedure was the result of research performed at the University of Illinois, Champaign-Urbana [2]. To use this design procedure a permissible rut depth for the road must be decided so as to develop the rut geometry. Knowing the rut geometry and assuming no slip at the interface tension in the geotextile can be calculated. The tensioning of the geotextile results in reduction of the vertical stresses transferred to the subgrade. The design procedure developed by Barenberg [3] is summarized in the main body of this report. Included here is a design example and design charts based on this procedure. It is important to mention that the design procedure and design charts (Fig. A.4, A.5, A.6, A.7) were developed for use with Mirafi® 500X and Mirafi® 600X. However, once this procedure is understood it can easily be applied when designing unpaved roads with other geotextiles.

Example

1. Determine wheel load and contact pressure anticipated on the soil-fabric-aggregate system surface.

- dual wheel load = 44.5 kN (10 kips)
per dual tire print
- tire pressure = 460 kPa (67 psi)



assume contact pressure = $0.75(460 \text{ kPa}) = 345 \text{ kPa}$ (50 psi)

2. Determine the maximum allowable stress, σ_{all} , on the subgrade.

$$\sigma_{all} = 3.2Ac_u$$

- soil undrained shear strength, c_u , determined from soil evaluations
(assume 21 kPa or 3 psi)
- coefficient A is often taken as 2

$$\sigma_{all} = 132 \text{ kPa} (19.2 \text{ psi})$$

3. Determine the rut geometry.

rut width, W , estimated as 1270 mm (50 in.) for track width of the dual-tire set plus “wander”

$$W = 1270 \text{ mm (50 in.)}$$

allowable rut depth, d , for this particular haul road set by engineer as 150 mm (6 in.)

$$d = 150 \text{ mm (6 in.)}$$

rut radius, R :

$$R = \frac{9W^2}{80d} + \frac{5}{16}d \quad R = \frac{9(1270)^2}{80(150)} + \frac{5}{16}(150)$$

$$R = 1240 \text{ mm (48.8 in.)}$$

arc, θ , for the rut geometry

$$\theta = 2 \tan^{-1} \left(\frac{10d}{6W} \right) \quad \theta = 2 \tan^{-1} \left(\frac{10(150)}{6(1270)} \right)$$

$$\theta = 22.6^\circ$$

4. Determine the strain in the fabric, ε_f .

$$\varepsilon_f = \left[\frac{4\pi R \theta}{135W} - 2 \right] \times 100\% \quad \varepsilon_f = \left[\frac{4\pi(1240)(22.6)}{135(1270)} - 2 \right] \times 100\%$$

$$\varepsilon_f = 5.32\%$$

5. Determine the tension in the fabric, t_f .

t_f is calculated by multiplying the fabric modulus (stiffness), K , by the fabric strain, ε_f .

$K = 260 \text{ N per mm (1500 lb/in)}$ for Mirafi® 600X

$K = 193 \text{ N per mm (1100 lb/in.)}$ for Mirafi® 500X

K values can be obtained from the manufacturer

$$t_f = K\varepsilon_f \quad t_f = 260 (0.0532)$$

$$t_f = 14 \text{ N per mm (79.8 lb/in.)}$$

6. Determine the differential normal stress carried by the fabric, $\Delta\sigma_{z-f}$.

$$\Delta\sigma_{z-f} = \frac{t_f}{R} \quad \Delta\sigma_{z-f} = \frac{14}{1240}$$

$$\Delta\sigma_{z-f} = 11.3 \text{ kPa (1.64 psi)}$$

7. Determine the permissible stress on the fabric, σ_{p-f} .

$$\sigma_{p-f} = \Delta\sigma_{z-f} + A3.2c_u \quad \sigma_{p-f} = 143 \text{ kPa (20.8 psi)}$$

8. Determining the required aggregate thickness, z .

actual vertical stress, σ_z , imposed on the fabric by the wheel load:

$$\sigma_z = p \left[1 - \left(\frac{1}{1 + (a/z)^2} \right)^{3/2} \right]$$

p = average surface contact pressure from wheel load

a = radius of loaded area = $\sqrt{L/\pi p}$

L = applied load

required aggregate layer thickness, z :

setting the permissible stress on the fabric, σ_{p-f} , equal to the actual vertical stress, σ_z , the following expression for the required aggregate layer thickness, z , can be developed:

$$z = \left(\frac{L/\pi p}{1/(1 - \sigma_{p-f}/p)^{2/3} - 1} \right)^{1/2} \quad z = \left(\frac{44.5/\pi(345)}{1/(1 - 143)^{2/3} - 1} \right)^{1/2}$$

$$z = 312 \text{ mm (12.3 in.)}$$

9. Comparison to conventional method without fabric.

from step 2:

$$\sigma_{all} = 3.2Ac_u$$

set $A = 1.0$ without fabric

$$\sigma_{all} = 239 \text{ kPa (9.42 psi)}$$

from step 8:

$$z = 523 \text{ mm (20.6 in.)}$$

add 75 mm (3 in.) of aggregate to account for subgrade intrusion

$$z = 523 + 75 = 598 \text{ mm (23.66 in.)}$$

10. Conclusion:

Use of Mirafi® 600X fabric with 330 mm (13 in.) of aggregate results in an 280 mm (11 in.) or 48% savings in aggregate.

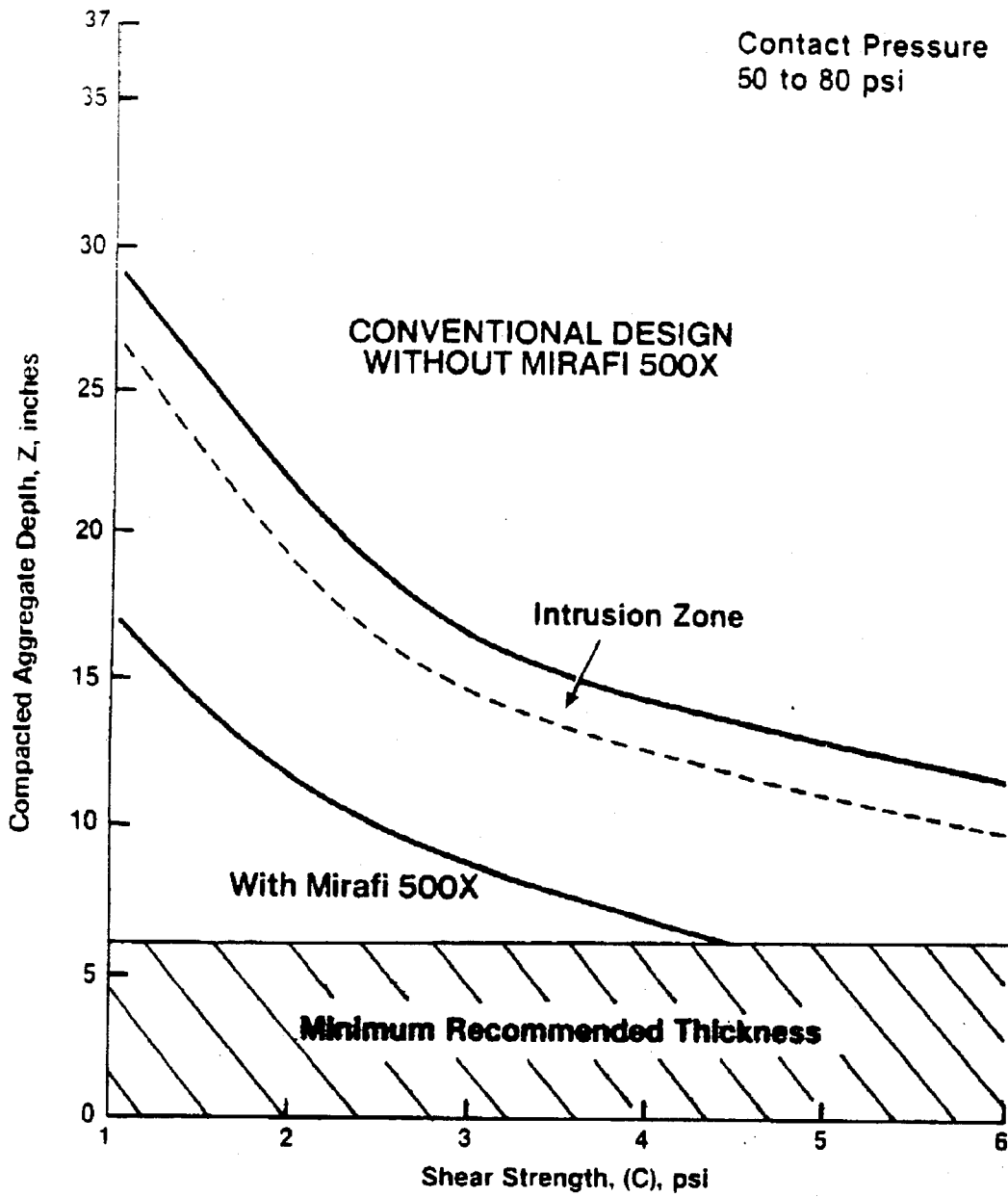


Figure A.4: Haul-road stabilization design curves for a 22 kN (5,000 lb) wheel load [3]

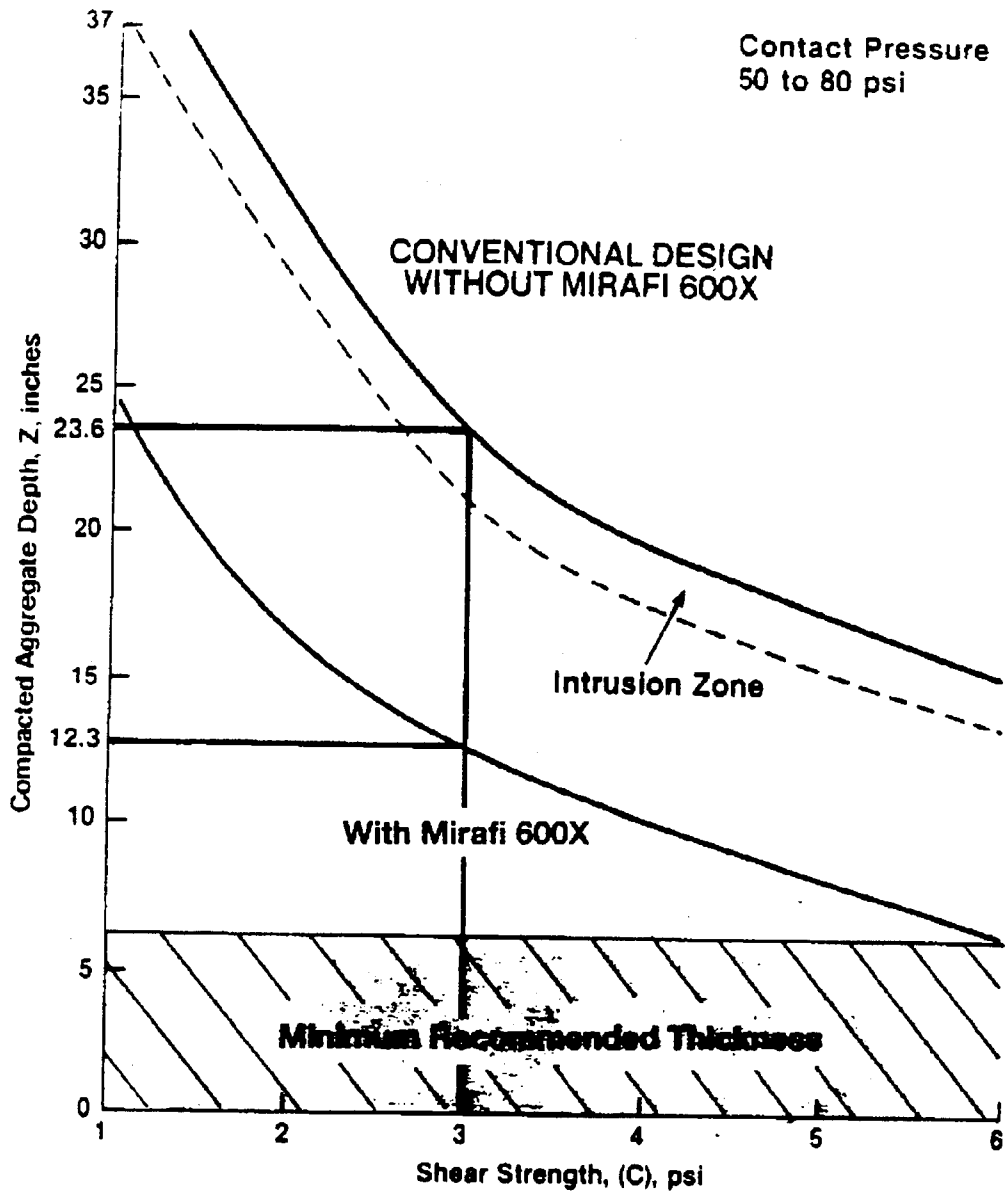


Figure A.5: Haul-road stabilization design curves for a 44.5 kN (10,000 lb) wheel load [3]

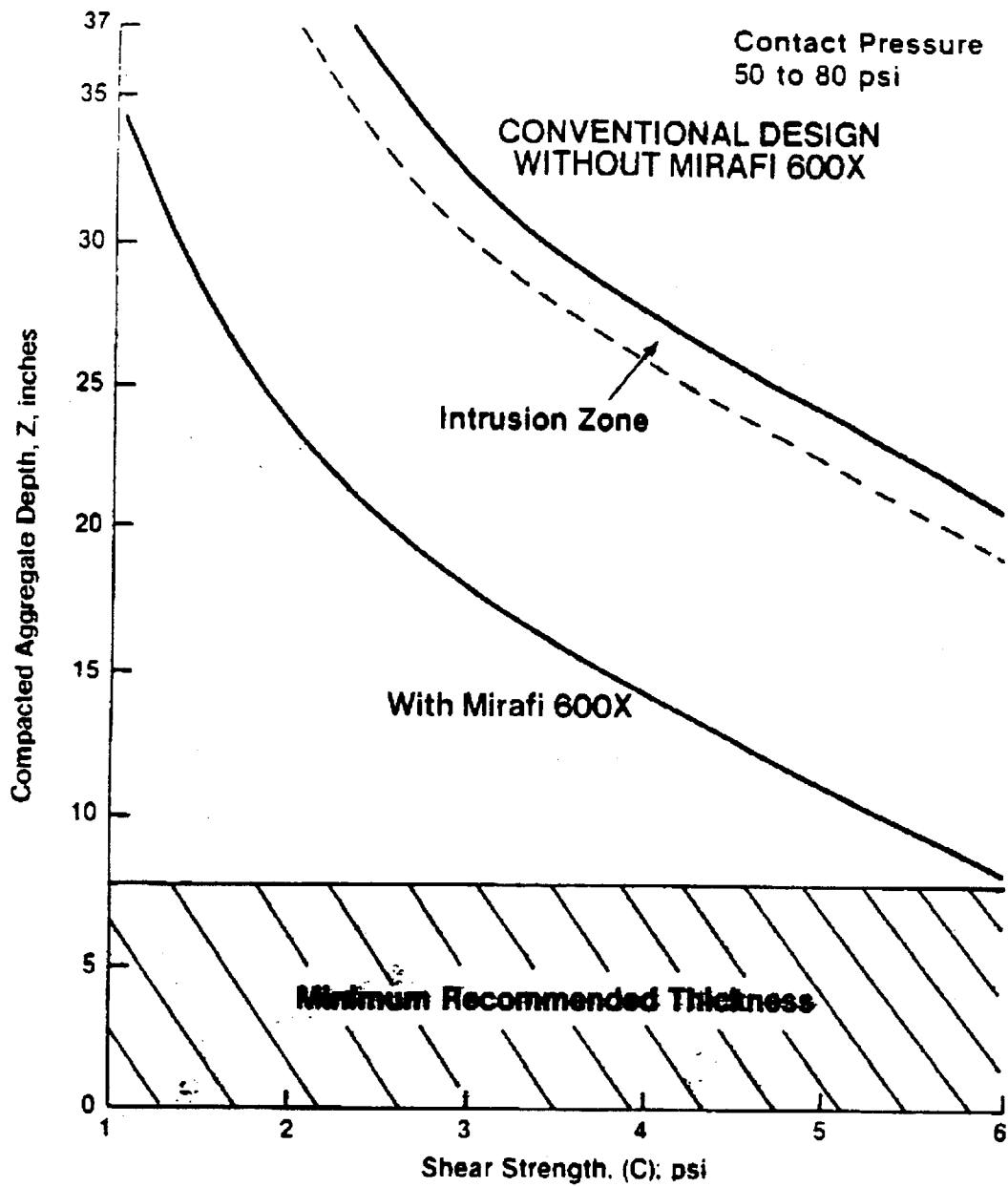


Figure A.6: Haul-road stabilization design curves for a 67 kN (15,000 lb) wheel load [3]

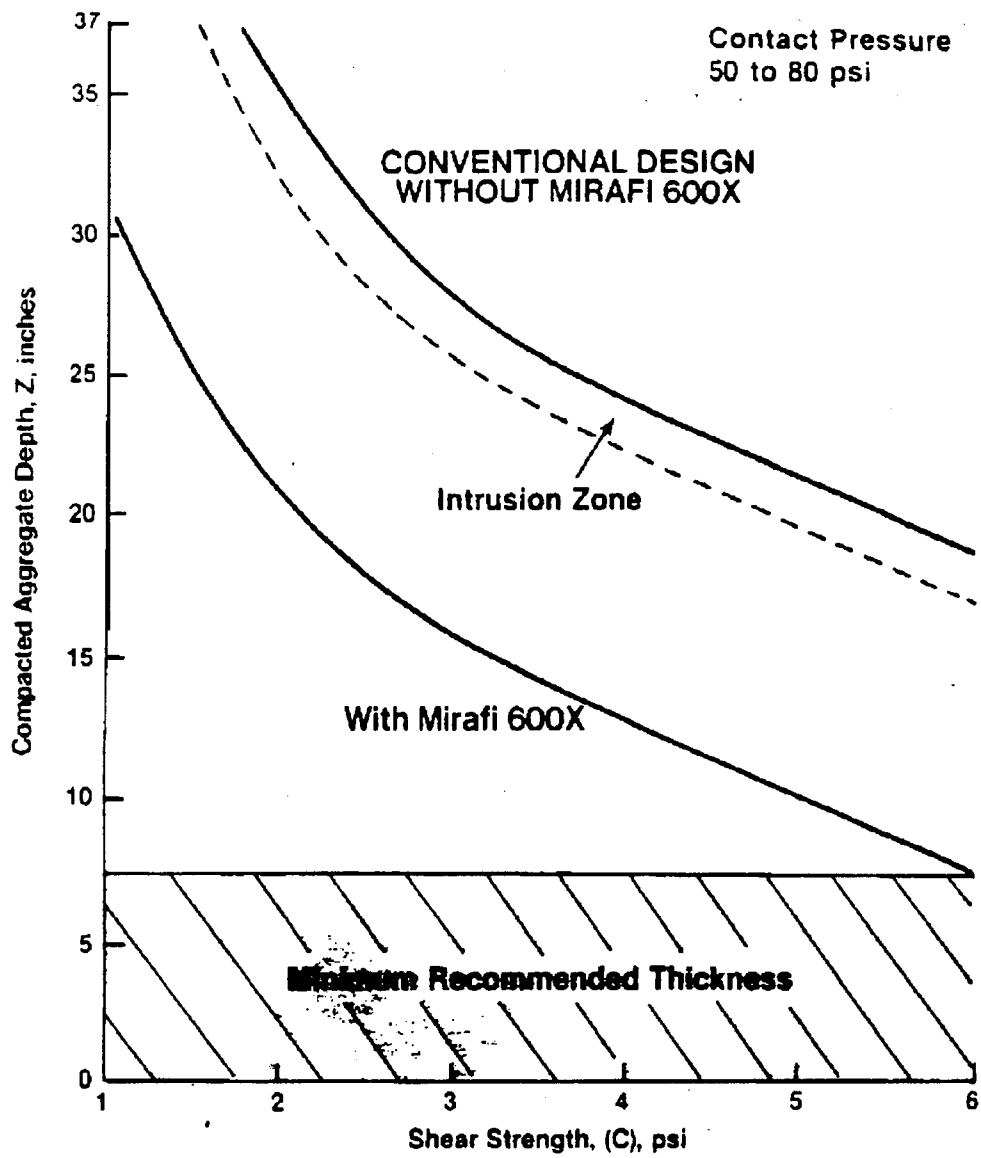


Figure A.7: Haul-road stabilization design curves for a 90 kN (20,000 lb) wheel load [3]

